NASA TECHNICAL REPORT

NASA TR R-421

NASA TR R-421

A STUDY OF THE NONLINEAR AERODYNAMICS OF BODIES IN NONPLANAR MOTION

by Lewis Barry Schiff

Ames Research Center

Moffett Field, Calif. 94035

NATIONAL AERONAUTICS AND SPACE ADMINISTRATION • WASHINGTON, D. C. • JANUARY 1974

1. Report No.	2. Government Accession No.	3. Recipient's Catalog No.
TR-421		

4. Title and Subtitle	5. Report Date
A Study of the Nonlinear Aerodynamics of Bodies in Nonplanar Motion	January 1974
	6. Performing Organization Code
7. Author(s)	8. Performing Organization Report No.
Lewis Barry Schiff	A-5057
9. Performing Organization Name and Address	10. Work Unit No.
Ames Research Center, Moffett Field, Calif. 94035 and Stanford University, Stanford, Calif.	501-06-01-23
	11. Contract or Grant No.
12. Sponsoring Agency Name and Address	13. Type of Report and Period Covered
National Aeronautics and Space Administration Washington, D.C. 20546	Technical Report
	14. Sponsoring Agency Code

15. Supplementary Notes

Submitted to Stanford University as partial fulfillment of Ph.D. degree, August 1973.

16. Abstract

Concepts from the theory of functionals are used to develop nonlinear formulations of the aerodynamic force and moment systems acting on bodies in large-amplitude, arbitrary motions. The analysis, which proceeds formally once the functional dependence of the aerodynamic reactions upon the motion variables is established, ensures the inclusion, within the resulting formulation, of pertinent aerodynamic terms that normally are excluded in the classical treatment. Applied to the large-amplitude, slowly varying, nonplanar motion of a body, the formulation suggests that the aerodynamic moment can be compounded of the moments acting on the body in four basic motions: steady angle of attack, pitch oscillations, either roll or yaw oscillations, and coning motion. Coning, where the nose of the body describes a circle around the velocity vector, characterizes the nonplanar nature of the general motion.

With the above motivation, a numerical finite-difference technique is developed for computing the inviscid flow field surrounding a body in coning motion in a supersonic stream. Computations carried out for circular cones in coning motion both at low supersonic and hypersonic Mach numbers confirm the adequacy of a linear moment formulation at low angles of attack. At larger angles of attack, however, the forces and moments become nonlinear functions of the angle of attack. Computational results for the reactions on the circular cone at the higher angles of attack agree well with experimental measurements within the range of variables investigated. This indicates that the initial nonlinear behavior of the aerodynamic forces and moments is governed primarily by the inviscid flow.

17. Key Words (Suggested by Author(s))	18. Distribution Statement
Nonlinear aerodynamics Nonsteady aerodynamics Nonplanar motion Supersonic aerodynamics Large angles of attack	Unclassified

19. Security Classif. (of this report)	20. Security Classif. (of this page)	21. No. of Pages	22. Price*
Unclassified	Unclassified	93	Domestic, $3.75 Foreign, $6.25

*For sale by the National Technical Information Service, Springfield, Virginia 22151

TABLE OF CONTENTS

NOMENCLATURE

C_Y	side-force coefficient in the aerodynamic axis system (along y), 2(side force)/$\rho_o V^2 S$
C_Z	normal-force coefficient in the aerodynamic axis system (along z), 2(normal force)/$\rho_o V^2 S$
$\hat{C}_Y, \hat{C}_Z$	side-force and normal-force coefficients in the body-axis system; along y_B, z_B, respectively
C_ℓ	rolling-moment coefficient in the aerodynamic axis system (along x_B), $2\bar{L}/\rho_o V^2 S\ell$
C_m	pitching-moment coefficient in the aerodynamic axis system (along y), $2\bar{M}/\rho_o V^2 S\ell$
C_n	side-moment coefficient in the aerodynamic axis system (along z), $2\bar{N}/\rho_o V^2 S\ell$
$\hat{C}_\ell, \hat{C}_m, \hat{C}_n$	rolling-, pitching-, and yawing-moment coefficients in the body-axis system; along x_B, y_B, z_B, respectively
h_o	total enthalpy
$\bar{L}, \bar{M}, \bar{N}$	moment components along the x_B,y,z aerodynamic axes, respectively
ℓ_{cg}	distance from center of gravity to nose of body $(-s_{tip})$
ℓ	reference length (body length, $(s_{final} - s_{tip})$)
p	pressure
p_B, q_B, r_B	components along the x_B, y_B, z_B axes, respectively, of the total angular velocity of the body axes relative to inertial space
q,r	components of the total angular velocity along the y,z aerodynamic axes, respectively, Eq. (2.6)
S	reference area (body base area)

s,τ,θ	computational axes, origin at center of gravity, s positive in the negative x_B direction, τ and θ polar coordinates in planes normal to s, Fig. 1
t	time
u_B,v_B,w_B	components of flight velocity along x_B,y_B,z_B axes, respectively, Fig. 1
u,v,w	components of local flow velocity in the s,τ,θ directions, respectively
V	flight velocity
x_B,y_B,z_B	body-fixed axes, origin at center of gravity, x_B coincident with a longitudinal axis of the body, Fig. 1
x_B,y,z	aerodynamic axes, origin at center of gravity, x_B,z in the plane of the resultant angle of attack, y in the crossflow plane normal to the resultant angle-of-attack plane, Fig. 1
α,β	angle of attack and sideslip in body axes, respectively, Eq. (2.7)
$\hat{\alpha}$	angle-of-attack parameter in body-axis system, w_B/V
$\hat{\beta}$	angle-of-sideslip parameter in body-axis system, v_B/V
γ	dimensionless axial component of flight velocity (along x_B), Fig. 1 and Eq. (2.2)
$\bar{\gamma}$	ratio of specific heats
δ	magnitude of the dimensionless crossflow flight velocity in the aerodynamic axis system, Fig. 1 and Eq. (2.2)
η	transformed circumferential independent coordinate, Eq. (3.6)
μ	transformed radial independent coordinate, Eq. (3.6)
ρ	local flow mass density
ρ_o	atmospheric mass density

σ resultant angle of attack defined by x_B axis and flight velocity vector, Fig. 1

Φ centrifugal potential, Eq. (3.3)

$\dot{\phi}$ coning rate of x_B axis about the flight velocity vector, Fig. 1 (for body in coning motion, total angular velocity of body-fixed axes with respect to inertial space)

ψ angular inclination of the z_B axis from the z axis in the crossflow plane, Fig. 1

$\omega_1, \omega_2, \omega_3$ components of total angular velocity in the s, τ, θ directions, respectively

$(\dot{})$ $\frac{d}{dt}(\ )$

A STUDY OF THE NONLINEAR AERODYNAMICS OF BODIES IN NONPLANAR MOTION*

Lewis Barry Schiff

Ames Research Center

SUMMARY

Concepts from the theory of functionals are used to develop nonlinear formulations of the aerodynamic force and moment systems acting on bodies in large-amplitude, arbitrary motions. The analysis, which proceeds formally once the functional dependence of the aerodynamic reactions upon the motion variables is established, ensures the inclusion, within the resulting formulation, of pertinent aerodynamic terms that normally are excluded in the classical treatment. Applied to the large-amplitude, slowly varying, nonplanar motion of a body, the formulation suggests that the aerodynamic moment can be compounded of the moments acting on the body in four basic motions: steady angle of attack, pitch oscillations, either roll or yaw oscillations, and coning motion. Coning, where the nose of the body describes a circle around the velocity vector, characterizes the nonplanar nature of the general motion.

With the above motivation, a numerical finite-difference technique is developed for computing the inviscid flow field surrounding a body in coning motion in a supersonic stream. Computations carried out for circular cones in coning motion both at low supersonic and hypersonic Mach numbers confirm the adequacy of a linear moment formulation at low angles of attack. At larger angles of attack, however, the forces and moments become nonlinear functions of the angle of attack. Computational results for the

*Presented as Ph.D. Thesis to Stanford University, Stanford, California.

reactions on the circular cone at the higher angles of attack agree well with experimental measurements within the range of variables investigated. This indicates that the initial nonlinear behavior of the aerodynamic forces and moments is governed primarily by the inviscid flow.

1. INTRODUCTION

Linear formulations of the aerodynamic force and moment systems do not properly describe the aerodynamic reactions on flight vehicles in nonplanar motions at large resultant angles of attack. As a result, equations of vehicle motion incorporating linear aerodynamic formulations have often failed to correctly predict the variety of motion such flight vehicles can experience. In the past this has been a problem primarily associated with the flight of slender bodies of revolution. However, the requirements for increased angle-of-attack ranges for proposed high performance aircraft and space shuttle vehicles, as well as those envisioned for STOL aircraft, have tended to make the deficiencies of the linear formulation a problem of more widespread concern in the analysis of vehicle motions.

In the linear formulation, a reference flight condition is chosen, for example, the steady level flight of an airplane, and the deviations of the angular orientation and angular velocities of the body are measured from the reference state. The aerodynamic reactions are expressed in a Taylor series expansion in terms of the deviations and only terms linear in the disturbance quantities are retained. The coefficients of the expansion are called the aerodynamic derivatives and are evaluated at the reference state. When applied to a combined pitching and yawing motion, the linear formulation can be shown to be equivalent to the vector decomposition of the nonplanar motion into two orthogonal planar motions, to the subsequent

treatment of each planar motion as if the other were absent, and to the superposition of the results. This approach has had a great deal of success, particularly for the case of airplane motions where the deviations from the reference state are small. A rather complete treatment of the linear formulation has been presented by Etkin.[1] At large resultant angles of attack, however, it is physically clear that the reactions due to motion in one plane will be influenced by the presence of the other motion, and thus a more precise formulation will be necessary to account for this coupling.

The form that extensions of the linear formulation should take to account for the large angular deviations from the reference state has not yet been settled. Guided by the fact that the static forces acting on a body of revolution lie in the plane of the resultant angle of attack, Nicolaides *et al.*[2] and Ingram,[3] concerned with missile aerodynamics, assumed that the form of the nonlinear generalization for a body of revolution was the same as that of the linear formulation, but that the aerodynamic derivatives were nonlinear functions of the *magnitude* of the resultant angle of attack. If this formulation is applied to the combined pitching and yawing motions of a nonspinning axisymmetric body, it predicts that the aerodynamic damping in the plane of the resultant angle of attack is equal to that acting perpendicularly to the angle-of-attack plane. It can be shown by a comparison of the experimental results of Iyengar[4] with those of Schiff and Tobak[5] that this is untrue for such bodies at large angles of attack. Murphy[6] proposed an extension of the linear formulation which allowed for the possibility of unequal aerodynamic dampings in and normal to the angle-of-attack plane. Unlike the previous one, Murphy's formulation is therefore capable of correctly distinguishing between the

out-of-plane damping and the out-of-plane classical Magnus forces in the case of the nonplanar motion of a spinning body of revolution.

Another approach has been developed by Tobak *et al.*,[7-10] who used concepts from nonlinear functional analysis to develop a formulation of the aerodynamic force and moment system for an arbitrarily shaped body that does not depend on a linearity assumption. This formulation has been shown to be equivalent to that of Murphy for the special case of a body of revolution,[9] and reduces to the form of the linear formulation for small resultant angles of attack. The formulation suggests that the aerodynamic reactions on a body in an arbitrary nonplanar motion can be compounded of the forces and moments acting on the body in four characteristic motions, three of which are well known. The fourth, coning motion, in which the nose of the body describes a circle around the velocity vector, is seen to have particular significance since the nonlinear behavior, with increasing angle of attack, of the contribution to the total force and moment due to coning motion cannot be evaluated from the contributions due to any planar motions. Experimental evaluations[5,8] of the contribution due to the coning of a body of revolution have confirmed this and have shown this contribution to be a potential cause of circular limit motions at large resultant angles of attack. In addition, it is anticipated that the contribution due to coning motion will be important in correctly describing the pre- and post-stall behavior of aircraft-like bodies at large angles of attack.

The objectives of the present work are twofold. The first is to review and unify the development of the nonlinear formulation proposed by Tobak *et al.* and to remove from this analysis an unnecessary assumption of constant flight speed. The second, and more important, objective is to present a numerical method for computing the flow field surrounding a body

in coning motion in a supersonic stream. A finite-difference scheme of MacCormack,[11] developed as a shock-capturing technique for computing complex, steady, three-dimensional, inviscid flow fields by Kutler and Lomax,[12] is extended to the case of coning motion. The capabilities and limitations of the method are described. Results of computations for slender conical bodies in coning motion at various supersonic Mach numbers are presented and are compared with experimental results and with the results of other analytical and numerical methods, where applicable. The results will be seen to exhibit significant nonlinear behavior with increasing resultant angle of attack, and the significance of the nonlinearities will be discussed.

The author wishes to acknowledge and thank Professor Samuel McIntosh, Jr., and Professor Holt Ashley for their advice and encouragement during the course of this work. Grateful acknowledgment is also given to Murray Tobak of the NASA Ames Research Center for his valuable advice and helpful consultation, and to Susan Schiff for her encouragement and for her help in preparing the manuscript.

Finally, acknowledgment is given to the National Aeronautics and Space Administration for support of the research and of the author's graduate study through the Honors Cooperative Program with Stanford University.

2. NONLINEAR FORMULATION - REVIEW AND EXTENSION

In a series of papers,[7-10] concepts from the theory of functionals were used to develop a nonlinear formulation of the aerodynamic force and moment system acting on a body performing motions of interest, the first being the planar motion of an airplane at large angle of attack.[7] The analysis was extended to the large-amplitude, nonplanar angular motions of a body of revolution whose mass center traversed a straight-line path,[8] and showed that the total moment could be compounded of the contributions from four simple motions. Further extensions of the analysis to the free flight of a body of revolution[9] and of an arbitrarily shaped body[10] showed that even in these more general cases the total moment still could be determined from the contributions from the same four simple motions. The resulting formulation allows the angular deviations of the body to be large, but is valid only for the low angular rates typical of aircraft motions. Unfortunately, a uniform notation was not employed throughout the series, while the assumptions of the analysis, covered in detail for the planar case, were abbreviated in the later works. Additionally, it was unnecessarily assumed that the flight speed remained constant over the course of the motion considered. In this chapter the development of the nonlinear moment system is reviewed for the large-amplitude planar motion of an arbitrary body whose flight speed varies, and it is indicated how the formulation can be extended to more accurately represent motions of higher frequencies. The formulation is then developed for the most general case, that of an arbitrarily shaped body in free flight, again removing the restriction of constant flight speed. Finally, the resulting formulation is specialized to the previously reported cases.

2.1 Coordinate Systems

Three axis systems having a common origin at the body's mass center, and a common axis x_B aligned with a longitudinal axis of the body, will be used to describe the motion in all cases considered. Some latitude exists in the choice of the longitudinal axis, and this freedom can be used to simplify the description of a particular motion. For example, when describing the motions of an airplane-like body, the x_B axis is usually chosen to be initially coincident with the direction of steady flight. Alternatively, when describing the flight of a body of revolution, the x_B axis is most often, but not necessarily, chosen as the axis of axial symmetry.

Axes x_B, y_B, z_B are fixed to the moving body (Fig. 1). The components of the flight velocity vector of magnitude V, resolved along the x_B, y_B, z_B body-fixed axes, are u_B, v_B, w_B, respectively. Thus

$$V = \sqrt{u_B^2 + v_B^2 + w_B^2} \tag{2.1}$$

The resultant angle of attack σ is defined by the flight velocity vector and the x_B axis. The plane formed by the y_B, z_B axes is the crossflow plane, illustrated in Fig. 1(a). The projection of a unit vector in the flight velocity direction onto the crossflow plane is a vector with magnitude δ, and will be called the dimensionless crossflow velocity vector. Reference to Fig. 1(b) gives

$$\delta = \sqrt{\left(\frac{v_B}{V}\right)^2 + \left(\frac{w_B}{V}\right)^2} = \sin \sigma \tag{2.2a}$$

$$\gamma = \frac{u_B}{V} = \cos \sigma \tag{2.2b}$$

$$\varepsilon = \frac{\delta}{\gamma} = \tan \sigma \tag{2.2c}$$

The components of the angular velocity vector of the body relative to inertial space, resolved along the x_B, y_B, z_B body axes, are p_B, q_B, r_B, respectively.

A second axis system, x_B, $\tilde{y}$, $\tilde{z}$, is chosen to be nonrolling with respect to inertial space. Specifically, the component of the angular velocity vector of the x_B, $\tilde{y}$, $\tilde{z}$ axes measured with respect to inertial space, resolved along the x_B axis, is zero, while the components resolved along the $\tilde{y}$, $\tilde{z}$ axes are $\tilde{q}$, $\tilde{r}$, respectively. The nonrolling axis system has been used extensively in the field of missile aerodynamics, since its use, together with the assumption of small angular deviations, leads to closed-form solutions of the equation of vehicle motion. The angle $\tilde{\phi}$ through which the body axes have rolled at any time t can be defined relative to the nonrolling axis system as

$$\tilde{\phi} = \int_0^t p_B \, d\tau \tag{2.3}$$

The angular inclination λ of the crossflow velocity vector δ is measured relative to the nonrolling axis system, while ψ is the angular inclination of the body axes from the crossflow velocity vector. With the aid of Fig. 1(a), the body roll rate is seen to be the sum

$$p_B = \dot{\lambda} + \dot{\psi} \tag{2.4}$$

The components of the angular velocity of the body relative to inertial space resolved in the nonrolling axis system, p_B, $\tilde{q}$, $\tilde{r}$, are related to those resolved in the body axis system, p_B, q_B, r_B, through

$$\tilde{q} + i\tilde{r} = e^{i\tilde{\phi}}(q_B + ir_B) \tag{2.5}$$

Finally, axes x_B, y, z will be called the aerodynamic axes. Axis z lies in the crossflow plane and is coincident with the crossflow velocity vector; axis y lies in the crossflow plane normal to the direction of δ. The components of the angular velocity of the body resolved in the aerodynamic axis system, p_B, q, r, are related to those resolved in the body axes through

$$q + ir = e^{i\psi}(q_B + ir_B) \tag{2.6}$$

In accordance with Ref. 10, w_B/V will be called the angle-of-attack parameter $\hat{\alpha}$, and v_B/V will be called the angle-of-sideslip parameter $\hat{\beta}$. They are related to the standard NASA definitions of angle of attack α and angle of sideslip β through

$$\tan \alpha = \frac{w_B}{u_B} = \frac{\hat{\alpha}}{\gamma} \tag{2.7a}$$

$$\sin \beta = \frac{v_B}{V} = \hat{\beta} \tag{2.7b}$$

and to δ and ψ through

$$\hat{\alpha} + i\hat{\beta} = \delta e^{i\psi} \tag{2.8}$$

The components of the aerodynamic force coefficient resolved along the x_B, y_B, z_B body axes are $\hat{C}_X$, $\hat{C}_Y$, $\hat{C}_Z$, respectively, while the corresponding components of the aerodynamic moment coefficient (acting about the mass center) are $\hat{C}_\ell$, $\hat{C}_m$, $\hat{C}_n$, respectively. Analogously, the components of the force and moment coefficients resolved along the aerodynamic axes x_B, y, z are C_X, C_Y, C_Z and C_ℓ, C_m, C_n, respectively. The components of the aerodynamic moment coefficient resolved in the aerodynamic axis system are related to those resolved in the body-fixed axes through

$$C_\ell = \hat{C}_\ell \tag{2.9a}$$

$$C_m + iC_n = e^{i\psi}(\hat{C}_m + i\hat{C}_n) \tag{2.9b}$$

The corresponding relations between the components of the aerodynamic force coefficient are obtained by replacing ℓ, m, n by X, Y, Z, respectively, in Eq. (2.9).

To completely describe the state of a six-degree-of-freedom free-flight motion, it is necessary to specify the velocity and angular velocity vectors of the body. These may be expressed in terms of their scalar components resolved in the body-fixed axes u_B, v_B, w_B, p_B, q_B, r_B, or equivalently by $\hat{\alpha}$, $\hat{\beta}$, V, p_B, q_B, r_B. Analogously, in the aerodynamic axis system, the motion is specified by the scalar variables δ, ψ, V, p_B, q, r, or by δ, ψ, V, $\dot{\lambda}$, q, r since p_B is related to $\dot{\lambda}$ and $\dot{\psi}$ through

Eq. (2.4). In those motions where the mass center traverses a straight-line path (i.e., with no lateral plunging), it is easy to show that, in the aerodynamic axes,

$$q = \dot{\sigma} = \frac{1}{\gamma}\dot{\delta} \tag{2.10a}$$

$$r = \delta\dot{\phi} \tag{2.10b}$$

$$\dot{\lambda} = \gamma\dot{\phi} \tag{2.10c}$$

where $\dot{\phi}$ is the coning rate of the resultant angle-of-attack plane around the velocity vector. When the plunging of the mass center is eliminated, two of the motion variables can be expressed in terms of the remaining four. In the aerodynamic axes, a nonplunging motion can thus be described by the variables δ, ψ, V, $\dot{\phi}$ since knowledge of δ and ψ implies knowledge of $\dot{\delta}$ and $\dot{\psi}$. The relations between variables in the body-fixed axes for the case of zero plunging, corresponding to Eq. (2.10), are

$$q_B = \frac{1}{\gamma}\left(\dot{\hat{\alpha}} + \hat{\beta}p_B\right) \tag{2.11a}$$

$$r_B = -\frac{1}{\gamma}\left(\dot{\hat{\beta}} - \hat{\alpha}p_B\right) \tag{2.11b}$$

$$p_B = \gamma\dot{\phi} + \dot{\psi} \tag{2.11c}$$

Thus it can be shown that, in the body-fixed axes, a nonplunging motion can be described by the variables $\hat{\alpha}$, $\hat{\beta}$, V, $\dot{\phi}$.

When, in addition to eliminating the plunging of the mass center, the angle of attack σ, the bank angle ψ, the coning rate, and the flight speed are all held fixed, the nose of the vehicle describes a circle around the velocity vector. This motion (σ = const, ψ = const, V = const, $\dot{\phi}$ = const) will be called steady coning motion. In the case of coning motion, one sees, with the aid of Eq. (2.11), that

$$p_B = \gamma\dot{\phi} \tag{2.12a}$$

$$q_B = \hat{\beta}\dot{\phi} \tag{2.12b}$$

$$r_B = \hat{\alpha}\dot{\phi} \tag{2.12c}$$

2.2 Development for Planar Motion

To illustrate the ideas behind the development of a nonlinear aerodynamic force and moment formulation, we consider, for simplicity, the large-amplitude planar oscillations of an aircraft as shown in Fig. 2. Assume that prior to time zero the aircraft is in steady level flight. At time zero it begins a longitudinal planar motion such that u_B and w_B, the components of the flight velocity vector resolved along the x_B, z_B body-fixed axes, respectively, and the angular velocity of the aircraft, q_B, all vary, while the wings remain level. Thus v_B, the component of the flight velocity resolved along the y_B axis, and the angular velocity components p_B and r_B all remain zero throughout the maneuver. The altitude excursions of the aircraft are assumed to be small enough for the atmospheric temperature and density to be considered constant. Further, the variation in the total flight speed is assumed to be small enough for the effect of Reynolds number variation on the aerodynamic reactions to be negligible. Under these conditions the aerodynamic force and moment acting on the body at time t after the start of the motion are dependent solely on the velocity components u_B and w_B, on the angular velocity q_B, and on all values taken by these variables over the time interval from zero to t.

2.2.1 Concept of a Functional

The fact that the aerodynamic reactions on the body at time t are dependent not only on the instantaneous values of the motion variables,

but also on the past history of the motion, can be expressed mathematically by introducing the concept of a functional.[13] Focussing specifically on the pitching-moment coefficient (the development for the other force and moment components is analogous), one designates the coefficient $\hat{C}_m(t)$ as a *functional* of u_B, w_B, q_B, or alternately as a functional of $\hat{\alpha}$, V, q_B by the use of the square bracket notation introduced by Volterra:

$$\hat{C}_m(t) = E[u_B(\xi), w_B(\xi), q_B(\xi)] = E'[\hat{\alpha}(\xi), V(\xi), q_B(\xi)] \qquad (2.13)$$

where ξ is a variable in time running from zero to t. The alternate designation is possible since in the case of planar motion, where $\hat{\beta}$, p_B, r_B are all zero, $\hat{\alpha}$ and V are related to u_B and w_B through Eqs. (2.1) and (2.7).

In brief, just as an ordinary function $f(x)$ assigns a number to each x for which it is defined, a functional $G[y(\xi)]$ assigns a number to each function $y(\xi)$ of the set of functions (all of which are defined in some interval $a \leq \xi \leq b$) for which the functional is defined. Thus Eq. (2.13) may be interpreted as follows: Given any triad of functions $\hat{\alpha}(\xi)$, $V(\xi)$, $q_B(\xi)$ out of the collection of all such triads defined in the interval $0 \leq \xi \leq t$, the functional E' assigns a number to $\hat{C}_m(t)$.

2.2.2 Nonlinear Indicial Response

Following Ref. 7, one defines the nonlinear indicial pitching-moment response as illustrated in Fig. 3. As shown for the case of a step change in V/V_R (where V_R is a constant reference speed), two motions are considered. The first begins at time zero, and at time τ the motion is constrained so that the motion variables $\hat{\alpha}(\xi)$, $V(\xi)$, and $q_B(\xi)$ are held constant thereafter. The second motion differs only in the step imposed at time τ. The difference between the pitching-moment coefficients

measured at time t for each of the two motions is divided by the magnitude of the step. The limit of the ratio, as the step size approaches zero, is defined as the indicial pitching-moment response at the time t per unit step in V/V_R at time τ. The indicial responses to step changes in $\hat{\alpha}$ and q_B are defined analogously. In functional notation these are

$$\lim_{\Delta(V/V_R)\to 0} \frac{\Delta \hat{C}_m(t)}{\Delta(V/V_R)} = \hat{C}_{m_V}[\hat{\alpha}(\xi), V(\xi), q_B(\xi); t, \tau] \tag{2.14a}$$

$$\lim_{\Delta\hat{\alpha}\to 0} \frac{\Delta C_m(t)}{\Delta\hat{\alpha}} = \hat{C}_{m_{\hat{\alpha}}}[\hat{\alpha}(\xi), V(\xi), q_B(\xi); t, \tau] \tag{2.14b}$$

$$\lim_{\Delta(q_B\ell/V_R)\to 0} \frac{\Delta C_m(t)}{\Delta(q_B\ell/V_R)} = \hat{C}_{m_{q_B}}[\hat{\alpha}(\xi), V(\xi), q_B(\xi); t, \tau] \tag{2.14c}$$

As indicated by the notation, the indicial response is dependent not only on the levels $\hat{\alpha}(\tau)$, $V(\tau)$, and $q_B(\tau)$ at which the steps occur, but may depend on all values taken by them over the time interval zero to τ. Thus, in general, the indicial responses may themselves be functionals.

Breaking the time histories of the motion variables $\hat{\alpha}$, V, and q_B into a series of step changes and summing the incremental responses to each of the steps over the interval from zero to t gives an exact integral form for $\hat{C}_m(t)$:

$$\begin{aligned}\hat{C}_m(t) = \hat{C}_m(0) &+ \int_0^t \hat{C}_{m_{\hat{\alpha}}}[\hat{\alpha}(\xi), V(\xi), q_B(\xi); t, \tau] \frac{d}{d\tau}(\hat{\alpha})\, d\tau \\ &+ \int_0^t \hat{C}_{m_V}[\hat{\alpha}(\xi), V(\xi), q_B(\xi); t, \tau] \frac{d}{d\tau}(V/V_R)\, d\tau \\ &+ \int_0^t \hat{C}_{m_{q_B}}[\hat{\alpha}(\xi), V(\xi), q_B(\xi); t, \tau] \frac{d}{d\tau}(q_B\ell/V_R)\, d\tau\end{aligned} \tag{2.15}$$

2.2.3 Approximate Formulation for Slowly Varying Motions

While exact in principle, Eq. (2.15) cannot generally be evaluated since the functionals appearing within the integrals may depend on the entire past history of the motion. It is desired to develop an approximate, more easily evaluated form of the expression in which the functionals are replaced by ordinary functions. To do so, it is first seen from physical considerations that the indicial response to a step at time τ is not equally affected by all past events, but is most strongly influenced by events of the most recent past. This is most easily illustrated for supersonic flight, where the flow field around the aircraft at the time τ, and thus the subsequent indicial response, can only be influenced by events that have occurred during the time interval $\tau - t_a \leq \xi \leq \tau$. The characteristic time t_a is approximately the maximum time required for a fluid element to travel from the bow shock wave to the tail shock. The indicial response to a step at time τ is unaffected by events that have occurred prior to $\tau - t_a$. In subsonic flight the vorticity shed by the aircraft will influence the local flow field for all later times, but the magnitude of the influence decreases as the vorticity is convected far downstream. In this case t_a is the time required for the shed vorticity to have negligible further effect on the flow field. Additional discussion concerning the diminishing dependence on the past can be found in Ref. 7.

The periods of oscillatory aircraft motions are typically large compared to the characteristic time t_a. For these slowly varying motions, the simplest way of accounting for the dependence of the indicial response on the past is to assume that the response is dependent only on the levels $\hat{\alpha}(\tau)$, $V(\tau)$, and $q_B(\tau)$ at which the steps occur. As shown in Fig. 4 for a step in $\hat{\alpha}$ at τ, this assumes that the response for motion B in which

$\hat{\alpha}$, V, and q_B are held fixed over the time interval $\tau - t_a < \xi < \tau$ which can influence the response is a good approximation of the response to the response for the arbitrary motion A. Under this assumption the response is no longer a functional, but is a *function* of the parameters $\hat{\alpha}(\tau)$, $V(\tau)$, and $q_B(\tau)$ and of the variables t and τ. In addition, with the motion held fixed prior to the step, the response is independent of the time at which the step is made and is seen to be a function only of $t-\tau$ rather than of t and τ separately. This is expressed in functional notation as

$$\hat{C}_{m_{\hat{\alpha}}}[\hat{\alpha}(\xi),V(\xi),q_B(\xi);t,\tau] \approx \hat{C}_{m_{\hat{\alpha}}}[\hat{\alpha}(\tau),V(\tau),q_B(\tau);t,\tau]$$

$$= \hat{C}_{m_{\hat{\alpha}}}(\hat{\alpha}(\tau),V(\tau),q_B(\tau);t-\tau) \qquad (2.16)$$

Under this assumption, the desired approximate form of Eq. (2.15) is

$$\hat{C}_m(t) = \hat{C}_m(0) + \int_o^t \hat{C}_{m_{\hat{\alpha}}}(\hat{\alpha}(\tau),V(\tau),q_B(\tau);t-\tau)\,\frac{d}{d\tau}(\hat{\alpha})d\tau$$

$$+ \int_o^t \hat{C}_{m_V}(\hat{\alpha}(\tau),V(\tau),q_B(\tau);t-\tau)\,\frac{d}{d\tau}(V/V_R)d\tau$$

$$+ \int_o^t \hat{C}_{m_{q_B}}(\hat{\alpha}(\tau),V(\tau),q_B(\tau);t-\tau)\,\frac{d}{d\tau}(q_B\ell/V_R)d\tau \qquad (2.17)$$

When the deficiency functions (which vanish for $t-\tau > t_a$) are introduced and defined as

$$F(\hat{\alpha}(\tau),V(\tau),q_B(\tau);t-\tau) = \hat{C}_{m_{\hat{\alpha}}}(\hat{\alpha}(\tau),V(\tau),q_B(\tau);\infty) - \hat{C}_{m_{\hat{\alpha}}}(\hat{\alpha}(\tau),V(\tau),q_B(\tau);t-\tau) \qquad (2.18a)$$

$$G(\hat{\alpha}(\tau),V(\tau),q_B(\tau);t-\tau) = \hat{C}_{m_V}(\hat{\alpha}(\tau),V(\tau),q_B(\tau);\infty) - \hat{C}_{m_Y}(\hat{\alpha}(\tau),V(\tau),q_B(\tau);t-\tau) \qquad (2.18b)$$

$$H(\hat{\alpha}(\tau),V(\tau),q_B(\tau);t-\tau) = \hat{C}_{m_{q_B}}(\hat{\alpha}(\tau),V(\tau),q_B(\tau);\infty) - \hat{C}_{m_{q_B}}(\hat{\alpha}(\tau),V(\tau),q_B(\tau);t-\tau) \qquad (2.18c)$$

where $\hat{C}_{m_{\hat{\alpha}}}(\hat{\alpha}(\tau),V(\tau),q_B(\tau);\infty)$ is the steady-state value of the indicial response, Eq. (2.17) can be expressed in the alternate form:

$$\hat{C}_m(t) = \hat{C}_m(\infty;\hat{\alpha}(t),V(t),q_B(t)) - \int_o^t F(\hat{\alpha}(\tau),V(\tau),q_B(\tau);t-\tau)\,\frac{d}{d\tau}(\hat{\alpha})d\tau$$

$$- \int_o^t G(\hat{\alpha}(\tau),V(\tau),q_B(\tau);t-\tau)\,\frac{d}{d\tau}(V/V_R)d\tau$$

$$- \int_o^t H(\hat{\alpha}(\tau),V(\tau),q_B(\tau);t-\tau)\,\frac{d}{d\tau}(q_B\ell/V_R)d\tau \qquad (2.19)$$

since the terms involving the steady-state values form a perfect differential. The term $\hat{C}_m(\infty;\hat{\alpha}(t),V(t),q_B(t))$ is the steady pitching-moment coefficient that would be measured in a steady pullup maneuver in which $\hat{\alpha}$, V, and q_B are held fixed at $\hat{\alpha}(t)$, $V(t)$, and $q_B(t)$, respectively. Equation (2.19) can be further simplified consistent with the assumption of slowly varying motions used to approximate the functional indicial responses. The functions are expanded in a Taylor series about the point $\hat{\alpha} = \hat{\alpha}(t)$, $V = V(t)$, $q_B = 0$, and only first-order frequency terms are retained. The resulting nonlinear formulation is

$$\hat{C}_m(t) = \hat{C}_m(\infty;\hat{\alpha}(t),V(t),0) + \frac{q_B(t)\ell}{V_R}\hat{C}_{m_{q_B}}(\infty;\hat{\alpha}(t),V(t),0)$$

$$+ \frac{\dot{\hat{\alpha}}(t)\ell}{V_R}\hat{C}_{m_{\dot{\hat{\alpha}}}}(\hat{\alpha}(t),V(t),0) + \frac{\dot{V}(t)\ell}{V_R^2}\hat{C}_{m_{\dot{V}}}(\hat{\alpha}(t),V(t),0) \qquad (2.20)$$

where

$$\hat{C}_{m_{\dot{\hat{\alpha}}}} = -\frac{V_R}{\ell}\int_o^t F(\hat{\alpha}(t),V(t),0;\tau)d\tau$$

$$\hat{C}_{m_{\dot{V}}} = -\frac{V_R}{\ell}\int_o^t G(\hat{\alpha}(t),V(t),0;\tau)d\tau$$

Each term in Eq. (2.20) is again identified with a particular motion from which it may be evaluated. The first term is the static pitching coefficient measured with $\hat{\alpha}$ and V held fixed at their instantaneous values, with q_B held fixed at zero. With the reference velocity V_R chosen to be equal to the instantaneous value of the flight velocity $V(t)$, the second term is seen to be the rate of change with q_B, evaluated at $q_B = 0$, of the pitching-moment coefficient that would be measured in a steady vertical pullup with $q_B = \text{const}$, $\hat{\alpha}$ and V held fixed. The third term is the damping coefficient that would be measured for small oscillations in $\hat{\alpha}$ about the instantaneous value $\hat{\alpha}(t) = \text{const}$, with V held fixed at $V(t)$, $q_B = 0$, a plunging oscillation normal to the velocity direction. The last term is the damping coefficient measured for small oscillations in V about the fixed flight speed $V(t)$, with $\hat{\alpha}$ held fixed at $\hat{\alpha}(t)$, $q_B = 0$, i.e., the damping due to lunging oscillations of the mass center along the flight velocity direction. Thus the specification of the moment acting on the aircraft performing an arbitrary planar motion requires knowledge of the moment acting on the body in four characteristic motions.

The number of characteristic motions required can be reduced in those cases where the lateral plunging of the mass center is small. To demonstrate this we rewrite Eq. (2.20) as

$$\hat{C}_m(t) = \hat{C}_m(\infty;\hat{\alpha}(t),V(t),0) + \frac{1}{\gamma}\frac{\dot{\hat{\alpha}}(t)\ell}{V_R}\left\{\hat{C}_{m_{q_B}}(\infty;\hat{\alpha}(t),V(t),0) + \gamma \hat{C}_{m_{\dot{\hat{\alpha}}}}(\hat{\alpha}(t),V(t),0)\right\}$$

$$+ \frac{\dot{V}(t)\ell}{V_R^2}\hat{C}_{m_{\dot{V}}}(\hat{\alpha}(t),V(t),0) + \frac{1}{\gamma}\frac{(\gamma q_B(t) - \dot{\hat{\alpha}}(t))\ell}{V_R} C_{m_{q_B}}(\infty;\hat{\alpha}(t),V(t),0) \tag{2.21}$$

The terms in Eq. (2.21) are identified by comparing them with those obtained for the case of nonplunging motion at constant flight speed. Under these conditions, $\dot{V} = 0$, $q_B = (1/\gamma)\dot{\hat{\alpha}}$, and the last two terms of Eq. (2.21) vanish. With the plunging of the mass center eliminated, changes in $\hat{\alpha}$ correspond to angular motion of the body about the fixed y_B axis. Thus the term $(\hat{C}_{m_{q_B}} + \gamma\hat{C}_{m_{\dot{\hat{\alpha}}}})$ is seen to be the planar pitch damping coefficient that would be measured in a single-degree-of-freedom experiment in which the body performs small angular oscillations about a mean angle of attack, i.e., small oscillations in $\hat{\alpha}$ about $\hat{\alpha} = \text{const}$, with V held fixed and $q_B = (1/\gamma)\dot{\hat{\alpha}}$. In a general motion, the contributions from the last two terms of Eq. (2.21) are not zero. However, for motions in which the plunging is small, and where the flight speed makes only small oscillations about a mean speed, the contributions from these terms can be justifiably neglected since, in equations of vehicle motion, they would appear only as products of (relatively small) damping terms. In such cases the total moment acting on the aircraft is due to the contributions from only two characteristic motions: steady angle of attack and damping-in-pitch. Here $V(t)$ need not appear explicitly within the notation, it being understood that the characteristic motions will be evaluated at a fixed speed equal to the mean value of the flight speed.

2.2.4 Extensions to Describe More General Motions

To obtain the approximate integral aerodynamic formulation, Eq. (2.17), from the exact functional form, Eq. (2.15), the aircraft motions were assumed to be slowly varying. The nonlinear indicial response for these arbitrary large-amplitude motions was assumed to be the same as the response to a motion with fixed past. For flutter motions involving small-amplitude, high-frequency oscillations of the motion variables about

fixed mean values, the assumption of a constant past history is also justified. Here the maximum excursions of the motion variables are small and the motion can be considered to be generated by a series of steps applied not at the instantaneous values but rather at the mean values of the motion variables. The approximate integral form is thus valid for flutter motions, but cannot be simplified as was done in the case of slowly varying motions.

When considering large-amplitude motions of higher frequencies, the simple assumption that the general nonlinear indicial response is the same as the response for fixed past may no longer be adequate. A more precise way to account for the dependence of the indicial response on past events, for the planar motion discussed above, is to assume that the response to a step at time τ is dependent not only on the levels $\hat{\alpha}(\tau)$, $V(\tau)$, and $q_B(\tau)$, but also on their rates of change at the time of the step, $\dot{\hat{\alpha}}(\tau)$, $\dot{V}(\tau)$, and $\dot{q}_B(\tau)$. This is illustrated in Fig. 4 for a step in $\hat{\alpha}$. In motion C, $\hat{\alpha}$, V, and q_B vary linearly in time with rates $\dot{\hat{\alpha}}(\tau)$, $\dot{V}(\tau)$, and $\dot{q}_B(\tau)$ over the time interval $\tau - t_a < \xi < \tau$ during which events may influence the subsequent response. The response to motion C is assumed to be a closer representation of the response to the arbitrary motion A than is the previously discussed response to motion B, whose past history is held fixed. The approximate response is again a function rather than a functional and is dependent on the parameters $\hat{\alpha}(\tau)$, $\dot{\hat{\alpha}}(\tau)$, $V(\tau)$, $\dot{V}(\tau)$, $q_B(\tau)$, and $\dot{q}_B(\tau)$. Since the motion is uniquely specified by these parameters over the interval of influence prior to the step, the response is again dependent on the time variable $t-\tau$ rather than on t and τ separately. In functional notation this is indicated as

$$\hat{C}_{m_{\hat{\alpha}}}[\hat{\alpha}(\xi),V(\xi),q_B(\xi);t,\tau]$$

$$\approx \hat{C}_{m_{\hat{\alpha}}}[\hat{\alpha}(\tau)+\dot{\hat{\alpha}}(\tau)(\xi-\tau),V(\tau)+\dot{V}(\tau)(\xi-\tau),q_B(\tau)+\dot{q}_B(t)(\xi-\tau);t,\tau]$$

$$= \hat{C}_{m_{\hat{\alpha}}}(\hat{\alpha}(\tau),\dot{\hat{\alpha}}(\tau),V(\tau),\dot{V}(\tau),q_B(\tau)\dot{q}_B(\tau);t-\tau) \qquad (2.22)$$

In addition to more accurately describing large-amplitude, high-frequency motions, the expanded approximate indicial response can describe motions involving hysteresis effects, where, for example, the response to a step imposed at a given level of the motion variables may be different, depending on whether the variable was increasing or decreasing prior to the application of the step. The expanded approximate integral form corresponding to Eq. (2.17) is

$$\hat{C}_m(t) = C_m(0) + \int_o^t \hat{C}_{m_{\hat{\alpha}}}(\hat{\alpha}(\tau),\dot{\hat{\alpha}}(\tau),V(\tau),\dot{V}(\tau),q_B(\tau),\dot{q}_B(\tau);t-\tau)\,\frac{d}{d\tau}(\hat{\alpha})d\tau$$

$$+\int_o^t \hat{C}_{m_V}(\hat{\alpha}(\tau),\dot{\hat{\alpha}}(\tau),V(\tau),\dot{V}(\tau),q_B(\tau),\dot{q}_B(\tau);t-\tau)\,\frac{d}{d\tau}(V/V_R)d\tau$$

$$+\int_o^t \hat{C}_{m_{q_B}}(\hat{\alpha}(\tau),\dot{\hat{\alpha}}(\tau),V(\tau),\dot{V}(\tau),q_B(\tau),\dot{q}_B(\tau);t-\tau)\,\frac{d}{d\tau}(q_B\ell/V_R)d\tau \qquad (2.23)$$

which is seen to be identical to the simplified form if the indicial response functions are found to be independent of the rates $\dot{\hat{\alpha}}$, $\dot{V}$, and $\dot{q}_B$.

2.3 Development for General Body in Free Flight

One advantage of using the theory of functionals to develop nonlinear aerodynamic formulations is the ease with which the analysis may be extended to include additional independent variables. Once the functional dependence of the force and moment on the variables is established, the succeeding analysis corresponds formally to that presented for the case of planar motion. We now use this formalism to develop a nonlinear formulation

for a general body in free flight. Under the same restrictions on the altitude and flight speed variations as were imposed on the planar case, the force and moment acting on the body are dependent solely on the velocity and angular velocity history of the motion. The reactions and the motion variables can be expressed in terms of their components resolved in the body-fixed axes or, equivalently, by their components resolved in the aerodynamic axis system. The resulting nonlinear formulations are equivalent, but lead to different sets of characteristic motions from which the total reactions are determined. However, as will be seen, the importance of coning motion is evidenced by the fact that it appears as one of the characteristic motions of the formulations developed in both axis systems.

2.3.1 Body-Fixed Axes

The components of the flight velocity vector resolved in the body-fixed axes, u_B, v_B, w_B, are related to $\hat{\alpha}$, $\hat{\beta}$, V through Eqs. (2.1) and (2.7). Thus the expanded dependence of the pitching-moment coefficient can be specified as a functional of the form

$$\hat{C}_m(t) = E[\hat{\alpha}(\xi),\hat{\beta}(\xi),V(\xi),p_B(\xi),q_B(\xi),r_B(\xi)] \qquad (2.24)$$

The formulation of the nonlinear indicial responses and of the exact and approximate integral forms for $\hat{C}_m(t)$ parallels that of the planar case, Eqs. (2.14), (2.15), and (2.17), respectively. When the integral form is expanded about the point $\hat{\alpha} = \hat{\alpha}(t)$, $\hat{\beta} = \hat{\beta}(t)$, $V = V(t)$, $p_B = q_B = r_B = 0$, and only terms linear in the rates are retained, the resulting nonlinear formulation corresponding to Eq. (2.20) is

$$\hat{C}_m(t) = \hat{C}_m(\infty;\hat{\alpha}(t),\hat{\beta}(t),V(t)) + \frac{p_B(t)\ell}{V_R}\hat{C}_{m_{p_B}}(\infty;\hat{\alpha}(t),\hat{\beta}(t),V(t))$$

$$+ \frac{q_B(t)\ell}{V_R}\hat{C}_{m_{q_B}}(\infty;\hat{\alpha}(t),\hat{\beta}(t),V(t)) + \frac{r_B(t)\ell}{V_R}\hat{C}_{m_{r_B}}(\infty;\hat{\alpha}(t),\hat{\beta}(t),V(t))$$

$$+ \frac{\dot{\hat{\alpha}}(t)\ell}{V_R}\hat{C}_{m_{\dot{\hat{\alpha}}}}(\hat{\alpha}(t),\hat{\beta}(t),V(t)) + \frac{\dot{\hat{\beta}}(t)\ell}{V_R}\hat{C}_{m_{\dot{\hat{\beta}}}}(\hat{\alpha}(t),\hat{\beta}(t),V(t))$$

$$+ \frac{\dot{V}(t)\ell}{V_R^2}\hat{C}_{m_{\dot{V}}}(\hat{\alpha}(t),\hat{\beta}(t),V(t)) \qquad (2.25)$$

where, for brevity, the zeros corresponding to p_B, q_B, r_B have been omitted.

Just as was done in the planar case, the formulation can be further simplified for motions where the plunging of the mass center is small and where the flight speed makes only small oscillations about a mean speed. As before, we rewrite Eq. (2.25) and, guided by Eq. (2.11), neglect terms multiplied by $\gamma q_B - (\dot{\hat{\alpha}} + \hat{\beta}p_B)$, $\gamma r_B + (\dot{\hat{\beta}} - \hat{\alpha}p_B)$, and $\dot{V}$ (their contributions vanish identically in the case of zero plunging and constant flight speed). The reference velocity V_R is taken as the mean flight velocity $V(t)$ and is omitted from the functional notation of Eq. (2.25) for conciseness. The simplified nonlinear formulation is

$$\hat{C}_m(t) = \hat{C}_m(\infty;\hat{\alpha},\hat{\beta}) + \frac{1}{\gamma}\frac{\dot{\hat{\alpha}}\ell}{V}\left(\hat{C}_{m_{q_B}}(\infty;\hat{\alpha},\hat{\beta}) + \gamma\hat{C}_{m_{\dot{\hat{\alpha}}}}(\hat{\alpha},\hat{\beta})\right)$$

$$- \frac{1}{\gamma}\frac{\dot{\hat{\beta}}\ell}{V}\left(\hat{C}_{m_{r_B}}(\infty;\hat{\alpha},\hat{\beta}) - \gamma\hat{C}_{m_{\dot{\hat{\beta}}}}(\hat{\alpha},\hat{\beta})\right) + \frac{p_B\ell}{V}\left(\gamma\hat{C}_{m_{p_B}}(\infty;\hat{\alpha},\hat{\beta})\right.$$

$$\left. + \hat{\beta}\hat{C}_{m_{q_B}}(\infty;\hat{\alpha},\hat{\beta}) + \hat{\alpha}\hat{C}_{m_{r_B}}(\infty;\hat{\alpha},\hat{\beta})\right) \qquad (2.26)$$

Equation (2.26) is identical to Eq. (22) of Tobak and Schiff,[10] derived for the case of constant flight speed. Analogous expressions for the

other moment coefficients $\hat{C}_n$ and $\hat{C}_\ell$, and for the force coefficients $\hat{C}_X$, $\hat{C}_Y$, $\hat{C}_Z$ are obtained by substituting them wherever $\hat{C}_m$ appears in Eq. (2.26).

Each term of Eq. (2.26) is associated with a particular motion from which it may be evaluated. The first two terms are identified by comparing them with those previously obtained for the case of planar motion, where $p_B = 0$, $\hat{\beta} = \text{const} = 0$. The first term is thus the pitching-moment coefficient that would be measured in a steady planar motion with $\hat{\alpha}$, $\hat{\beta}$ (and V) held fixed. The term $(\hat{C}_{m_{q_B}} + \gamma \hat{C}_{m_{\dot{\hat{\alpha}}}})$ is the planar damping-in-pitch coefficient that would be measured for small angular oscillations in $\hat{\alpha}$ about fixed $\hat{\alpha}$, with $\hat{\beta}$ held fixed at $\hat{\beta}(t)$ and $p_B = 0$. Similarly, $(\hat{C}_{m_{r_B}} - \gamma \hat{C}_{m_{\dot{\hat{\beta}}}})$ is the change in the pitching-moment coefficient due to damping-in-yaw motion (small angular oscillations in $\hat{\beta}$ about fixed $\hat{\beta}$, with $\hat{\alpha}$ held fixed, $p_B = 0$). As was pointed out in Ref. 10, the term $(\hat{C}_{m_{r_B}} - \gamma \hat{C}_{m_{\dot{\hat{\beta}}}})$ and the analogous term in $\hat{C}_n(t)$, $(\hat{C}_{n_{q_B}} + \gamma \hat{C}_{n_{\dot{\hat{\alpha}}}})$, are the cross-coupling terms normally excluded in the classical treatment. These terms are missed by attempts to generalize to the nonlinear case from linear formulations based on the principle of superposition.

The last term in Eq. (2.26) is identified by comparing it to the result that would be obtained for the case of steady coning motion ($\hat{\alpha} = \text{const}$, $\hat{\beta} = \text{const}$, $\dot{\phi} = \text{const}$), where, as seen from Eq. (2.12), $p_B = \gamma\dot{\phi}$, $q_B = \hat{\beta}\dot{\phi}$, $r_B = \hat{\alpha}\dot{\phi}$. When these conditions are substituted in Eq. (2.25), the result is

$$\hat{C}_m(t) = \hat{C}_m(\infty;\hat{\alpha},\hat{\beta}) + \frac{\dot{\phi}\ell}{V}\left(\gamma \hat{C}_{m_{p_B}}(\infty;\hat{\alpha},\hat{\beta}) + \hat{\beta}\hat{C}_{m_{q_B}}(\infty;\hat{\alpha},\hat{\beta}) + \hat{\alpha}\hat{C}_{m_{r_B}}(\infty;\hat{\alpha},\hat{\beta})\right) \tag{2.27}$$

The group $(\gamma\hat{C}_{m_{p_B}} + \hat{\beta}\hat{C}_{m_{q_B}} + \hat{\alpha}\hat{C}_{m_{r_B}})$ is thus seen to be the rate of change with $\dot{\phi}$, evaluated at $\dot{\phi} = 0$, of the pitching-moment coefficient measured in steady coning motion, and is designated $\hat{C}_{m_{\dot{\phi}}}(\infty;\hat{\alpha},\hat{\beta})$.

In summary, Eq. (2.26) suggests that for the free flight of a general body with small plunging and near-constant flight speed, the total moment may be compounded of the contributions from four characteristic motions: steady angle of attack and sideslip, planar pitch and yaw oscillations at constant angles of attack and sideslip, and coning at steady angle of attack and sideslip. These motions are illustrated schematically in Fig. 5.

2.3.2 Aerodynamic Axes

As can be seen in section 2.1, the velocity vector of a general motion can be specified in the aerodynamic axes by the scalar variables δ, ψ, V. The angular velocity vector is specified by p_B, q, r or, equivalently, by $\dot{\lambda}$, q, r, since p_B is related to $\dot{\lambda}$ and $\dot{\psi}$ through Eq. (2.4). The pitching-moment coefficient in the aerodynamic axes, $C_m(t)$, thus may be specified as a functional of the form

$$C_m(t) = F[\delta(\xi),\psi(\xi),V(\xi),\dot{\lambda}(\xi),q(\xi),r(\xi)] \tag{2.28}$$

Proceeding formally, one finds that the nonlinear formulation in the aerodynamic axes corresponding to Eq. (2.25) is

$$\begin{aligned} C_m(t) = {} & C_m(\infty;\delta(t),\psi(t),V(t)) + \frac{\dot{\lambda}(t)\ell}{V_R} C_{m_{\dot{\lambda}}}(\infty;\delta(t),\psi(t),V(t)) \\ & + \frac{q(t)\ell}{V_R} C_{m_q}(\infty;\delta(t),\psi(t),V(t)) + \frac{r(t)\ell}{V_R} C_{m_r}(\infty;\delta(t),\psi(t),V(t)) \\ & + \frac{\dot{\delta}(t)\ell}{V_R} C_{m_{\dot{\delta}}}(\delta(t),\psi(t),V(t)) + \frac{\dot{\psi}(t)\ell}{V_R} C_{m_{\dot{\psi}}}(\delta(t),\psi(t),V(t)) \\ & + \frac{\dot{V}(t)\ell}{V_R^2} C_{m_{\dot{V}}}(\delta(t),\psi(t),V(t)) \end{aligned} \tag{2.29}$$

As before, Eq. (2.29) may be simplified in the case of small plunging and near-constant flight speed by rearranging terms and neglecting those terms multiplied by $q-\dot{\sigma}$, $r-\varepsilon\dot{\lambda}$, and $\dot{V}$ (which vanish identically for zero plunging and constant flight speed, e.g., Eq. (2.10)) to obtain

$$C_m(t) = C_m(\infty;\delta,\psi) + \frac{\dot{\sigma}\ell}{V}\left(C_{m_q}(\infty;\delta,\psi) + \gamma C_{m_{\dot{\delta}}}(\delta,\psi)\right) + \frac{\dot{\psi}\ell}{V} C_{m_{\dot{\psi}}}(\delta,\psi)$$

$$+ \frac{1}{\gamma}\frac{\dot{\lambda}\ell}{V}\left(\gamma C_{m_{\dot{\lambda}}}(\infty;\delta,\psi) + \delta C_{m_r}(\infty;\delta,\psi)\right) \qquad (2.30)$$

Analogous expressions hold for the other force and moment coefficients. The characteristic motions from which the terms of Eq. (2.30) are evaluated differ from those in the body-fixed axes. Here the term $(C_{m_q}+\gamma C_{m_{\dot{\delta}}})$ is the planar damping-in-pitch coefficient that would be measured in a nonplunging motion for small oscillations of the resultant angle of attack σ about fixed σ with ψ and V held fixed, $\dot{\lambda} = 0$. This term is designated $C_{m_{\dot{\sigma}}}(\delta,\psi)$. The term $C_{m_{\dot{\psi}}}$ is the change in the pitching-moment coefficient due to damping-in-roll motion (small oscillations in ψ about fixed ψ with σ = const, V = const, $\dot{\lambda} = 0$). When the conditions of steady coning motion ($q = 0$, $r = \delta\dot{\phi}$, $\dot{\lambda} = \gamma\dot{\phi}$) are substituted in Eq. (2.29), it can be shown that the term $(\delta C_{m_r}+\gamma C_{m_{\dot{\lambda}}})$ is the rate of change with coning rate $\dot{\phi}$, evaluated at $\dot{\phi} = 0$, of the pitching-moment coefficient that would be measured in coning motion, and this term is designated $C_{m_{\dot{\phi}}}(\infty;\delta,\psi)$. Thus

$$C_{m_{\dot{\sigma}}}(\delta,\psi) = C_{m_q}(\infty;\delta,\psi) + \gamma C_{m_{\dot{\delta}}}(\delta,\psi) \qquad (2.31a)$$

$$C_{m_{\dot{\phi}}}(\infty;\delta,\psi) = \gamma C_{m_{\dot{\lambda}}}(\infty;\delta,\psi) + \delta C_{m_r}(\infty;\delta,\psi) \qquad (2.31b)$$

In the aerodynamic axis system, the characteristic motions are: steady resultant angle of attack and bank angle ψ, pitch and roll oscillations

at steady angles of attack and bank, and coning at steady resultant angle of attack with fixed bank angle. These motions are illustrated schematically in Fig. 6.

2.3.3 Correspondence Between Axis Systems

The formulation developed in the body-fixed axis system, Eq. (2.25), is related to the one developed in the aerodynamic axes, Eq. (2.29), through Eq. (2.9). These relations, presented in detail for convenient reference in appendix A, can be used to show the following significant equivalence:

$$C_{n_{\dot{\phi}}}(\infty;\delta,\psi) - \gamma C_{n_{\dot{\psi}}}(\delta,\psi) + \delta C_{m_{\sigma}}(\delta,\psi) = \delta\{(\hat{C}_{m_{q_B}}(\infty;\hat{\alpha},\hat{\beta}) + \gamma\hat{C}_{m_{\dot{\hat{\alpha}}}}(\hat{\alpha},\hat{\beta})) + (\hat{C}_{n_{r_B}}(\infty;\hat{\alpha},\hat{\beta}) - \gamma C_{n_{\dot{\hat{\beta}}}}(\hat{\alpha},\hat{\beta}))\} \tag{2.32}$$

The term $C_{n_{\dot{\phi}}}$ is the rate of change with $\dot{\phi}\ell/V$, evaluated at $\dot{\phi} = 0$, of the side-moment coefficient C_n that would be measured in steady coning motion, while the term $C_{n_{\dot{\psi}}}$ is the change in the side-moment coefficient due to damping-in-roll motion. Thus a determination of $C_{n_{\dot{\phi}}} - \gamma C_{n_{\dot{\psi}}}$ would be equivalent to a determination of the three planar damping coefficients. The identity is shown schematically in Fig. 7. There are two cases of special interest that lead to simplification of Eq. (2.32): when $\psi = 0$ ($\hat{\alpha} = \delta$, $\hat{\beta} = 0$), and when $\psi = \pi/2$ ($\hat{\alpha} = 0$, $\hat{\beta} = \delta$). In the first case, Eq. (2.32) becomes

$$C_{n_{\dot{\phi}}}(\infty;\delta,0) - \gamma C_{n_{\dot{\psi}}}(\delta,0) = \delta\{\hat{C}_{n_{r_B}}(\infty;\hat{\alpha},0) - \gamma\hat{C}_{n_{\dot{\hat{\beta}}}}(\hat{\alpha},0)\} \tag{2.33a}$$

while, in the second case, we obtain

$$C_{n_{\dot{\phi}}}(\infty;\delta,\pi/2) - \gamma C_{n_{\dot{\psi}}}(\delta,\pi/2) = \delta[\hat{C}_{m_{q_B}}(\infty;0,\hat{\beta}) + \gamma\hat{C}_{m_{\dot{\hat{\alpha}}}}(0,\hat{\beta})\} \tag{2.33b}$$

A determination of $(C_{n_{\dot{\phi}}}-\gamma C_{n_{\dot{\psi}}})$ as the resultant angle of attack becomes small ($\delta \to 0$) for these cases is seen to be equivalent to a determination of the classical (linear formulation) damping-in-yaw and damping-in-pitch coefficients, respectively.

Another important equivalence between terms of the formulations in the two-axis systems is

$$C_{m_\sigma}(\delta,\psi) = \{\hat{C}_{m_{q_B}}(\infty;\hat{\alpha},\hat{\beta})+\gamma\hat{C}_{m_{\dot{\hat{\alpha}}}}(\hat{\alpha},\hat{\beta})\}\cos^2\psi+\{\hat{C}_{n_{r_B}}(\infty;\hat{\alpha},\hat{\beta})-\gamma\hat{C}_{n_{\dot{\hat{\beta}}}}(\hat{\alpha},\hat{\beta})\}\sin^2\psi$$
$$-[\{\hat{C}_{n_{q_B}}(\infty;\hat{\alpha},\hat{\beta})+\gamma\hat{C}_{n_{\dot{\hat{\alpha}}}}(\hat{\alpha},\hat{\beta})\}+\{\hat{C}_{m_{r_B}}(\infty;\hat{\alpha},\hat{\beta})-\gamma\hat{C}_{m_{\dot{\hat{\beta}}}}(\hat{\alpha},\hat{\beta})\}]\sin\psi\cos\psi \tag{2.34}$$

which in the special cases of $\psi = 0$ and $\psi = \pi/2$ becomes, respectively,

$$C_{m_\sigma}(\delta,0) = \{\hat{C}_{m_{q_B}}(\infty;\hat{\alpha},0) + \gamma\hat{C}_{m_{\dot{\hat{\alpha}}}}(\hat{\alpha},0)\} \tag{2.35a}$$

$$C_{m_\sigma}(\delta,\pi/2) = \{\hat{C}_{n_{r_B}}(\infty;0,\hat{\beta}) - \gamma\hat{C}_{n_{\dot{\hat{\beta}}}}(0,\hat{\beta})\} \tag{2.35b}$$

Here, in contrast to Eq. (2.33), the determination of C_{m_σ} as the angle of attack becomes small is equivalent to the determination of the linear formulation damping-in-pitch and damping-in-yaw coefficients, respectively.

2.3.4 Bodies of Revolution

When the body has axial symmetry about the x_B axis, the value of ψ is arbitrary and will be chosen equal to $\pi/2$ for convenience. Also, in the case of a body of revolution, the damping-in-roll motion used to evaluate $C_{m_{\dot{\psi}}}$ and $C_{n_{\dot{\psi}}}$ can be replaced by the classical Magnus experiment where the body is placed at angle of attack and spun about the x_B axis (σ = const, $\dot{\psi}$ = const, $\dot{\lambda} = 0$). Here the term $C_{n_{\dot{\psi}}}$ is the rate of change with $\dot{\psi}\ell/V$, evaluated at $\dot{\psi} = 0$, of the side-moment coefficient that would be measured in the Magnus experiment. The only mechanisms for affecting the moments on the body in this experiment is the small

asymmetry of the flow field produced by viscous shear at the body surface. Thus numerous experimental investigations (e.g., Regan and Horanoff,[14] Platou and Sternberg,[15] Platou[16]) and a viscous theory (Sedney[17]) have shown that, when measured in this manner, the term $C_{n_{\dot{\psi}}}$ and the corresponding side force term, $C_{Y_{\dot{\psi}}}$, for a body of revolution are extremely small. Additionally, Schiff and Tobak[5] have demonstrated experimentally that, at least for a 10° half-angle cone, the term $C_{n_{\dot{\psi}}}$ can be neglected in comparison with $C_{n_{\dot{\phi}}}$, the change in the side moment due to steady coning motion. In this case the determination of $C_{n_{\dot{\phi}}}$ alone, for small resultant angle of attack, is seen from Eq. (2.33b) to be equivalent to the determination of the linear damping-in-pitch coefficient.

The form that the nonlinear formulation takes when applied to the nonplunging flight of a body of revolution illustrates an erroneous assumption that has frequently been made when attempting to generalize to the nonlinear case from linear formulations based on the principle of superposition. Here the terms $C_{m_{\dot{\phi}}}$, $C_{m_{\dot{\psi}}}$, $C_{n_{\dot{\sigma}}}$, and the static side-moment term $C_n(\infty;\delta,\psi)$ which appear in Eq. (2.30) and in the analogous expression for $C_n(t)$ can normally be neglected on the basis of symmetry arguments. With ψ chosen as $\pi/2$, the resulting formulation can, with the aid of Eqs. (2.10c) and (2.11c), be written as

$$C_m(t) = C_m(\infty;\delta,\pi/2) + \frac{\dot{\sigma}\ell}{V} C_{m_{\dot{\sigma}}}(\delta,\pi/2) \tag{2.36a}$$

$$C_n(t) = \frac{\dot{\phi}\ell}{V}\{C_{n_{\dot{\phi}}}(\infty;\delta,\psi) - \gamma C_{n_{\dot{\psi}}}(\delta,\psi)\} + \frac{p_B\ell}{V} C_{n_{\dot{\psi}}}(\delta,\pi/2) \tag{2.36b}$$

Although, as discussed above, $C_{n_{\dot{\psi}}}$ could be neglected in comparison with $C_{n_{\dot{\phi}}}$ in the first term of Eq. (2.36b), we shall retain it in the notation to avoid confusion. When Eqs. (2.33b) and (2.35b) are substituted in Eq. (2.36), we obtain

$$C_m(t) = C_m(\infty;\delta,\pi/2) + \frac{\dot{\sigma}\ell}{V}\{\hat{C}_{n_{r_B}}(\infty;0,\hat{\beta}) - \gamma\hat{C}_{n_{\hat{\beta}}}(0,\hat{\beta})\} \qquad (2.37a)$$

$$C_n(t) = \frac{\dot{\phi}\ell}{V}\delta\{\hat{C}_{m_{q_B}}(\infty;0,\hat{\beta}) + \gamma\hat{C}_{m_{\hat{\alpha}}}(0,\hat{\beta})\} + \frac{p_B\ell}{V}C_{n_\psi}(\delta,\pi/2) \qquad (2.37b)$$

When the linear formulation is valid (i.e., as $\hat{\alpha} \to 0$, $\hat{\beta} \to 0$), the axial symmetry of the body dictates that

$$\{\hat{C}_{m_{q_B}}(\infty;0,\hat{\beta}\to 0) + \gamma\hat{C}_{m_{\hat{\alpha}}}(0,\hat{\beta}\to 0)\} = \{\hat{C}_{n_{r_B}}(\infty;0,\hat{\beta}\to 0) - \gamma\hat{C}_{n_{\hat{\beta}}}(0,\hat{\beta}\to 0)\} \qquad (2.38)$$

This leads to the linear formulation result that

$$C_{m_\sigma} = \frac{C_{n_\phi} - \gamma C_{n_\psi}}{\delta} = \hat{C}_{m_{q_B}}(\infty) + \gamma\hat{C}_{m_{\hat{\alpha}}} \qquad (2.39)$$

where $\hat{C}_{m_{q_B}}(\infty) + \gamma\hat{C}_{m_{\hat{\alpha}}}$ denotes the planar pitch-damping coefficient evaluated at $\hat{\alpha} = 0$, $\hat{\beta} = 0$. As the resultant angle of attack becomes large, relation (2.38) is no longer valid. The damping measured for pitch oscillations at large sideslip angle (and $\hat{\alpha} = 0$) is not necessarily equal to the damping measured for yaw oscillations at the same angle of sideslip. Thus, for large δ, C_{m_σ} need not be equal to $(C_{n_\phi} - \gamma C_{n_\psi})/\delta$ and, in fact, neither need equal the linear formulation value of the pitch-damping coefficient. That this inequality does actually occur is demonstrated in Fig. 8, which compares the values of δC_{m_σ} measured by Iyengar[4] for a 10° half-angle cone at Mach number = 2 to the values of C_{n_ϕ} measured in steady coning motion at the same conditions, where $C_{n_\psi} << C_{n_\phi}$ (Ref. 5). Also shown is the theoretical value of $\delta\{\hat{C}_{m_{q_B}}(\infty) + \gamma\hat{C}_{m_{\hat{\alpha}}}\}$ (Tobak and Wehrend[18]). At the low values of δ the three values are in good agreement. However, as δ increases the equality breaks down. Consequently, extensions to the linear formulation that retain the equality between C_{m_σ} and the term $(C_{n_\phi} - \gamma C_{n_\psi})/\delta$, although they allow for the nonlinear

behavior of C_{m_σ} with increasing angle of attack, will lead to false results. In particular, when $(C_{n_\phi} - \gamma C_{n_\psi})/\delta$ is incorrectly forced to equal C_{m_σ}, the difference between the assigned value and the actual one must be absorbed in the remaining term of the side-moment equation, $\{p_B \ell/V\}C_{n_\psi}$. As discussed by Levy and Tobak,[9] this may cause methods that extract nonlinear aerodynamic coefficients from free-flight data, if based on such an aerodynamic formulation, to assign an unrealistically large value to C_{n_ψ}, although the value determined in the classical Magnus experiment would be negligibly small.

2.3.5 Potential Application to Airplane Spins

The ability to predict the pre-stall and post-stall spin behavior of high performance aircraft is currently hampered by the inadequacies of the linear aerodynamic moment system. The striking similarity between coning motion and the steady spin of an aircraft suggests that a moment formulation similar to Eq. (2.25) (or, alternately, Eq. (2.29)) will properly describe the aerodynamic reactions on a spinning airplane. It is known, however, that in the establishment of a spin the large asymmetric regions of separated flow on the wings of the vehicle cause the aerodynamic reactions to be highly nonlinear functions of the spin rate, even at low spin rates. This contradicts the assumption, used in the development of Eq. (2.25), that the reactions are linear functions of the rates. It is anticipated that by expanding the integral form for $\hat{C}_m(t)$ corresponding to Eq. (2.17) about the point $p_B = p_B(t)$ (the instantaneous spin rate) rather than about $p_B = 0$, a formulation corresponding to Eq. (2.25) could be obtained which would describe the nonlinear behavior of the aerodynamic reactions with coning rate as well as with angle of attack and sideslip. In such a formulation $p_B(t)$ would, of necessity, be retained in the notation.

3. NUMERICAL FLOW-FIELD SOLUTION

The previous chapter has shown that the nonlinear aerodynamic force and moment acting on a body performing large-amplitude nonplanar motions can be compounded of the contributions from four characteristic motions: steady angle of attack, pitch oscillations, either roll or yaw oscillations, and coning motion. It would be desirable to be able to apply methods of computational fluid dynamics to compute the flow fields about bodies performing these characteristic motions and so obtain their contributions to the aerodynamic reactions. Extensive study of the steady angle-of-attack case has led to the development of many numerical finite-difference methods for computing the steady inviscid flow field about two- and three-dimensional bodies for subsonic through hypersonic Mach numbers. The computation of the nonsteady flow fields generated by the oscillatory motions is more difficult. Here the flow variables are functions of time as well as of position, and thus the solution requires increased computation and larger computer data storage capacity than is necessary for the steady flow case. Coning motion, shown to have special significance in the nonlinear moment formulation, generates a flow field more amenable to numerical solution than do those of the oscillatory cases, since to an observer fixed on the coning body the surrounding flow is steady. Hence, techniques developed for the solution of steady flow fields can be applied to coning motion.

The study of steady supersonic flow has led to the development of a class of accurate numerical finite-difference methods termed marching methods. By taking advantage of the fact that the equations governing a supersonic flow are hyperbolic in the streamwise direction, the use of such methods advances an initial solution, specified at one transverse

plane, in the streamwise direction to obtain the entire flow field. These methods enable the solution of the full nonlinear gasdynamic equations, rather than the simplified equations obtained by the introduction of a velocity potential. The solutions obtained are therefore valid for flows at hypersonic Mach numbers where vorticity is generated by strong curved shock waves, as well as for flow at lower supersonic Mach numbers. One such method, the noncentered second-order scheme introduced by MacCormack[11] and developed by Kutler and Lomax[12] as a shock-capturing technique, has been shown to be both accurate and versatile. Results of computations of the complex steady hypersonic flow field surrounding a proposed space shuttle orbiter, obtained using this technique, show excellent agreement with experiment and with results obtained from a three-dimensional method of characteristics (Rakich and Kutler[19]). In a shock-capturing technique, the equations are expressed in conservation-law form and the finite-difference scheme is applied uniformly at all points of a computational mesh which extends into the undisturbed free stream ahead of the bow shock wave. The jump in the flow variables across the shock is spread over several points of the mesh. In a sharp-shock technique, the bow shock is treated as a discontinuity and the Rankine-Hugoniot relations are used to determine the flow conditions immediately behind the shock. One advantage of the shock-capturing technique is its ability to determine the position and strength of the bow shock without special computer coding. A second and more important advantage is its ability to determine the position and strength of embedded shock waves, such as the crossflow shocks that are seen on the leeward side of a body at large angles of attack, if they occur within the flow field. Because of its accuracy and simplicity, the shock-capturing technique was extended to the case of a body in coning motion in a supersonic stream.

3.1 Method of Solution

The nonlinear Eulerian gasdynamic equations are solved numerically to determine the totally supersonic inviscid flow field about a pointed body in coning motion. A body-fixed cylindrical coordinate system, designated the computational system, is introduced. The origin of these coordinates lies at the center of gravity of the body, with s, the axial coordinate, aligned with the negative x_B axis. The radial coordinate r lies in planes normal to the x_B axis (i.e., in crossflow planes) as illustrated in Fig. 1(a). The circumferential angle, θ, is seen to be measured from the resultant angle-of-attack plane. In coning motion at fixed coning rate $\dot{\phi}$, the flow is time-invariant with respect to an observer fixed in the computational coordinate system. Since the flow field is everywhere supersonic, the gasdynamic equations are hyperbolic in the axial direction. A computational mesh is established between the body surface and the free stream ahead of the bow shock wave in planes normal to the s axis. With the flow field specified at an initial data plane, $s = s_{initial}$, MacCormack's method is used to march the solution in the s direction over the length of the body. At the outer edge of the mesh, the flow variables are assigned free-stream values, while at the inner edge, the flow is kept tangent to the body. With the complete flow field thus determined, the forces and moments are obtained from a subsequent integration of the surface pressure distribution.

Computations have been carried out for conical bodies of circular and elliptical cross section. An approximate initial solution was generated at the initial data plane by assuming the flow upstream to be that about a cone at angle of attack and yaw, with a uniform sidewash velocity. Note that although the body geometry is conical, the free-stream sidewash generated by coning motion is a function of axial position along the body,

and the resulting flow field is not conical. Details of the method and a discussion of the approximate starting solution are given below.

The computations were carried out on an IBM 360/67 computer linked to a cathode-ray tube graphics device. The graphics unit, which possesses man-machine interaction capability, was used to study the flow field as it developed, and to control any numerical instabilities that evolved. Approximately 50 minutes of computer time were required per case (one angle of attack at one coning rate).

3.2 Gasdynamic Equations

The equations governing the unsteady inviscid flow of a non-heat-conducting perfect gas around a body performing an arbitrary motion, written with respect to a body-fixed coordinate system whose origin is at the center of gravity of the body, can be expressed as

(mass)
$$\frac{\partial}{\partial t}(\rho) + \operatorname{div}(\rho\bar{V}) = 0 \tag{3.1a}$$

(momentum)
$$\frac{\partial}{\partial t}(\rho\bar{V}) + \operatorname{grad} p + \rho\bar{V} \cdot \operatorname{grad} \bar{V} + \bar{V} \operatorname{div}(\rho\bar{V}) + \rho\left[2\bar{\Omega}\times\bar{V} + \frac{d}{dt}(\bar{V}_{cg}) + \frac{d}{dt}(\bar{\Omega})\times\bar{V} + \bar{\Omega}\times(\bar{\Omega}\times\bar{r})\right] = 0 \tag{3.1b}$$

(energy)
$$\frac{\partial}{\partial t}(\mathcal{E}) + \operatorname{div}[(p+\mathcal{E})\bar{V}] + \left[2\bar{\Omega}\times\bar{V} + \frac{d}{dt}(\bar{V}_{cg}) + \frac{d}{dt}(\bar{\Omega})\times\bar{V} + \bar{\Omega}\times(\bar{\Omega}\times\bar{r})\right] \cdot \rho\bar{V} = 0 \tag{3.1c}$$

(state)
$$p = (\bar{\gamma}-1)\rho e \tag{3.1d}$$

where

$\bar{r}$ position vector in the body coordinate system

$\bar{V}(\bar{r},t)$ velocity vector (having components u, v, w) of the fluid at the point $\bar{r}$, measured relative to the body-fixed coordinates

$\bar{V}_{cg}, \bar{\Omega}$ velocity and angular velocity, respectively, of the body-fixed coordinates measured with respect to an inertial system

$\mathscr{E} = \rho[e+(1/2)|\bar{V}|^2]$ total energy per unit volume of fluid

The terms $2\rho\bar{\Omega}\times\bar{V}$ and $\rho\bar{\Omega}\times(\bar{\Omega}\times\bar{r})$ in Eqs. (3.1b) and (3.1c) are Coriolis and centrifugal force terms that appear because the body-fixed coordinate system is noninertial.

In the case of steady coning motion, $\bar{V}_{cg}$ = const, $\bar{\Omega}$ = const, and the flow field is time-invariant in the body-fixed coordinates. Under these conditions, Eqs. (3.1) become

(mass)
$$\operatorname{div}(\rho\bar{V}) = 0 \tag{3.2a}$$

(momentum)
$$\operatorname{grad} p + \rho\bar{V} \cdot \operatorname{grad} \bar{V} + \bar{V} \operatorname{div}(\rho\bar{V}) + \rho[2\bar{\Omega}\times\bar{V} + \bar{\Omega}\times(\bar{\Omega}\times\bar{r})] = 0 \tag{3.2b}$$

(energy)
$$\operatorname{div}[(p+\mathscr{E})\bar{V}] + [2\bar{\Omega}\times\bar{V} + \bar{\Omega}\times(\bar{\Omega}\times\bar{r})] \cdot \rho\bar{V} = 0 \tag{3.2c}$$

Equation (3.2c) can be simplified upon recognizing that $(\bar{\Omega}\times\bar{V}) \cdot \bar{V} = \bar{\Omega} \cdot (\bar{V}\times\bar{V}) = 0$. Also it can be shown that with $\bar{\Omega}$ = const, $\operatorname{curl}[\bar{\Omega}\times(\bar{\Omega}\times\bar{r})] = 0$, and thus $\bar{\Omega}\times(\bar{\Omega}\times\bar{r})$ can be expressed as the gradient of a potential, i.e., $\bar{\Omega}\times(\bar{\Omega}\times\bar{r}) = \operatorname{grad}(-\Phi/2)$. Substituting in Eq. (3.2c), and using Eqs. (3.2a) and (3.1d), we obtain

$$\rho\bar{V} \cdot \operatorname{grad}\left(\bar{\gamma}e - \frac{1}{2}\Phi + \frac{1}{2}|\bar{V}|^2\right) = 0 \tag{3.3}$$

This states that $\left(\bar{\gamma}e - \frac{1}{2}\Phi + \frac{1}{2}|V|^2\right)$ is constant along streamlines of the flow field. Since the motion under consideration is that of a body through a uniform atmosphere at rest with respect to the inertial system, the constant is the same for all streamlines, and Eq. (3.3) becomes

$$\bar{\gamma}e - \frac{1}{2}\Phi + \frac{1}{2}|\bar{V}|^2 = \text{const} = \bar{\gamma}e_o = h_o \qquad (3.4a)$$

or

$$p = \frac{\bar{\gamma}-1}{2\bar{\gamma}}\rho[2h_o + \Phi - (u^2+v^2+w^2)] \qquad (3.4b)$$

The number of dependent variables is thus reduced from five (E, ρ, $\bar{V}$) to four (ρ, $\bar{V}$), with p related to ρ and $\bar{V}$ through Eq. (3.4b).

When the coordinate system is specialized to the body-fixed computational system, the gasdynamic equations (3.2a) and (3.2b) can be written in conservation-law form as

$$E'_s + F'_\tau + G'_\theta + H' = 0 \qquad (3.5)$$

where the subscripts denote differentiation and

$$E' = \begin{vmatrix} \rho u \\ p+\rho u^2 \\ \rho uv \\ \rho uw \end{vmatrix}, \quad F' = \begin{vmatrix} \rho v \\ \rho uv \\ p+\rho v^2 \\ \rho vw \end{vmatrix}, \quad G' = \frac{1}{\tau}\begin{vmatrix} \rho w \\ \rho uw \\ \rho vw \\ p+\rho w^2 \end{vmatrix}$$

$$H' = \frac{1}{\tau}\begin{vmatrix} \rho v \\ \rho uv + \rho\tau[2(\omega_2 w-\omega_3 v)+\omega_1\omega_2\tau-s(\omega_2^2+\omega_3^2)] \\ \rho(v^2-w^2) + \rho\tau[2(\omega_3 u-\omega_1 w)+\omega_1\omega_2 s-\tau(\omega_1^2+\omega_3^2)] \\ 2\rho vw + \rho\tau[2(\omega_1 v-\omega_2 u)+\omega_3(\omega_2\tau+\omega_1 s)] \end{vmatrix}$$

The components of the angular velocity vector of magnitude $\dot{\phi}$, resolved in the s,τ,θ directions are, respectively, $\omega_1 = -\dot{\phi}\cos\sigma$, $\omega_2 = \dot{\phi}\sin\sigma\cos\theta$, and $\omega_3 = -\dot{\phi}\sin\sigma\sin\theta$. The energy equation is given by Eq. (3.4b), while the centrifugal force potential, obtained from the integration of $\text{grad}(-\Phi/2) = \bar{\Omega}\times(\bar{\Omega}\times\bar{r})$, can be expressed as

$$\Phi = \dot{\phi}^2[(s\sin\sigma + \tau_s\cos\sigma\cos\theta)^2 + (\tau\sin\theta)^2]$$

For supersonic flow, Eq. (3.5) is hyperbolic with respect to s, and thus can be integrated in the s direction. Specifically, u, the component of the local flow velocity in the s direction, must be greater than

the local speed of sound at all points of the flow field. In regions where this condition does not hold, such as in the subsonic nose region of a blunted body, the marching method fails. In such a case the nonsteady form of the gasdynamic equations would have to be integrated with respect to time, and the steady solution would be obtained as the steady limit of an unsteady flow.

It is generally advantageous, when flow problems are solved with the use of finite-difference methods, to have the physical boundaries of the flow field lie along coordinate surfaces of the computational coordinate system. Under these conditions the application of the surface boundary conditions is greatly simplified. Further, to improve the accuracy of the solution, it is desirable to use a dense spacing of computational grid points in those regions of the flow field where large gradients of the flow variables are known or suspected to exist. Thus, in the present case, that of flow over cones of circular and elliptical cross section, the annular region of interest about the body (in the τ,θ plane) is transformed into a rectangular region (Fig. 9). A radial independent coordinate μ is chosen to map the region between the body surface and an outer boundary into the region $0 \leq \mu \leq 1$. The outer boundary is chosen to lie in the undisturbed stream outside the bow shock wave. It is known that when a cone of elliptical cross section is placed at incidence in a wing-like attitude (i.e., with the semimajor axis of the ellipse normal to the flow direction) rapid variations of the flow variables occur in the vicinity of the semimajor axis. A circumferential independent variable η, dependent on the body cross section, is therefore chosen to cluster the physical circumferential planes more closely in these regions. The transformations are:

$$s = s \; ; \quad s_{initial} \le s \le s_{final} \tag{3.6a}$$

$$\mu = (\tau-\tau_b)/(\tau_{ob}-\tau_b) \; ; \quad 0 \le \mu \le 1 \tag{3.6b}$$

$$\eta = \tan^{-1}\left(\frac{A}{B}\tan\theta\right) \; ; \quad 0 \le \eta \le 2\pi \tag{3.6c}$$

where

$\tau_b = \tau_b(\theta,s)$ value of τ at the body surface

$\tau_{ob} = \tau_{ob}(\theta,s)$ value of τ at the outer boundary

A sine of the angle subtended by the semimajor axis, a(s), of the elliptical cone

B sine of the angle subtended by the semiminor axis, b(s), of the elliptical cone

Applying these transformations to Eq. (3.5) gives

$$E_s + F_\mu + G_\eta + H = 0 \tag{3.7}$$

where

$$E = E'$$

$$F = \frac{1}{\tau_{ob}-\tau_b}\left\{[(\mu-1)\tau_{b_s}-\mu\tau_{ob_s}]E' + F' + [(\mu-1)\tau_{b_\theta}-\mu\tau_{ob_\theta}]G'\right\}$$

$$G = \sin\eta\cos\eta\left(\frac{A_s}{A}-\frac{B_s}{B}\right)E' + \frac{A^2\cos^2\eta + B^2\sin^2\eta}{AB}G'$$

$$H = H' + \left[\cos 2\eta\left(\frac{B_s}{B}-\frac{A_s}{A}\right) + \frac{\tau_{ob_s}-\tau_{b_s}}{\tau_{ob}-\tau_b}\right]E' + \left[\sin 2\eta\,\frac{A^2-B^2}{AB} + \frac{\tau_{ob_\theta}-\tau_{b_\theta}}{\tau_{ob}-\tau_b}\right]G'$$

Here B_s denotes differentiation of B with respect to s, τ_{ob_θ} denotes differentiation of τ_{ob} with respect to θ, etc.

3.3 Differencing Scheme

The rectangular region of interest in the μ,η plane is divided into an equispaced rectangular grid having 20 intervals $\Delta\mu$ in the μ direction

and 36 intervals $\Delta\eta$ in the η direction. Thus $\Delta\mu = 0.05$, and $\Delta\eta = \pi/18$. With the primitive flow variables (pressure, density, and velocity) known at all mesh points of an initial data plane at $s = n\,\Delta s$, MacCormack's two-step, predictor-corrector difference scheme is used to advance the solution to $s = (n+1)\Delta s$. As applied to Eq. (3.7), this method is

$$\tilde{E}^{n+1}_{j,k} = E^{n}_{j,k} - \frac{\Delta s}{\Delta\mu}\left(F^{n}_{j+1,k} - F^{n}_{j,k}\right) - \frac{\Delta s}{\Delta\eta}\left(G^{n}_{j,k+1} - G^{n}_{j,k}\right) - \Delta s H^{n}_{j,k} \tag{3.8a}$$

$$E^{n+1}_{j,k} = \frac{1}{2}\left\{E^{n}_{j,k} + \tilde{E}^{n+1}_{j,k} - \frac{\Delta s}{\Delta\mu}\left(\tilde{F}^{n+1}_{j,k} - \tilde{F}^{n+1}_{j-1,k}\right) - \frac{\Delta s}{\Delta\eta}\left(\tilde{G}^{n+1}_{j,k} - \tilde{G}^{n+1}_{j,k-1}\right) - \Delta s \tilde{H}^{n+1}_{j,k}\right\} \tag{3.8b}$$

where $\tilde{E}^{n}_{j,k} = \tilde{E}(n\,\Delta s, j\,\Delta\mu, k\,\Delta\eta)$, the predicted value of E at $s = n\,\Delta s$, $E^{n}_{j,k} = E(n\,\Delta s, j\,\Delta\mu, k\,\Delta\eta)$, the corrected value of E at $s = n\,\Delta s$, $F^{n}_{j,k} = F(E^{n}_{j,k})$, $\tilde{F}^{n}_{j,k} = F(\tilde{E}^{n}_{j,k})$, etc. To proceed, the conservation-law variables $E^{n}_{j,k}$, $F^{n}_{j,k}$, etc., are formed from the primitive variables at all points of the mesh since the body and outer boundary geometry are known. Predicted values $\tilde{E}^{n+1}_{j,k}$ of the conservation-law variables at $s = (n+1)\Delta s$ are obtained with the use of Eq. (3.8a), and these are decoded to obtain the predicted values of the primitive flow variables. Boundary conditions are then applied to ensure tangency of the flow at the body, and the proper flow conditions in the free stream. The conservation-law variables $\tilde{F}^{n+1}_{j,k}$, $\tilde{G}^{n+1}_{j,k}$, and $\tilde{H}^{n+1}_{j,k}$ are formed from the predicted primitive variables and the known body and outer boundary geometry at the new axial position. Corrected values $E^{n+1}_{j,k}$ are obtained using Eq. (3.8b), and are decoded to obtain the solution in terms of primitive variables at $s = (n+1)\Delta s$. The boundary conditions are again applied, thus completing the computational cycle. This cycle is repeated to advance the solution

from $s = (n+1)\Delta s$ to $s = (n+2)\Delta s$, and so on over the entire length of the body.

The primitive flow variables are obtained from the new (predicted or corrected) values of E and the energy equation (3.4b) in the following manner. Let

$$E = \begin{vmatrix} \rho u \\ p+\rho u^2 \\ \rho uv \\ \rho uw \end{vmatrix} = \begin{vmatrix} e_1 \\ e_2 \\ e_3 \\ e_4 \end{vmatrix} \qquad \begin{matrix} (3.9a) \\ (3.9b) \\ (3.9c) \\ (3.9d) \end{matrix}$$

With pressure eliminated from Eq. (3.9) by the use of Eq. (3.4b), the simultaneous solution of Eq. (3.9) gives

$$v = e_3/e_1 \qquad (3.10a)$$

$$w = e_4/e_1 \qquad (3.10b)$$

$$u = \frac{\bar{\gamma}}{\bar{\gamma}+1}\frac{e_2}{e_1} + \left[\left(\frac{\bar{\gamma}}{\bar{\gamma}+1}\frac{e_2}{e_1}\right)^2 - \frac{\bar{\gamma}-1}{\bar{\gamma}+1}\left(2h_o + \Phi - v^2 - w^2\right)\right]^{1/2} \qquad (3.10c)$$

$$\rho = e_1/u \qquad (3.10d)$$

The pressure p is determined from the energy equation (3.4). The positive sign appearing before the radical in Eq. (3.10c) is used because the axial component of the local flow velocity is supersonic throughout the flow field. That the flow was supersonic in the cases considered was assured since the maximum effective deflection angle, defined as the sum of the resultant angle of attack and the cone half-angle, was always less than the shock detachment angle for axisymmetric supersonic cone flow at the same Mach number.

It is desirable, both for reasons of numerical accuracy and for computational efficiency, to take as large a step size Δs as possible. However, explicit numerical schemes such as this one become unstable if too large a step is employed. To determine the maximum step size that may

be used at a particular s station, the nonlinear equation (3.7) is expressed in a locally linear form as

$$E_s + ME_\mu + NE_\eta + H = 0 \tag{3.11}$$

where M and N are the Jacobian matrices $\partial F/\partial E$ and $\partial G/\partial E$, respectively. The maximum allowable step sizes determined from applying linear one-dimensional stability analyses successively in the μ,s and η,s planes (e.g., Richtmyer and Morton[20]) are

$$\frac{\Delta s}{\Delta \mu} \leq \frac{1}{|\sigma_M|_{max}} \tag{3.12a}$$

$$\frac{\Delta s}{\Delta \eta} \leq \frac{1}{|\sigma_N|_{max}} \tag{3.12b}$$

where σ_M and σ_N are the eigenvalues of M and N. The eigenvalues are evaluated for all points in the flow field at the current s location, and the most restrictive condition on Δs is selected. While the use of uncoupled one-dimensional analyses is not exact, the results are useful provided the step size thus determined is further reduced by approximately 10 percent. Further, if the local Mach number tends toward unity, the step size determined in this manner tends toward zero, thus providing a warning that the assumptions of the analysis may no longer be valid.

3.4 Boundary Conditions

The outer edge, $\mu = 1$, of the computational grid is chosen to lie in the undisturbed free stream ahead of the bow shock. Here the pressure and density are the free-stream values, while the velocity components, determined from geometrical considerations, are

$$u = V \cos \sigma - \dot{\phi} r_{ob} \sin \sigma \sin \theta \tag{3.13a}$$

$$v = -V \sin \sigma \cos \theta + \dot{\phi} s \sin \sigma \sin \theta \tag{3.13b}$$

$$w = V \sin \sigma \sin \theta + \dot{\phi}(s \sin \sigma \cos \theta + r_{ob} \cos \sigma) \tag{3.13c}$$

At the sides ($\eta = 0$ and $\eta = 2\pi$) of the computational grid, a periodic continuation principle is applied, i.e., $p(\mu,\eta = 0) = p(\mu,\eta = 2\pi)$, $\rho(\mu,\eta = 0) = \rho(\mu,\eta = 2\pi)$, etc. The tangency boundary condition at the body, $\mu = 0$, is due to a scheme of Abbett[21] and is briefly summarized here. The flow variables are known at the new axial position after the predictor step. In general, the local flow velocity at the body is not tangent to the body. A local two-dimensional Prandtl-Mayer expansion or an isentropic compression is used as needed to turn the flow into the local tangent plane. This satisfies the tangency condition and determines a corrected value of the surface pressure. A corrected value of the surface density is then determined since it is assumed that flow along surface streamlines is isentropic. The magnitude of the corrected flow velocity is then determined from the energy equation, Eq. (3.4), while its direction is that obtained from satisfying the tangency condition. This tangency condition scheme has been shown to give good results. The surface flow conditions for a circular cone at angle of attack computed by Kutler *et al.*[22] using this scheme were found to be in good agreement with the numerical results of Babenko *et al.*[23] and with the method of characteristics results of Rakich.[24]

Crossflow shocks were observed to exist in the flow field for the high angle-of-attack computations and to extend to the body surface. In such cases, the assumption that the flow is isentropic along surface streamlines is no longer valid. In principle, the value of surface entropy (used in the tangency scheme to compute the corrected surface density) for points behind the embedded shocks should be different from those points unaffected by the shocks. However, if the embedded shocks are relatively weak this refinement to the tangency condition can be justifiably neglected. This

was found to be the case in the present computations, and a single value of surface entropy was used for all points on the surface.

3.5 Initial Solution

The flow field surrounding even a conical body is not conical when the body is in coning motion since the sidewash velocity of the undisturbed stream, measured by an observer on the body, is a function of axial position. This is illustrated in Fig. 10(a) for the conical tip of a body in coning motion. The velocity component normal to the angle-of-attack plane varies linearly from $\dot{\phi}s_{tip} \sin\sigma$ at $s = s_{tip}$ to $\dot{\phi}s_{initial} \sin\sigma$ at $s = s_{initial}$, changes direction at $s = 0$, and increases linearly with s behind the mass center. The exact computation of the flow field upstream of the initial data plane at $s = s_{initial}$ would require the use of a three-dimensional, time-dependent technique with the steady solution approached as the limit of an unsteady flow. To avoid this complication, an approximate initial solution, valid for bodies with conical tips and capable of being generated by the marching method, is employed. The flow field upstream of the initial data plane for the conical tip in coning motion ($\dot{\phi} = \text{const}$) is assumed to be that of the body in steady planar motion at the same values of angle of attack and bank, with a uniform imposed sidewash velocity of $\dot{\phi}s_{initial} \sin\sigma$ acting normal to the angle-of-attack plane. This is illustrated in Fig. 10(b). Under these conditions the flow field around the conical tip is conical.

The marching method is used to generate the approximate conical solution in a "distance asymptotic" technique. The outer boundary of the flow field is chosen as a cone whose apex is coincident with that of the body. Corresponding points in successive $s = \text{const}$ planes thus lie along rays of the flow field. The flow variables are set to convenient values, such

as free-stream values, and the gasdynamic equations are integrated downstream. As the integration proceeds, the arbitrarily chosen initial values of the flow variables have less and less effect on the current values. The current solution is increasingly affected only by the boundary conditions at the body surface and at the outer boundary. When, at corresponding points, no change in the flow variables is detected with further integration downstream, the flow variables are constant along rays and the solution has been determined. The conical field is then scaled to place it at $s = s_{initial}$.

When the surface tangency condition is applied during the determination of the conical starting solution, the value of the surface entropy is allowed to vary. At each step the position of the crossflow stagnation streamline is determined numerically, and the surface entropy is chosen as that of stagnation streamline one mesh interval above the body. As the conical solution is approached, the surface entropy, too, remains constant with further integration downstream. The numerical method differences across the vortical layer known to exist in the flow fields about circular and noncircular cones at angle of attack (cf. Ferri[25]). Although differencing across these regions of high gradients causes some small spatial oscillations of the flow variables close to the body, it has no effect on the stability of the method.

The errors associated with the use of the approximate initial solution should be small, particularly when $s_{initial}$ is chosen close to s_{tip}, and should diminish as the integration (for the body in coning motion) proceeds downstream from the initial data plane. Further, these errors should have only negligible effect on the forces and moments since the surface area of the body is small near its apex. The magnitude of

these errors was assessed by carrying out a series of computations at one coning rate, Mach number, and angle of attack, in which the position of the initial data plane was varied. No changes in the forces and moments were observed as $s_{initial}$ was varied for values of $(s_{initial} - s_{tip})/(s_{final} - s_{tip})$ less than 0.05. The solutions were thus started 5 percent downstream from the nose for the remainder of the cases considered.

3.6 Results

Flow fields were computed for a 10° half-angle circular cone in coning motion at $M = 2$ and $M = 10$, and for an elliptic cone in coning motion at $M = 2$. These cases were selected both to demonstrate various capabilities of the numerical method and to enable a comparison of the numerical results with experimental measurements (and indirectly with the results of other analytical and numerical methods).

3.6.1 10° Circular Cone at $M = 2$; Nonlinear vs. Viscous Effects

Computations were carried out for a 10° half-angle cone in coning motion for angles of attack ranging from 0° to 25° ($0 \leq \delta \leq 0.42$) and for values of the coning-rate parameter $\dot{\phi}\ell/V$ ranging from 0 to 0.15. The center of mass ($s = 0$) was located at 61 percent of the body length from the nose; thus $s_{tip} = -0.61$, $s_{initial} = -0.56$, and $s_{final} = 0.39$. These conditions duplicate those of the experiment described in Ref. 5. Briefly, in that experiment a six-component balance mounted on a rotating sting was used to measure the forces and moments acting on a cone in coning motion. In addition, the viscosity-induced vortex patterns present on the leeward side of the body at high angles of attack were investigated using the vapor screen flow visualization technique (Allen and Perkins[26]).

3.6.1.1 Flow-Field Results

3.6.1.1a *Surface pressure* - Circumferential plots of the surface pressure for the conical initial solutions generated at $s = s_{initial} = -0.56$ are presented in Fig. 11. These plots show the surface pressure, normalized by the free-stream pressure, as a function of the circumferential angle θ for each of the angles of attack σ computed. These pressure plots are not symmetrical about $\theta = 0°$ due to the presence of the imposed sidewash velocity, but rather are symmetrical about the direction of the resultant crossflow velocity vector, i.e., $\tan \theta_{sym} = -\dot{\phi} s_{initial}/V$. Results for two values of the coning rate $\dot{\phi}$ are presented in the figure. A value of $\dot{\phi}/V = 0.12$ was used for $\sigma \leq 12.5°$, and for $\sigma \geq 15°$, $\dot{\phi}/V$ was chosen as 0.15, giving values of θ_{sym} of 3.84° and 4.80°, respectively. At angles of attack less than the cone half-angle, the pressure drops smoothly from a maximum at the windward ray ($\theta = \theta_{sym}$) to a minimum at the leeward ray ($\theta = \theta_{sym} + 180°$). As the angle of attack is increased beyond the cone half-angle, the surface pressure is observed to drop to a minimum approximately 115° from the windward ray, and then to increase gradually toward the leeward ray. At angles of attack of 20° and 25°, the surface pressure drops to a minimum located 125° and 135°, respectively, from the windward ray. The pressure then undergoes an abrupt jump followed by a slight increase as θ increases toward the leeward ray, thus indicating the presence of a pair of crossflow shocks extending from the body surface into the flow field.

3.6.1.1b *Crossflow shocks* - The strength and location of the crossflow shocks can also be determined from the circumferential plots of the surface crossflow Mach number of the conical initial solutions which are presented in Fig. 12. The surface crossflow Mach number, M_c, defined as

the surface crossflow velocity, w_s, normalized by the local speed of sound, is shown as a function of θ for angles of attack of 15°, 20°, and 25°. These plots are symmetric about the windward ray, whose location, indicated by $M_c = 0$, is again seen to be displaced to $\theta_{sym} = 4.8°$ due to the imposed sidewash velocity. For angles of attack up to 15°, the crossflow velocity is everywhere subsonic. At $\sigma \doteq 15°$ the surface Mach number reaches a maximum of 0.88 located 115° from the windward ray, which corresponds to the location of the minimum surface pressure, and decreases smoothly to zero at the leeward ray ($\theta = 185°$). At $\sigma = 20°$ and 25°, the crossflow velocity is observed to become supersonic approximately 85° and 75°, respectively, from the windward ray, and reach a maximum Mach number followed by an abrupt drop, indicating the crossflow shock, at values of θ which correspond to the locations of the jump in the surface pressure. In a conical flow field, the crossflow shocks lie along rays from the apex and thus the component of the Mach number normal to these shocks at the body surface is just the surface crossflow Mach number, M_c. The best estimates of the upstream (supersonic) surface Mach numbers, M_{c_1}, and shock locations, obtained from the numerical results for $\sigma = 20°$ and 25°, are indicated in Fig. 12. The corresponding downstream Mach numbers, M_{c_2}, which together with the pressure ratio across the shock are determined from M_{c_1} using the normal shock relations (e.g., Liepmann and Roshko[27]) are also shown. The pressure behind the crossflow shocks, determined from numerically obtained values of the pressure ahead of the shocks and the pressure ratio corresponding to M_{c_1}, is shown in Fig. 11 and is in good agreement with the numerical results.

3.6.1.1c *Flow-field contour maps* - Qualitative characteristics of the conical flow field, including the strength and location of the bow shock

wave and the changes in the flow field due to increasing angle of attack, can be determined from the flow-field cross-section contour maps presented in Fig. 13. These maps show contours of constant, equispaced values of the pressure, normalized by the free-stream pressure, in the plane $s = s_{initial}$ for each of the angles of attack computed. Also shown in Fig. 13 are the body cross section and the selected outer boundary of the computational region. The contours are generated by a contour mapping program directly from the numerical data. The contour mapping routine generates fewer points along contour segments running from the lower left to the upper right of the μ,η computational mesh than for other segments. This relatively large spacing between contour points causes the more jagged appearance of the contours in the lower right section of the maps. As before, the flow field is observed to be symmetric about θ_{sym} due to the imposed sidewash velocity, and the location of the symmetry plane is shown in the figure.

At low angles of attack, the bow shock location, indicated by closely spaced contour lines within the computational region, is well defined both on the windward and leeward sides of the body. As the angle of attack is increased beyond the cone half-angle, the windward side shock strength increases. On the leeward side, the bow shock becomes weak, tending toward a Mach wave, and its location is not easily identified. In these cases the shock location is indicated by a contour of $p/p_\infty = 1.005$. The small closed contours seen in the free stream outside the bow shock at angles of attack of 20° and 25° are indicative of overshoots in the numerical data to values of p/p_∞ greater than 1.10, caused by third-order dispersive errors in the numerical scheme. This is also the cause of the jaggedness of the contours in the shock layer close to the shock. Experience with higher-order

differencing schemes that minimize these effects (Kutler *et al.*[22]), as well as with sharp shock techniques, indicates that the oscillations have negligible effect on the solution in regions away from the immediate vicinity of the shock. Thus, for example, the surface pressure distribution is not adversely affected by the dispersive effects.

At angles of attack of 20° and 25°, shocks are seen to extend from the body surface into the flow. The crossflow shocks are situated at the rear of a region of supersonic crossflow located adjacent to the body and surrounded by a larger subsonic crossflow region. This is similar to the mixed flow pattern that would be observed on a wing section in a transonic flow ($M_\infty < 1$). As in the transonic case, the shock is strongest at the body, and its strength decreases with distance from the body surface. The crossflow shock terminates in the flow field where it joins the sonic line delineating the front of the supersonic region. The locations of the crossflow shocks and of the sonic lines, determined from the numerical data, are indicated on the contour maps. At $\sigma = 20°$ the shocks extend about 1/2 body radius into the flow, while at $\sigma = 25°$ they extend about 1 body radius and, as discussed previously, are stronger.

3.6.1.1d *Surface pressure contours* - Starting with the conical solutions at $s = s_{initial}$, the gasdynamic equations were integrated over the length of the body. The resulting three-dimensional flow fields are observed to vary only slightly and gradually with distance along the body. To best demonstrate this variation, contours of constant values of the surface pressure, normalized by the free-stream pressure, are presented in Fig. 14 for each angle of attack computed. The contours are plotted on the developed body surface, which is unrolled at the leeward ($\theta = 180°$) ray. For zero coning rate ($\dot{\phi} = 0$), the flow field surrounding the body

would be conical, and the flow quantities, including the surface pressure, would be constant along rays. In Fig. 14, the surface pressure contours would merely be straight lines passing through the apex. Thus the deviation of the pressure contours from such straight lines is a measure of the effect of coning on the flow field. For the small values of the coning-rate parameter $\dot{\phi}\ell/V$ used in the cases computed, the contours are only slightly curved, and no large differences are observed between the low angle-of-attack and the high angle-of-attack cases. The contours that originate part way along the body indicate a gradual change in the pressure with distance on the leeward side of the body. Although the curvature of the contours is small, the cumulative effect of the curvature is significant. To obtain a quantitative measure of the effects of coning, the surface pressure distributions were integrated to obtain force- and moment-coefficient data.

3.6.1.2 Force and Moment Coefficients

3.6.1.2a *Normal-force and pitching-moment coefficients* - The normal-force and pitching-moment coefficients are presented in Figs. 15(a) and 15(b), respectively. These coefficients were obtained from computations at fixed angles of attack for various coning rates. At each angle of attack, no change in the normal-force or the pitching-moment coefficient was observed as the coning-rate parameter was varied. This result, which agrees with the experimental observations, indicates that $C_{Z_{\dot{\phi}}}(\infty;\delta,\psi)$ and $C_{m_{\dot{\phi}}}(\infty;\delta,\psi)$, the contributions to the normal-force and pitching-moment coefficients due to coning motion, are negligible.

Also shown in Figs. 15(a) and 15(b) are the experimental measurements (Schiff and Tobak[5]) of the normal-force and pitching-moment coefficients, respectively. The theoretical values (Tobak and Wehrend[18]) of the linear

normal-force and pitching-moment coefficients, $\hat{C}_{Z_{\hat{\alpha}}}(\infty)$ and $\hat{C}_{m_{\hat{\alpha}}}(\infty)$, are also presented. At low values of δ, the computational results, the experimental measurements, and the linear theory values agree well. As δ increases the computational results and the experimental measurements become nonlinear functions of δ, and both are greater than the linear theory values. However, the computational results and the experimental measurements remain in good agreement.

3.6.1.2b *Side-force and side-moment coefficients* - At fixed angle of attack, the computational results indicate that the side-force and side-moment coefficients C_Y and C_n are linear functions of the coning-rate parameter over the range of $\dot{\phi}$ investigated. This result, which agrees with the experimental findings, demonstrates the adequacy of the moment formulation, Eq. (2.30), in which only terms linear in the rates are retained.

Since C_Y and C_n are linear functions of $\dot{\phi}$, normalizing by the coning-rate parameter yields $C_{Y_{\dot{\phi}.}}(\infty;\delta,\psi)$ and $C_{n_{\dot{\phi}.}}(\infty;\delta,\psi)$. Computational results for $C_{Y_{\dot{\phi}.}}$ and $C_{n_{\dot{\phi}.}}$ are presented in Figs. 16(a) and 16(b), respectively, together with the experimentally measured values. Also shown in Figs. 16(a) and 16(b) are the theoretical values (Tobak and Wehrend[18]) of the equivalent linear planar pitch damping derivatives, $\delta[\hat{C}_{Z_{q_B}}(\infty)+\gamma\hat{C}_{Z_{\hat{\alpha}.}}]$ and $\delta[\hat{C}_{m_{q_B}}(\infty)+\gamma\hat{C}_{m_{\hat{\alpha}.}}]$, respectively. These equivalences follow from Eq. (2.39) since in an inviscid computation for a body of revolution, where there is no viscous shear at the body surface, $C_{n_{\dot{\psi}.}}$ is identically zero. At low values of δ, $C_{Y_{\dot{\phi}.}}$ and $C_{n_{\dot{\phi}.}}$ are linear functions of δ and there is excellent agreement among the computational results, the experimental measurements, and the linear theory values. As δ increases, the computational results and the experimental measurements become nonlinear functions

of δ and depart significantly from the linear theory results. In contrast, the computational results agree well with the measurements for values of δ up to 0.34, even as C_{Y_ϕ} peaks and then tends toward negative values. As δ increases beyond 0.35, the computational results diverge from those obtained experimentally.

3.6.1.2c *Vapor screen results* - Previous attempts to explain the experimentally measured nonlinear behavior of the coefficients with increasing angle of attack (Schiff and Tobak,[5] Kuhn *et al.*[28]) postulated that their deviation from the linear theory values was due to the formation of a viscosity-induced leeward-side vortex pattern. In contrast, the present inviscid computational results, which neglect such a vortex pattern, follow the initial nonlinear behavior of the coefficients. This suggests that the initial nonlinearities are caused primarily by inviscid effects. An examination of the vapor screen studies of the experiment of Ref. 5 tends to support the latter hypothesis. Photographs of the leeward-side vortex patterns as they appeared in the vapor screen are presented in Fig. 17. The vortex cores are visible as dark spots on a light plane normal to the velocity vector. Distinct vortices are not visible in the vapor screen for values of δ less than 0.34 ($\sigma \leq 15°$). At $\delta = 0.34$ ($\sigma = 20°$), vortices are visible but are small and lie close to the body near the leeward ray. Under these conditions the inviscid flow field should be a good approximation of the actual one, and the forces and moments derived from the computation should, and do, agree well with the experimentally measured values. With further increases in the angle of attack, the vortices gradually increase in size, and presumably in strength, and lie farther from the body. Here the inviscid flow field is a poorer approximation of the actual one, and the computationally derived

forces and moments begin to diverge from those measured experimentally. Nonetheless, where the viscosity-induced effects are small, the inviscid computations agree well with experiment and demonstrate significantly nonlinear behavior of the forces and moments.

3.6.2 10° Circular Cone at M = 10

A computation was carried out for a 10° half-angle cone in coning motion for an angle of attack of 2° and a coning-rate parameter, $\dot{\phi}\ell/V$, of 0.2. At this low angle of attack, good agreement is expected between the side-moment coefficient $C_{n_{\dot{\phi}}}$ and the planar damping-in-pitch coefficient, as predicted by Eq. (2.39). Results of the computation are presented in Table 1 and are compared with the corresponding planar coefficients obtained from the unsteady inviscid flow-field results of Brong.[29] The agreement between the two methods is excellent with the maximum difference seen to be less than 2 percent. This demonstrates the capability of the present method to yield accurate results at hypersonic as well as at low supersonic Mach numbers.

Table 1.- Comparison of Force and Moment Coefficients due to Coning with Corresponding Planar Coefficients; 10° Half-Angle Cone, M = 10.0, $\sigma = 2.0°$, $\dot{\phi}\ell/V = 0.2$, $\ell_{cg}/\ell = 0.61$.

	C_Z $\left(\delta C_{Z_{\hat{\alpha}}}(\infty)\right)$	C_m $\left(\delta C_{m_{\hat{\alpha}}}(\infty)\right)$	$C_{Y_{\dot{\phi}}}$ $\left(\delta\left[\hat{C}_{Z_{q_B}}(\infty)+\gamma\hat{C}_{Z_{\dot{\hat{\alpha}}}}\right]\right)$	$C_{n_{\dot{\phi}}}$ $\left(\delta\left[\hat{C}_{m_{q_B}}(\infty)+\gamma\hat{C}_{m_{\dot{\hat{\alpha}}}}\right]\right)$
Coning	-0.06717	-0.00588	0.01623	-0.00626
(Planar)[29]	-0.0671	-0.00586	0.0164	-0.00634

3.6.3 Elliptic Cone at $M = 2$

Computations were carried out for a cone of elliptic cross section in coning motion at $M = 1.97$. The ratio of the major to minor axes of the cone was 3:2, and the base area was equal to that of a 7.75° half-angle circular cone of the same length. The angle of attack was fixed at 4° for $\psi = 0$ and $\pi/2$, and the coning-rate parameter ranged from 0 to 0.15. Computations were also carried out for the equivalent circular cone in coning motion.

3.6.3.1 Normal-Force Coefficient

The normal-force coefficients obtained from the computations with the bodies in coning motion are presented in Fig. 18(a). Again, at fixed angle of attack no change in the normal-force coefficient was obtained as the coning-rate parameter was varied. Also shown in Fig. 18(a) are experimental values of the normal-force coefficients of these bodies measured at zero coning rate by Jorgenson.[30] The good agreement between the computational results and the experimental measurements demonstrates the capability of the method to compute the flow field about bodies of noncircular cross section. The method can be extended to bodies of arbitrary shape (i.e., airplane-like configurations).

3.6.3.2 Side-Moment Coefficient

Computed values of the side-moment coefficient $C_{n_{\dot{\phi}}}(\infty;\delta,\psi)$ are presented in Fig. 18(b). Also shown is the theoretical value (Tobak and Wehrend[18]) of the linear planar damping-in-pitch derivative $\delta[\hat{C}_{m_{q_B}}(\infty)+\gamma\hat{C}_{m_{\dot{\hat{\alpha}}}}]$ for the equivalent circular cone. As before, for the circular cone $C_{n_{\dot{\psi}}} \equiv 0$ and there is good agreement between the computed value of $C_{n_{\dot{\phi}}}$ and the linear damping-in-pitch derivative, as predicted by Eq. (2.39). For the elliptic cone, $C_{n_{\dot{\psi}}}$ does not vanish but can probably

be neglected in comparison with $C_{n_{\dot{\phi}}}$. Under these conditions, Eq. (2.33) indicates that $C_{n_{\dot{\phi}}}(\infty;\delta,\pi/2) = \delta[\hat{C}_{m_{q_B}}(\infty) + \gamma\hat{C}_{m_{\dot{\hat{\alpha}}}}]$ and $C_{n_{\dot{\phi}}}(\infty;\delta,0) = \delta[\hat{C}_{n_{r_B}}(\infty) - \gamma\hat{C}_{n_{\dot{\hat{\beta}}}}]$. These are the planar damping coefficients for oscillations in the directions indicated by the double-headed arrows in Fig. 18(b). The computational results confirm the expectation that oscillations parallel to the major axis of the elliptical cone should be less strongly damped than those parallel to the minor axis.

4. CONCLUDING REMARKS

Concepts from the theory of functionals have been applied to develop nonlinear formulations of the aerodynamic force and moment systems acting on bodies in arbitrary, slowly varying, large-amplitude motions. The analysis, which proceeds formally once the functional dependence of the aerodynamic reactions upon the motion variables has been established, ensures the inclusion of all pertinent aerodynamic terms within the resulting formulations. The results confirm formally the intuitive notion that the instantaneous reactions on a body in an arbitrary motion can be compounded of the contributions from several characteristic motions: a steady motion with the instantaneous large values of the motion variables held fixed, and suitable perturbations about the steady motion.

The analysis indicates that coning, where the nose of the body describes a circle around the velocity vector, characterizes the nonplanar nature of a general motion. With this motivation, a numerical method was developed for computing the inviscid flow field surrounding a body in coning motion. Computations carried out for circular cones in coning motion both at low supersonic and hypersonic Mach numbers confirm the adequacy of a linear formulation at low angles of attack. At larger angles of attack,

however, the forces and moments become nonlinear functions of the angle of attack. Computational results for the reactions on the circular cone at the higher angles of attack agreed well with experimental measurements within the range of variables investigated. This indicates that the initial nonlinear behavior of the aerodynamic forces and moments is governed primarily by the inviscid flow and not, as previously postulated, by the viscosity-induced leeward-side vortices.

Ames Research Center

National Aeronautics and Space Administration

Moffett Field, Calif., 94035, August 24, 1973

APPENDIX A

The formulation developed in the body-fixed axis system is

$$\hat{C}_k(t) = \hat{C}_k(\infty;\hat{\alpha}(t),\hat{\beta}(t),V(t)) + \frac{p_B \ell}{V_R}\hat{C}_{k_{p_B}}(\infty;\hat{\alpha}(t),\hat{\beta}(t),V(t))$$

$$+ \frac{q_B \ell}{V_R}\hat{C}_{k_{q_B}}(\infty;\hat{\alpha}(t),\hat{\beta}(t),V(t)) + \frac{r_B \ell}{V_R}\hat{C}_{k_{r_B}}(\infty;\hat{\alpha}(t),\hat{\beta}(t),V(t))$$

$$+ \frac{\dot{\hat{\alpha}}\ell}{V_R}\hat{C}_{k_{\dot{\hat{\alpha}}}}(\hat{\alpha}(t),\hat{\beta}(t),V(t)) + \frac{\dot{\hat{\beta}}\ell}{V_R}\hat{C}_{k_{\dot{\hat{\beta}}}}(\hat{\alpha}(t),\hat{\beta}(t),V(t))$$

$$+ \frac{\dot{V}\ell}{V_R^2}\hat{C}_{k_{\dot{V}}}(\hat{\alpha}(t),\hat{\beta}(t),V(t)) \; ; \quad k = \ell,m,n \tag{A1}$$

while the formulation developed in the aerodynamic axis system is

$$C_k(t) = C_k(\infty;\delta(t),\psi(t),V(t)) + \frac{\dot{\lambda}\ell}{V_R}C_{k_{\dot{\lambda}}}(\infty;\delta(t),\psi(t),V(t))$$

$$+ \frac{q\ell}{V_R}C_{k_q}(\infty;\delta(t),\psi(t),V(t)) + \frac{r\ell}{V_R}C_{k_r}(\infty;\delta(t),\psi(t),V(t))$$

$$+ \frac{\dot{\delta}\ell}{V_R}C_{k_{\dot{\delta}}}(\delta(t),\psi(t),V(t)) + \frac{\dot{\psi}\ell}{V_R}C_{k_{\dot{\psi}}}(\delta(t),\psi(t),V(t))$$

$$+ \frac{\dot{V}\ell}{V_R^2}C_{k_{\dot{V}}}(\delta(t),\psi(t),V(t)) \; ; \quad k = \ell,m,n \tag{A2}$$

The moments expressed in the two axis systems are related to each other through

$$C_\ell = \hat{C}_\ell \tag{A3a}$$

$$C_m + iC_n = e^{i\psi}(\hat{C}_m + i\hat{C}_n) \tag{A3b}$$

while the motion variables in the two axis systems are related by

$$p_B = \dot{\lambda} + \dot{\psi} \tag{A4a}$$

$$q_B + ir_B = e^{-i\psi}(q + ir) \tag{A4b}$$

$$\hat{\alpha} + i\hat{\beta} = \delta\, e^{i\psi} \tag{A4c}$$

Substituting the results of Eq. (A4) into Eq. (A1), we obtain

$$\begin{aligned}
\hat{C}_k(t) = {} & \hat{C}_k(\infty;\hat{\alpha}(t),\hat{\beta}(t),V(t)) + \frac{\dot{\lambda}\ell}{V_R}\hat{C}_{k_{p_B}}(\infty;\hat{\alpha}(t),\hat{\beta}(t),V(t)) \\
& + \frac{q\ell}{V_R}\left[\hat{C}_{k_{q_B}}(\infty;\hat{\alpha}(t),\hat{\beta}(t),V(t))\cos\psi - \hat{C}_{k_{r_B}}(\infty;\hat{\alpha}(t),\hat{\beta}(t),V(t))\sin\psi\right] \\
& + \frac{r\ell}{V_R}\left[\hat{C}_{k_{q_B}}(\infty;\hat{\alpha}(t),\hat{\beta}(t),V(t))\sin\psi + \hat{C}_{k_{r_B}}(\infty;\hat{\alpha}(t),\hat{\beta}(t),V(t))\cos\psi\right] \\
& + \frac{\dot{\delta}\ell}{V_R}\left[\hat{C}_{k_{\dot{\hat{\alpha}}}}(\hat{\alpha}(t),\hat{\beta}(t),V(t))\cos\psi + \hat{C}_{k_{\dot{\hat{\beta}}}}(\hat{\alpha}(t),\hat{\beta}(t),V(t))\sin\psi\right] \\
& + \delta\,\frac{\dot{\psi}\ell}{V}\left[-\hat{C}_{k_{\dot{\hat{\alpha}}}}(\hat{\alpha}(t),\hat{\beta}(t),V(t))\sin\psi + \hat{C}_{k_{\dot{\hat{\beta}}}}(\hat{\alpha}(t),\hat{\beta}(t),V(t))\cos\psi\right. \\
& \left. + \frac{1}{\delta}\hat{C}_{k_{p_B}}(\infty;\hat{\alpha}(t),\hat{\beta}(t),V(t))\right] + \frac{\dot{V}\ell}{V_R^2}\hat{C}_{k\dot{V}}(\hat{\alpha}(t),\hat{\beta}(t),V(t)) \quad ; \quad k = \ell,m,n
\end{aligned} \tag{A5}$$

When the results of Eq. (A5) are substituted into Eq. (A3), the following equivalences between coefficients formulated in the two-axis systems are obtained:

$$C_\ell(\infty;\delta,\psi,V) = \hat{C}_\ell(\infty;\hat{\alpha},\hat{\beta},V) \tag{A6a}$$

$$C_{\ell_{\dot{\lambda}}}(\infty;\delta,\psi,V) = \hat{C}_{\ell_{p_B}}(\infty;\hat{\alpha},\hat{\beta},V) \tag{A6b}$$

$$C_{\ell_q}(\infty;\delta,\psi,V) = \hat{C}_{\ell_{q_B}}(\infty;\hat{\alpha},\hat{\beta},V)\cos\psi - \hat{C}_{\ell_{r_B}}(\infty;\hat{\alpha},\hat{\beta},V)\sin\psi \tag{A6c}$$

$$C_{\ell_r}(\infty;\delta,\psi,V) = \hat{C}_{\ell_{q_B}}(\infty;\hat{\alpha},\hat{\beta},V)\sin\psi + \hat{C}_{\ell_{r_B}}(\infty;\hat{\alpha},\hat{\beta},V)\cos\psi \tag{A6d}$$

$$C_{\ell_{\dot{\delta}}}(\delta,\psi,V) = \hat{C}_{\ell_{\dot{\hat{\alpha}}}}(\hat{\alpha},\hat{\beta},V)\cos\psi + \hat{C}_{\ell_{\dot{\hat{\beta}}}}(\hat{\alpha},\hat{\beta},V)\sin\psi \tag{A6e}$$

$$C_{\ell_{\dot{V}}}(\delta,\psi,V) = \hat{C}_{\ell_{\dot{V}}}(\hat{\alpha},\hat{\beta},V) \tag{A6f}$$

$$C_{\ell_{\dot{\psi}}}(\delta,\psi,V) = \hat{C}_{\ell_{p_B}}(\infty;\hat{\alpha},\hat{\beta},V) + \delta[-\hat{C}_{\ell_{\dot{\hat{\alpha}}}}(\hat{\alpha},\hat{\beta},V)\sin\psi + \hat{C}_{\ell_{\dot{\hat{\beta}}}}(\hat{\alpha},\hat{\beta},V)\cos\psi] \tag{A6g}$$

and

$$C_m(\infty;\delta,\psi,V) = \hat{C}_m(\infty;\hat{\alpha},\hat{\beta},V)\cos\psi - \hat{C}_n(\infty;\hat{\alpha},\hat{\beta},V)\sin\psi \tag{A7a}$$

$$C_{m_{\dot{\lambda}}}(\infty;\delta,\psi,V) = \hat{C}_{m_{p_B}}(\infty;\hat{\alpha},\hat{\beta},V)\cos\psi - \hat{C}_{n_{p_B}}(\infty;\hat{\alpha},\hat{\beta},V)\sin\psi \tag{A7b}$$

$$\begin{aligned} C_{m_q}(\infty;\delta,\psi,V) = {} & \hat{C}_{m_{q_B}}(\infty;\hat{\alpha},\hat{\beta},V)\cos\psi + \hat{C}_{n_{r_B}}(\infty;\hat{\alpha},\hat{\beta},V)\sin^2\psi \\ & -[\hat{C}_{m_{r_B}}(\infty;\hat{\alpha},\hat{\beta},V) + \hat{C}_{n_{q_B}}(\infty;\hat{\alpha},\hat{\beta},V)]\cos\psi\sin\psi \end{aligned} \tag{A7c}$$

$$\begin{aligned} C_{m_r}(\infty;\delta,\psi,V) = {} & \hat{C}_{m_{r_B}}(\infty;\hat{\alpha},\hat{\beta},V)\cos^2\psi - \hat{C}_{n_{q_B}}(\infty;\hat{\alpha},\hat{\beta},V)\sin^2\psi \\ & +[\hat{C}_{m_{q_B}}(\infty;\hat{\alpha},\hat{\beta},V) - \hat{C}_{n_{r_B}}(\infty;\hat{\alpha},\hat{\beta},V)]\cos\psi\sin\psi \end{aligned} \tag{A7d}$$

$$\begin{aligned} C_{m_{\dot{\delta}}}(\delta,\psi,V) = {} & \hat{C}_{m_{\dot{\hat{\alpha}}}}(\hat{\alpha},\hat{\beta},V)\cos^2\psi - \hat{C}_{n_{\dot{\hat{\beta}}}}(\hat{\alpha},\hat{\beta},V)\sin^2\psi \\ & +[\hat{C}_{m_{\dot{\hat{\beta}}}}(\hat{\alpha},\hat{\beta},V) - \hat{C}_{n_{\dot{\hat{\alpha}}}}(\hat{\alpha},\hat{\beta},V)]\cos\psi\sin\psi \end{aligned} \tag{A7e}$$

$$C_{m_{\dot{V}}}(\delta,\psi,V) = \hat{C}_{m_{\dot{V}}}(\hat{\alpha},\hat{\beta},V)\cos\psi - \hat{C}_{n_{\dot{V}}}(\hat{\alpha},\hat{\beta},V)\sin\psi \tag{A7f}$$

$$\begin{aligned} C_{m_{\dot{\psi}}}(\delta,\psi,V) = {} & \hat{C}_{m_{p_B}}(\infty;\hat{\alpha},\hat{\beta},V)\cos\psi - \hat{C}_{n_{p_B}}(\infty;\hat{\alpha},\hat{\beta},V)\sin\psi \\ & +\delta\{\hat{C}_{m_{\dot{\hat{\beta}}}}(\hat{\alpha},\hat{\beta},V)\cos^2\psi + \hat{C}_{n_{\dot{\hat{\alpha}}}}(\hat{\alpha},\hat{\beta},V)\sin^2\psi \\ & -[\hat{C}_{m_{\dot{\hat{\alpha}}}}(\hat{\alpha},\hat{\beta},V) + \hat{C}_{n_{\dot{\hat{\beta}}}}(\hat{\alpha},\hat{\beta},V)]\sin\psi\cos\psi\} \end{aligned} \tag{A7g}$$

The correspondences for the coefficients in $C_n(t)$ may be obtained from Eq. (A7) by replacing $\hat{C}_m$ with $\hat{C}_n$ and $\hat{C}_n$ with $-\hat{C}_m$. Similarly, the analogous matches for the force coefficients may be obtained by replacing ℓ,m,n with X,Y,Z, respectively, in Eqs. (A6) and (A7).

REFERENCES

[1]Etkin, B., *Dynamics of Flight*, John Wiley & Sons, New York, 1959.

[2]Nicolaides, J. D., Eikenberry, R. S., Ingram, C. W., and Kryvoruka, J. K., "Non-Linear Aerodynamic Characteristics of Re-Entry Configurations with Aerodynamic and Mass Asymmetries," AIAA Paper 69-867, 1969.

[3]Ingram, C. W., "An Approximate Solution for the Nonlinear Differential Equation for the Complex Angle of Attack of a Symmetrical Missile," AFATL-TR-68-71, Air Force Armament Laboratory, Eglin Air Force Base, Florida, June 1968.

[4]Iyengar, S., "Experimental Damping-in-Pitch of Two Slender Cones at Mach 2 and Incidences Up to 30°," LTR-UA-19, National Research Council, Ottawa, Canada, Jan. 1968.

[5]Schiff, L. B., and Tobak, M., "Results from a New Wind-Tunnel Apparatus for Studying Coning and Spinning Motions of Bodies of Revolution," AIAA Journal, Vol. 8, No. 11, pp. 1953-1957, Nov. 1970.

[6]Murphy, C. H., "Free Flight Motion of Symmetric Missiles," Rept. BRL-1216, Ballistic Research Lab., Aberdeen Proving Ground, Maryland, July 1963.

[7]Tobak, M., and Pearson, W. E., "A Study of Nonlinear Longitudinal Dynamic Stability," TR R-209, NASA, Sept. 1964.

[8]Tobak, M., Schiff, L. B., and Peterson, V. L., "Aerodynamics of Bodies of Revolution in Coning Motion," AIAA Journal, Vol. 7, No. 1, pp. 95-99, Jan. 1969.

[9]Levy, L. L., Jr., and Tobak, M., "Nonlinear Aerodynamics of Bodies of Revolution in Free Flight," AIAA Journal, Vol. 8, No. 12, pp. 2168-2171, Dec. 1970.

[10]Tobak, M., and Schiff, L. B., "A Nonlinear Aerodynamic Moment Formulation and Its Implications for Dynamic Stability Testing," AIAA Paper 71-275, 1971.

[11]MacCormack, R. W., "The Effect of Viscosity in Hypervelocity Impact Cratering," AIAA Paper 69-364, 1969.

[12]Kutler, P., and Lomax, H., "Shock-Capturing, Finite-Difference Approach to Supersonic Flows," Journal of Spacecraft and Rockets, Vol. 8, No. 12, pp. 1175-1182, Dec. 1971.

[13]Volterra, V., *Theory of Functionals and of Integral and Integro-Differential Equations*, Dover Publications, Inc., New York, 1959.

[14]Regan, F. J., and Horanoff, E. V., "Wind Tunnel Magnus Measurements at the Naval Ordnance Laboratory," AIAA Paper 66-753, 1966.

[15]Platou, A. S., and Sternberg, J., "The Magnus Characteristics of a 30 mm Aircraft Bullet," Rept. 994, Ballistic Research Lab., Aberdeen Proving Ground, Maryland, 1954.

[16]Platou, A. S., "The Magnus Force on a Short Body at Supersonic Speeds," Rept. 1062, Ballistic Research Lab., Aberdeen Proving Ground, Maryland, 1959.

[17]Sedney, R., "Laminar Boundary Layer on a Spinning Cone at Small Angles of Attack in a Supersonic Flow," Journal of the Aeronautical Sciences, Vol. 24, No. 6, pp. 430-436, June 1957.

[18]Tobak, M., and Wehrend, W. R., "Stability Derivatives of Cones at Supersonic Speeds," TN 3788, NACA, 1956.

[19]Rakich, J. V., and Kutler, P., "Comparison of Characteristic and Shock-Capturing Methods with Application to the Space Shuttle," AIAA Paper 72-191, 1972.

[20]Richtmyer, R. D., and Morton, R. W., *Difference Methods for Initial-Value Problems*, Interscience, New York, pp. 304, 360-365, 1967.

[21]Abbett, M. J., "Boundary Condition Computational Procedures for Inviscid Supersonic Steady Flow Field Calculations," Final Rept. 71-41, Aerotherm Corp., Mountain View, California, Nov. 1971.

[22]Kutler, P., Lomax, H., and Warming, R. F., "Computation of Space Shuttle Flow Fields Using Noncentered Finite-Difference Schemes," AIAA Paper 72-193, 1972.

[23]Babenko, K. I., Voskresenskiy, G. P., Lyubimov, A. N., and Rusanov, V. V., "Three-Dimensional Flow of Ideal Gas Past Smooth Bodies," TT F-380, NASA, April 1966.

[24]Rakich, J. V., "Three-Dimensional Flow Calculations by the Method of Characteristics," AIAA Journal, Vol. 5, No. 10, pp. 1906-1908, Oct. 1967.

[25]Ferri, A., "Supersonic Flow Around Circular Cones at Angles of Attack," Rept. 1045, NACA, 1951.

[26]Allen, H. J., and Perkins, E. W., "A Study of the Effects of Viscosity on Flow Over Slender Inclined Bodies of Revolution," Rept. 1048, NACA, 1951.

[27]Liepmann, H. W., and Roshko, A., *Elements of Gasdynamics*, John Wiley & Sons, New York, pp. 57-61, 1957.

[28]Kuhn, G. D., Spangler, S. B., and Nielsen, J. N., "Theoretical Analysis of Vortex Shedding from Bodies of Revolution in Coning Motion," AIAA Journal, Vol. 9, No. 5, pp. 784-790, May 1971.

[29]Brong, E. A., "The Unsteady Flow Field About a Right Circular Cone in Unsteady Flight," FDL-TR-64-148, Flight Dynamics Lab., Wright-Patterson Air Force Base, Ohio, Jan. 1967.

[30]Jorgenson, L. H., "Elliptic Cones Alone and With Wings at Supersonic Speeds," TN 4045, NACA, 1957.

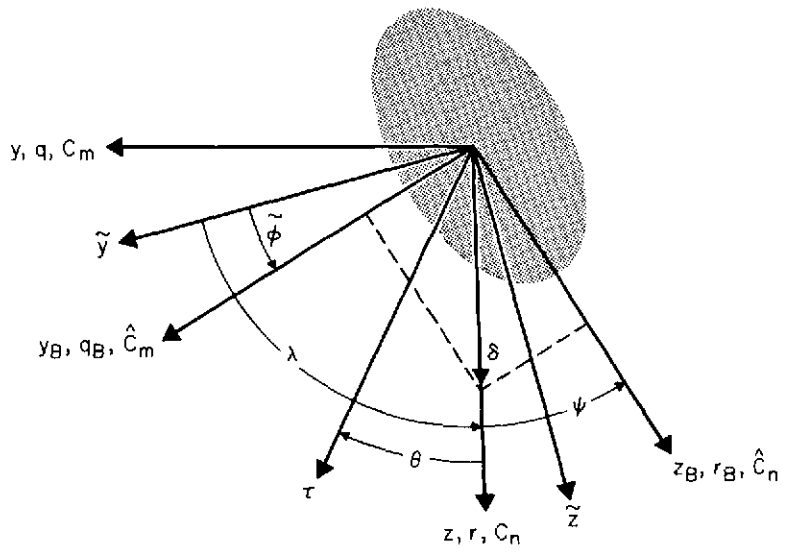

(a) Crossflow plane.

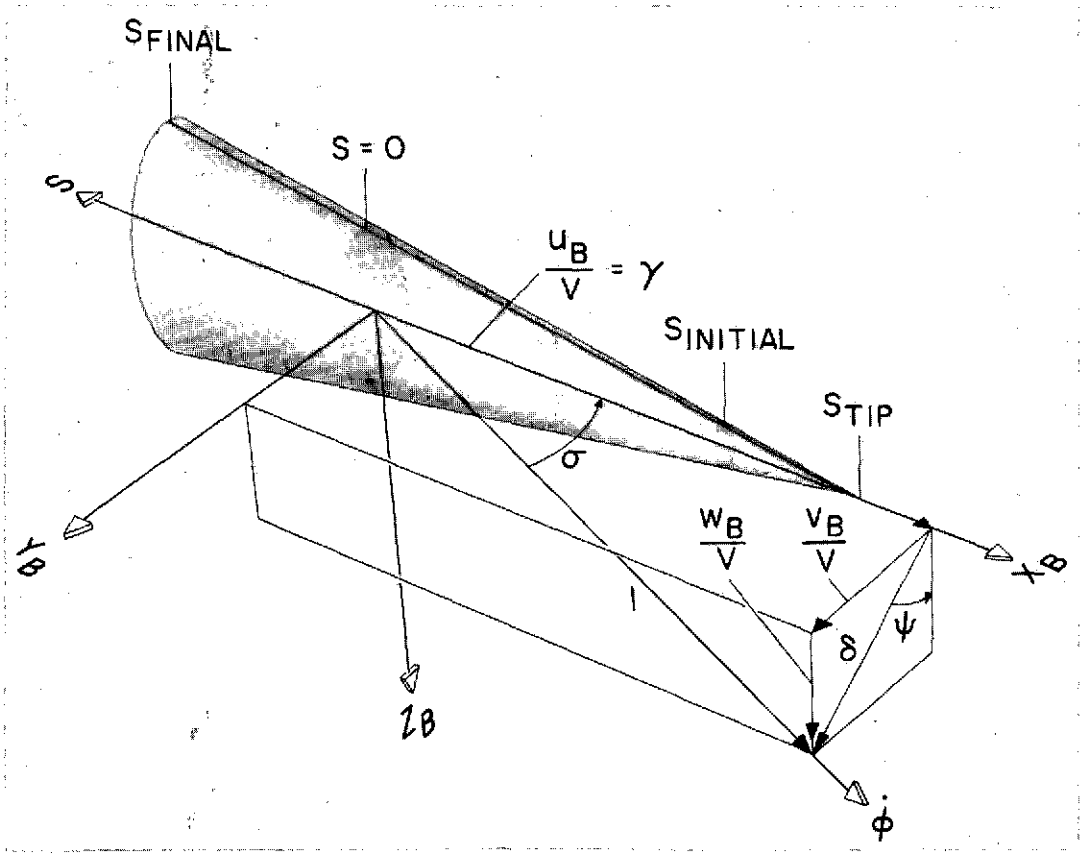

(b) Resultant angle-of-attack plane.

Figure 1.- Axes, angles, and velocity components in the crossflow and resultant angle-of-attack plane.

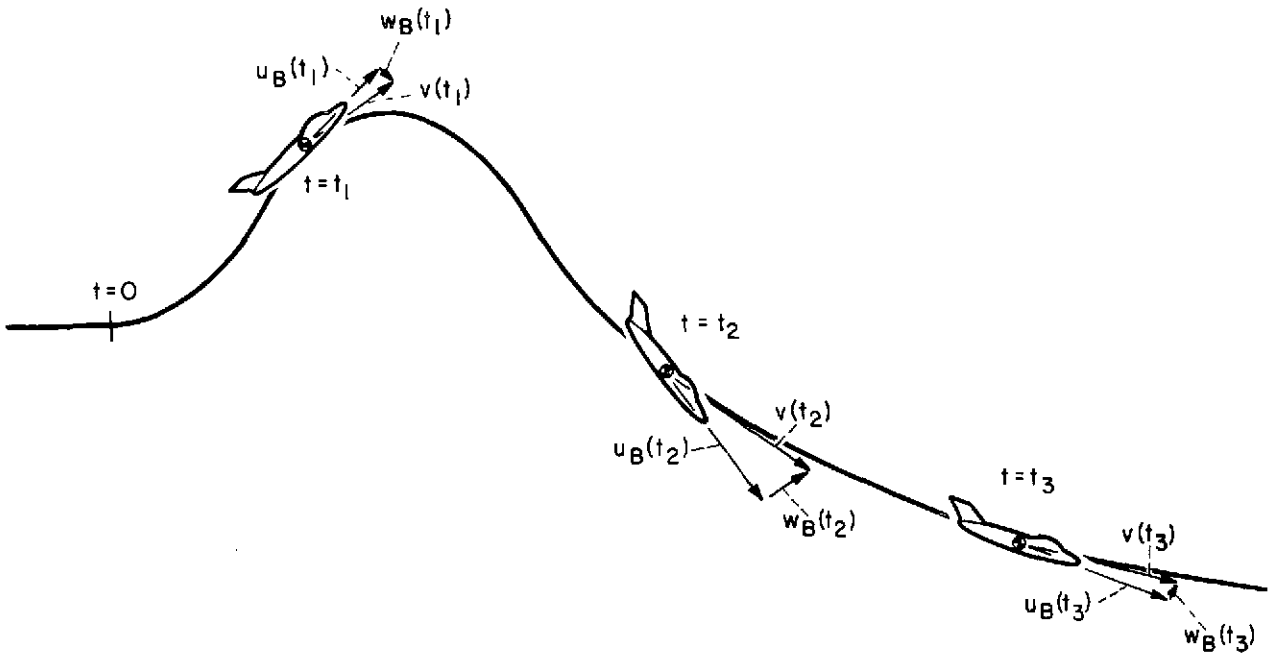

(a) Planar motion.

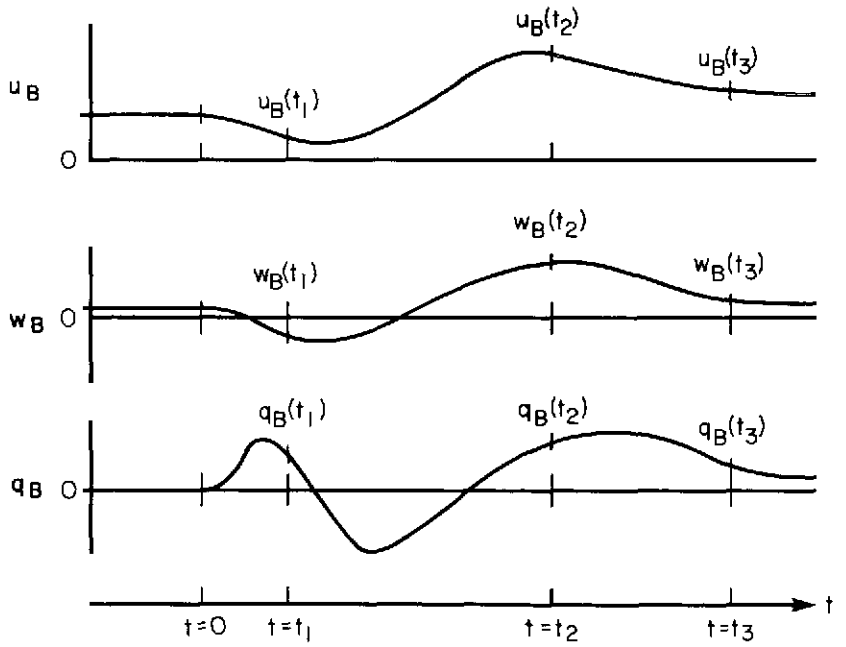

(b) Variation of motion variables.

Figure 2.- Arbitrary large-amplitude planar aircraft motion.

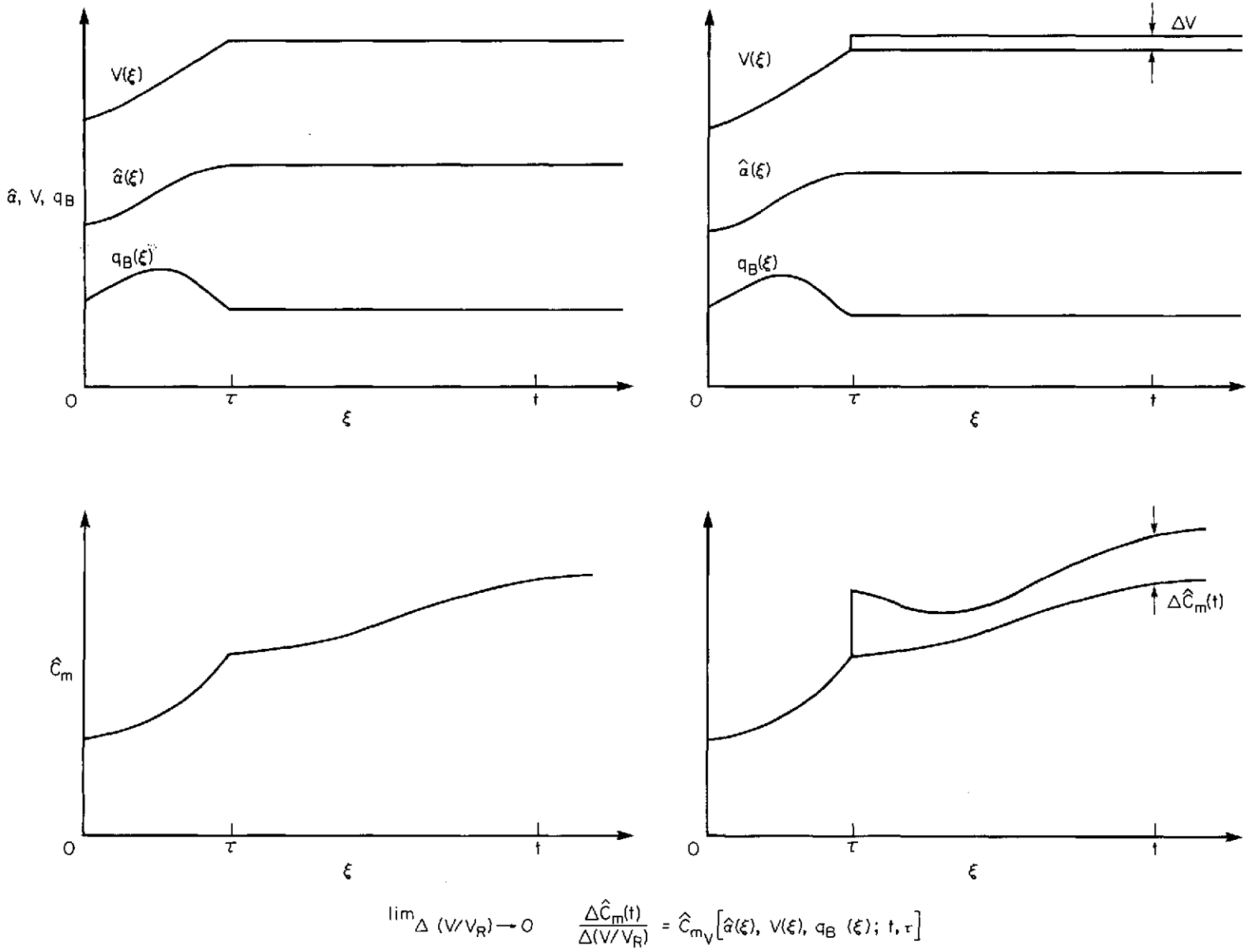

$$\lim_{\Delta\,(V/V_R)\to 0} \quad \frac{\Delta \hat{C}_m(t)}{\Delta(V/V_R)} = \hat{C}_{m_V}\left[\hat{a}(\xi),\ V(\xi),\ q_B\ (\xi);\ t, \tau\right]$$

Figure 3.- Definition of nonlinear indicial response.

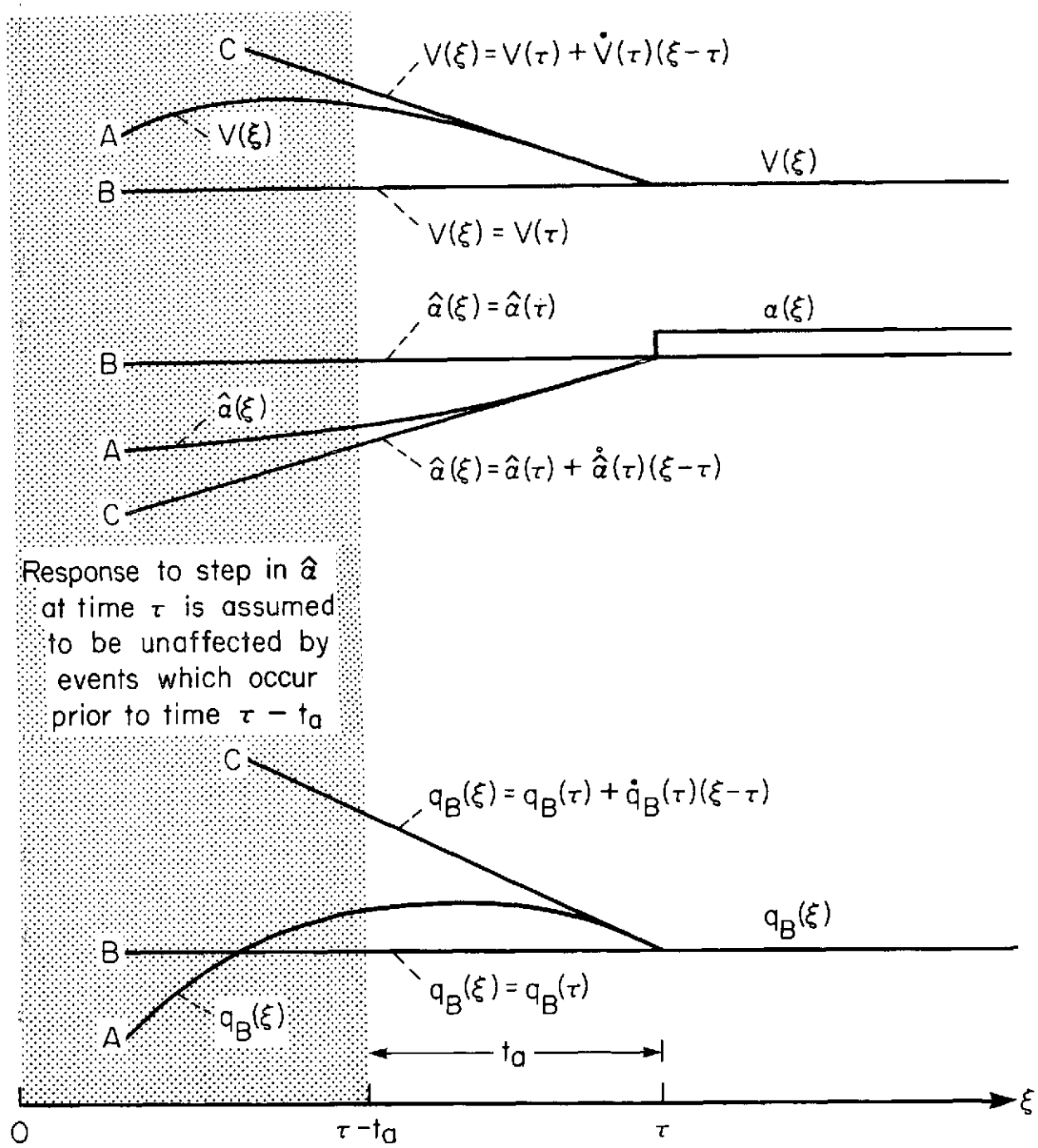

Figure 4.- Approximation of indicial response.

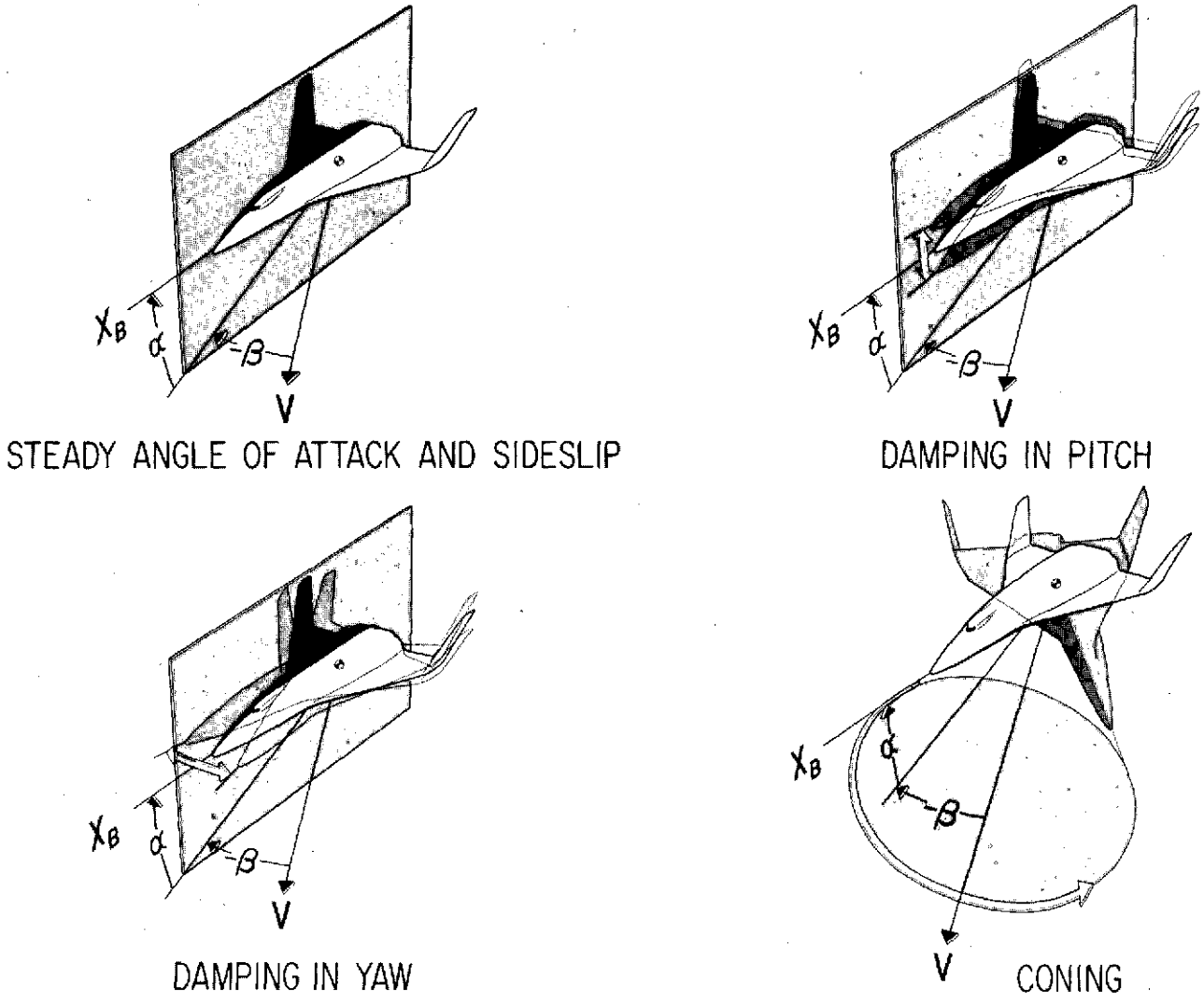

Figure 5.- Basic motions in body-fixed axes.

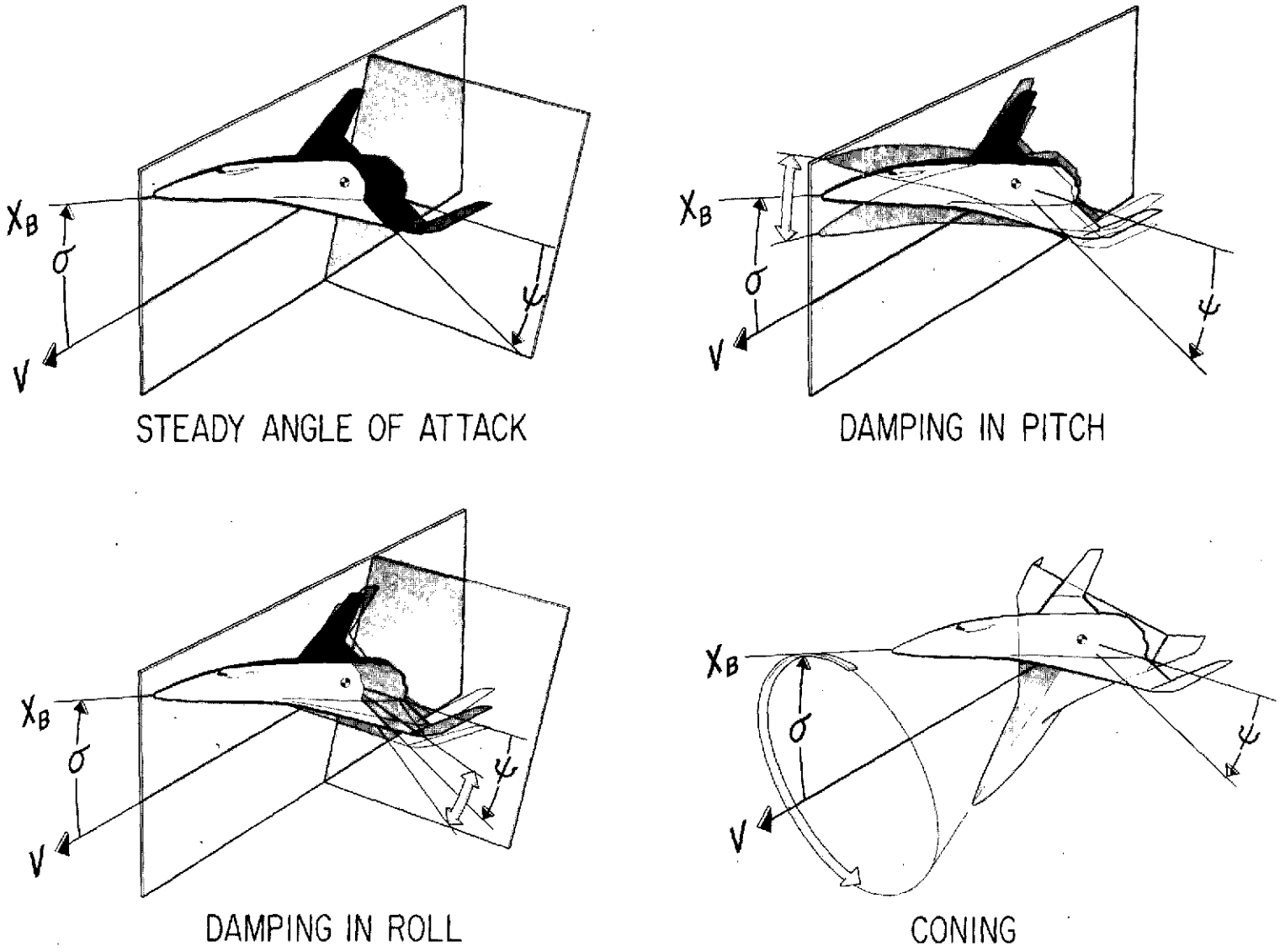

Figure 6.- Basic motions in aerodynamic axes.

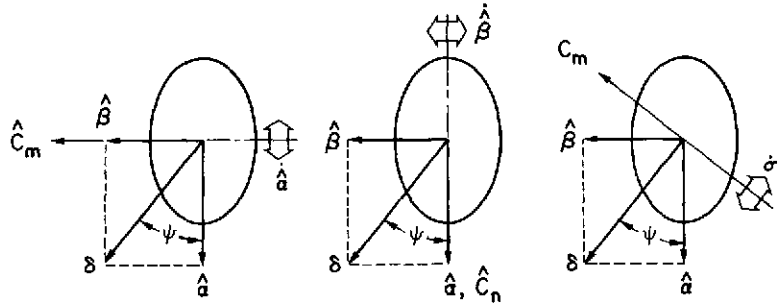

$$\frac{C_{n_{\dot{\phi}}} - \gamma C_{n_{\dot{\psi}}}}{\delta} = \left(\hat{C}_{m_{q_B}} + \gamma \hat{C}_{m_{\dot{\alpha}}}\right) + \left(\hat{C}_{n_{r_B}} - \gamma \hat{C}_{n_{\dot{\beta}}}\right) - C_{m_{\dot{\sigma}}}$$

Figure 7.- Schematic representation of the equality between $(C_{n_{\dot{\phi}}} - \gamma C_{n_{\dot{\psi}}})/\delta$ and the three damping coefficients.

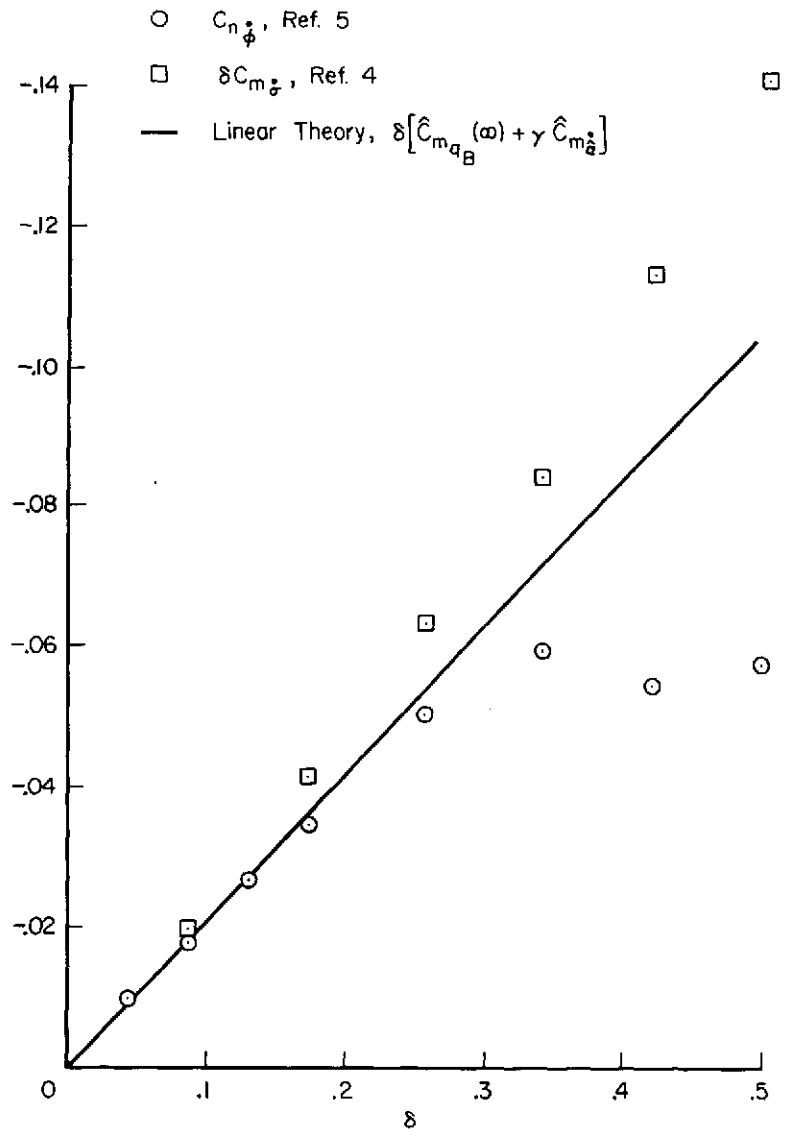

Figure 8.- Variation of $\delta C_{m_{\dot{\sigma}}}$ and $(C_{n_{\dot{\phi}}} - \gamma C_{n_{\dot{\psi}}})$ with increasing angle of attack; Mach number = 2.0, $\ell_{cg}/\ell = 0.61$.

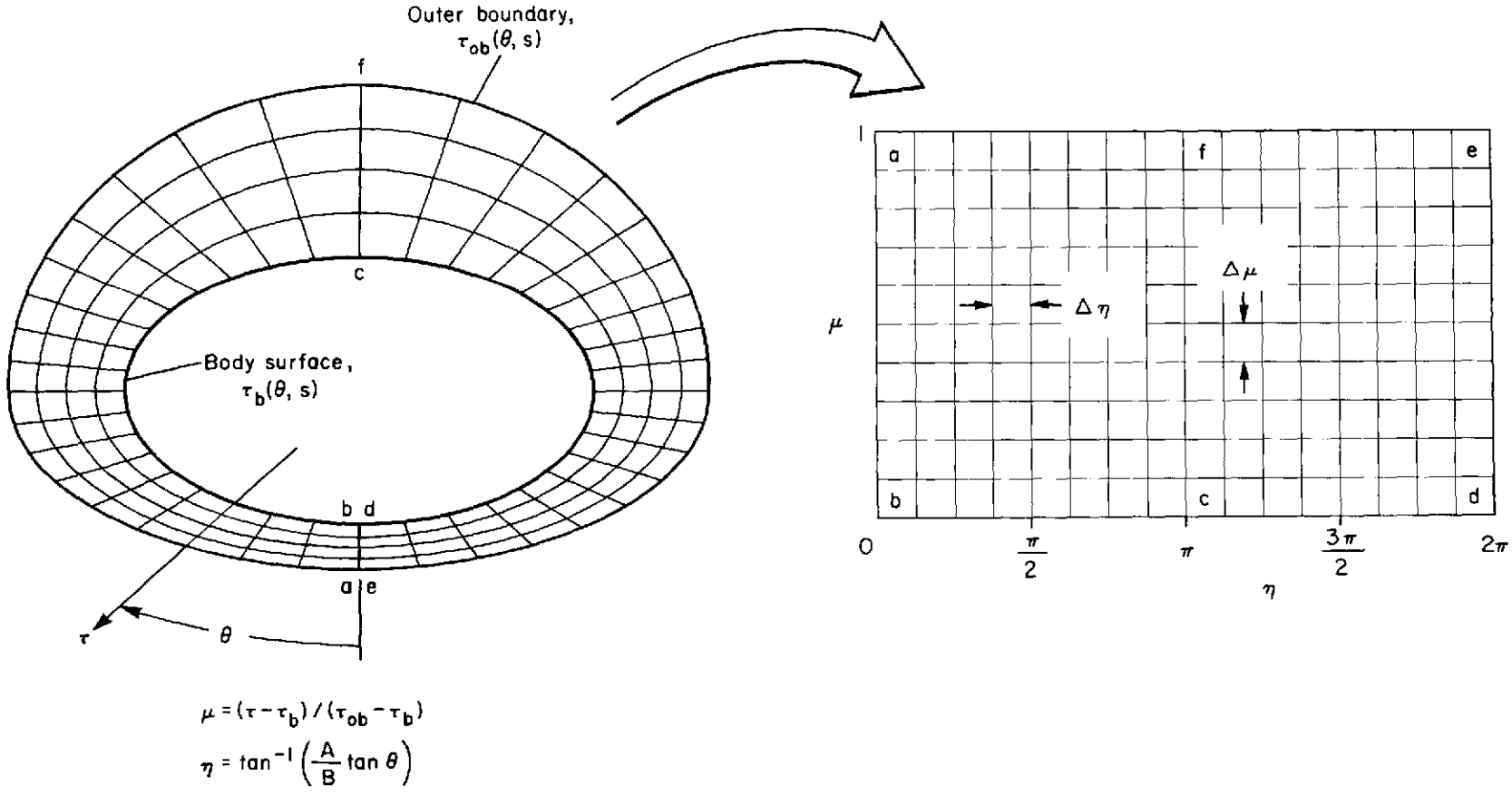

$$\mu = (\tau - \tau_b) / (\tau_{ob} - \tau_b)$$

$$\eta = \tan^{-1}\left(\frac{A}{B}\tan\theta\right)$$

Figure 9.- Transformation from physical to computational planes.

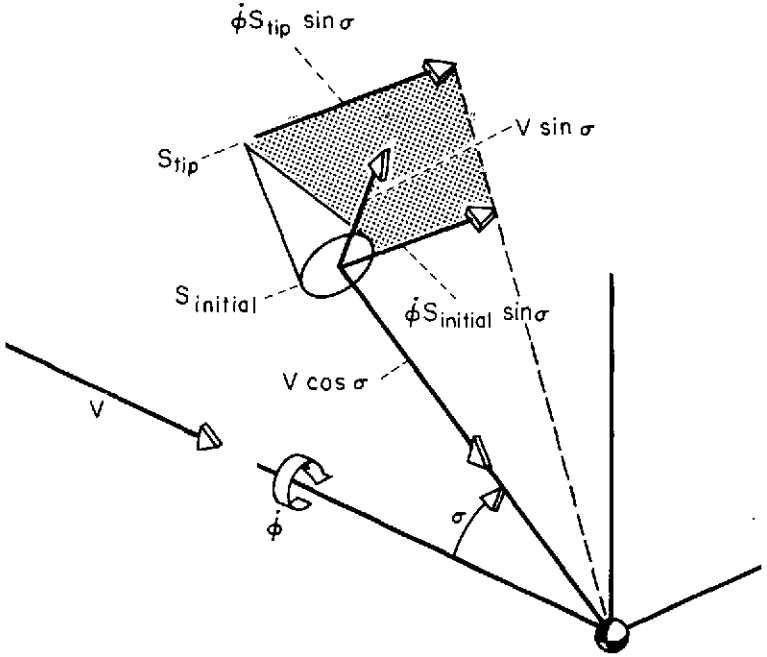

(a) Coning motion.

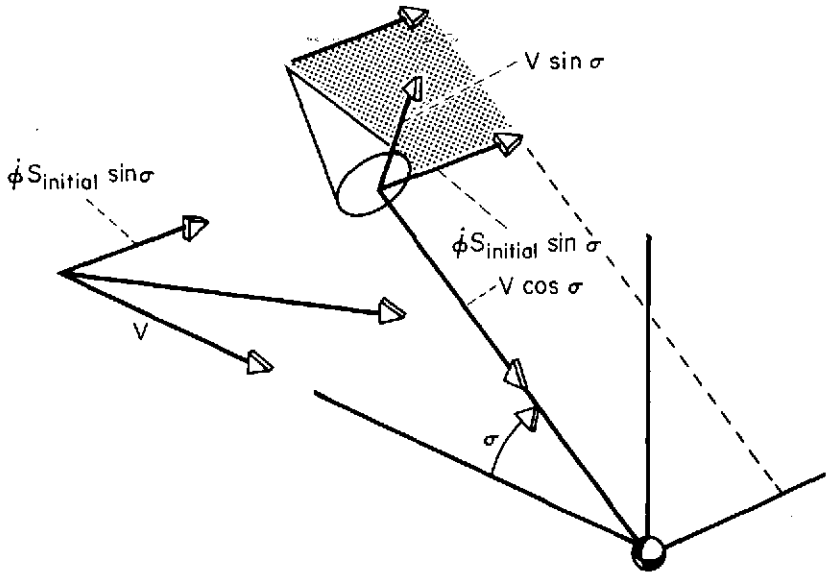

(b) Conical flow approximation.

Figure 10.- Approximation of initial solution.

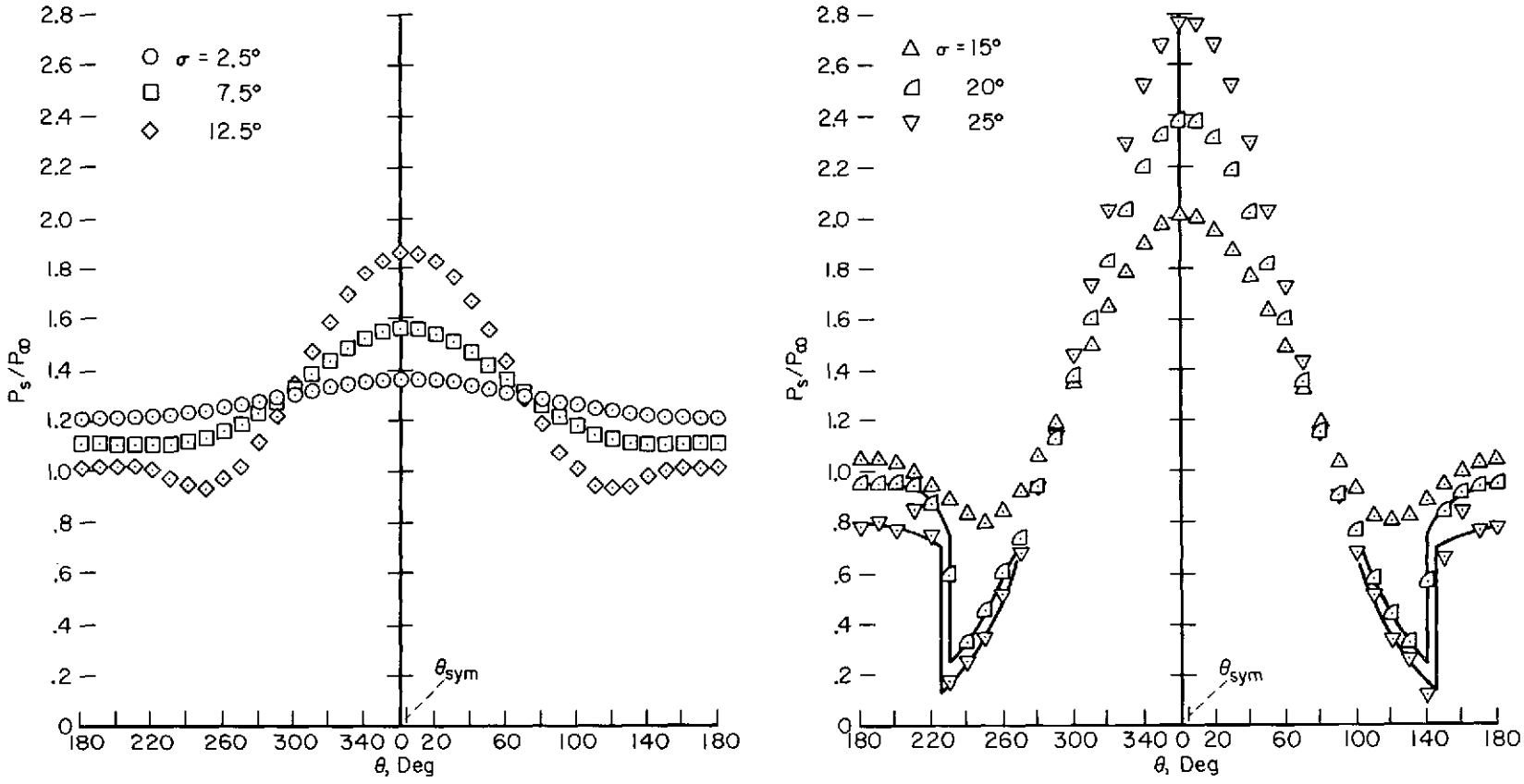

(a) $\dot{\phi}/V = 0.12$

(b) $\dot{\phi}/V = 0.15$

Figure 11.- Circumferential surface pressure distribution for 10° half-angle cone; Mach number = 2.0, $s = s_{initial}$.

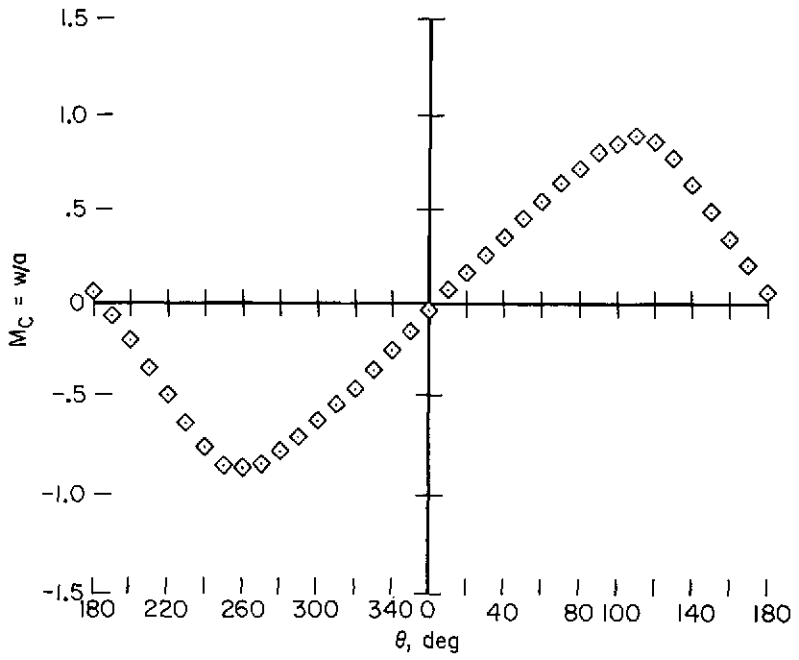

(a) $\sigma = 15°$

Figure 12.- Circumferential crossflow Mach number for 10° half-angle cone; Mach number = 2.0, $s = s_{initial}$, $\dot{\phi}/V = 0.15$.

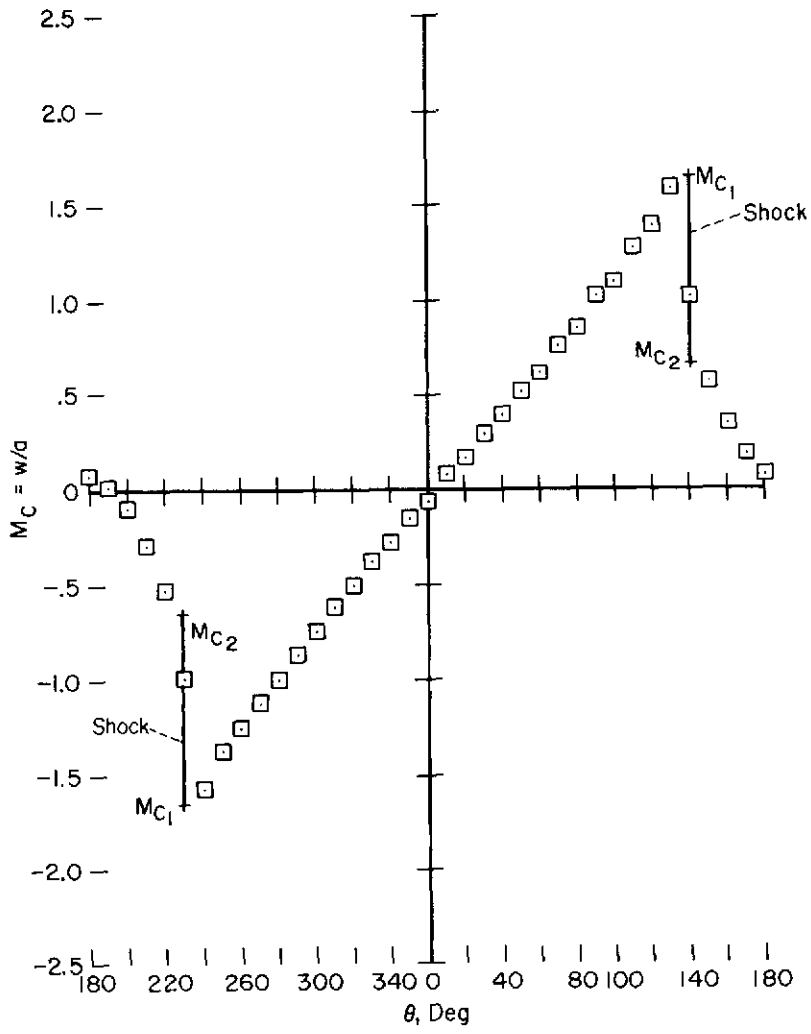

(b) $\sigma = 20°$

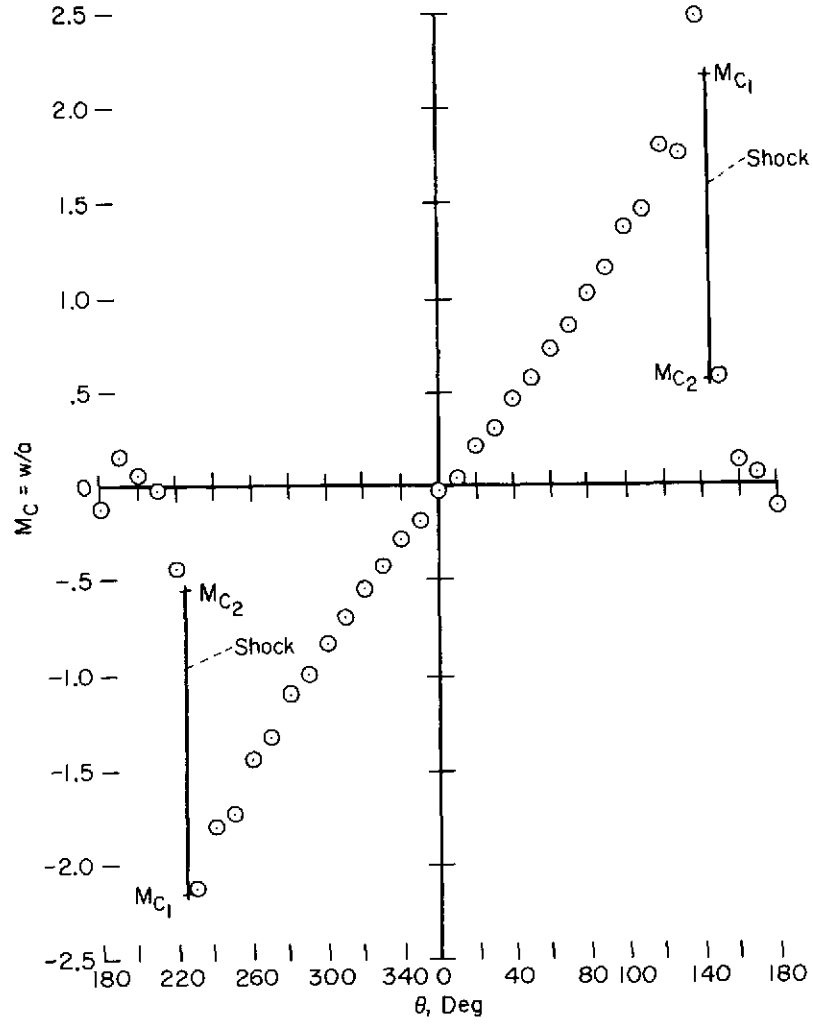

(c) $\sigma = 25°$

Figure 12.- Concluded.

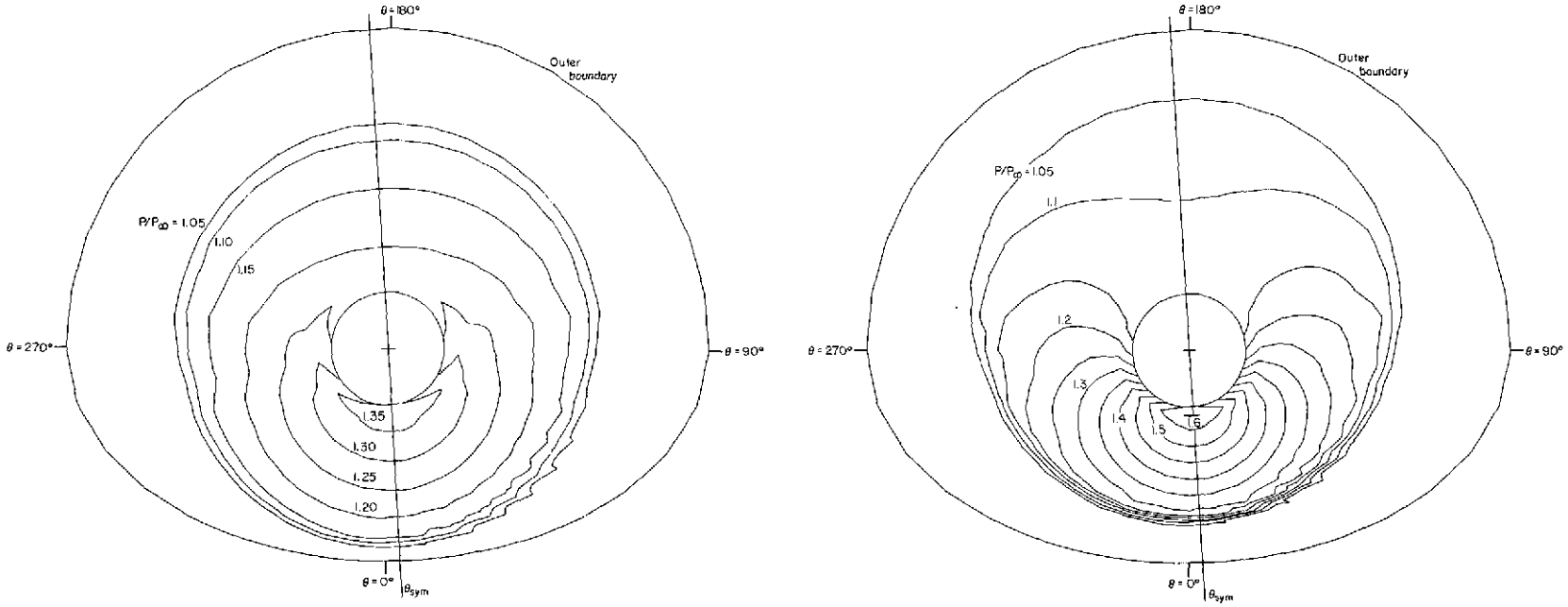

(a) $\sigma = 2.5°$, $\dot{\phi}/V = 0.12$

(b) $\sigma = 7.5°$, $\dot{\phi}/V = 0.12$

Figure 13.- Flow-field cross section pressure contours for 10° half-angle cone; Mach number = 2.0, s = $s_{initial}$.

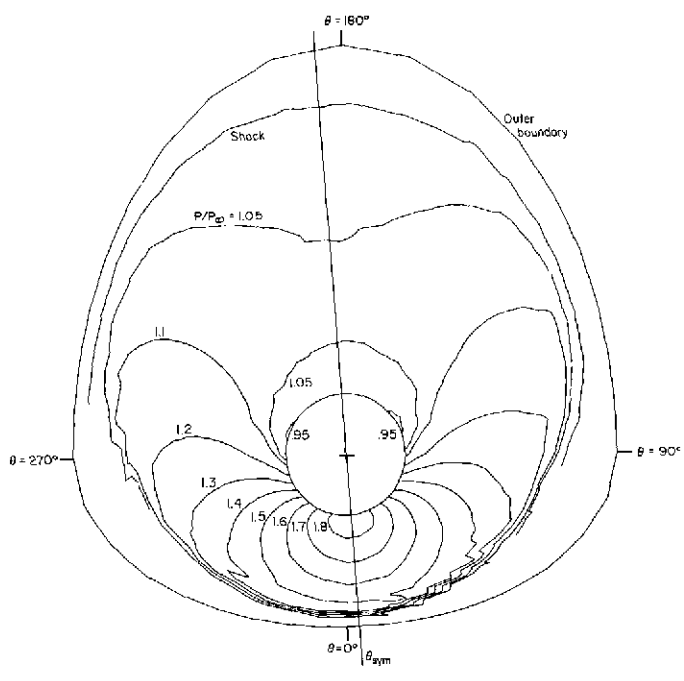

(c) $\sigma = 12.5°$, $\dot{\phi}/V = 0.12$

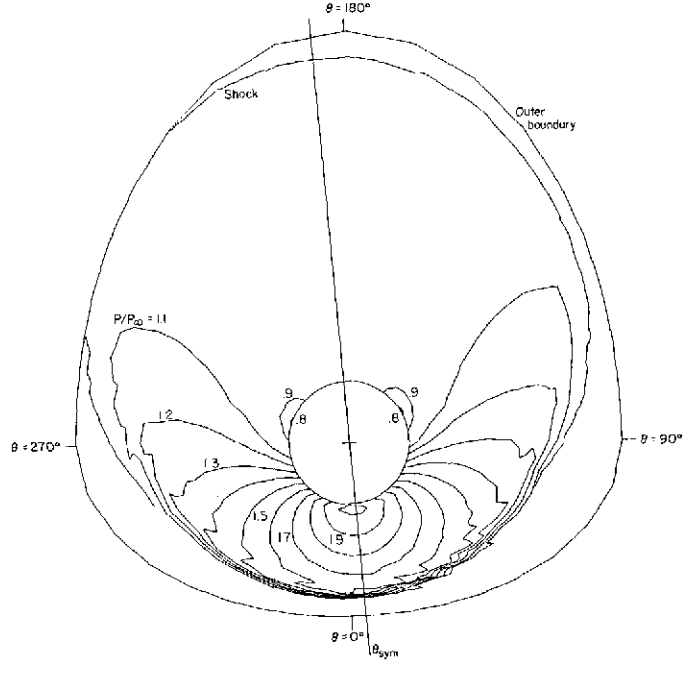

(d) $\sigma = 15.0°$, $\dot{\phi}/V = 0.15$

Figure 13.- Continued.

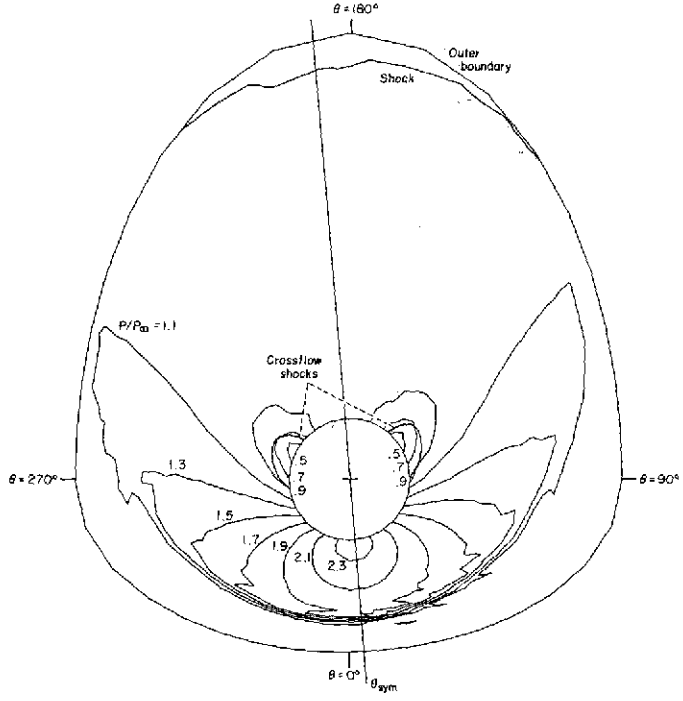

(e) $\sigma = 20.0°$, $\dot{\phi}/V = 0.15$

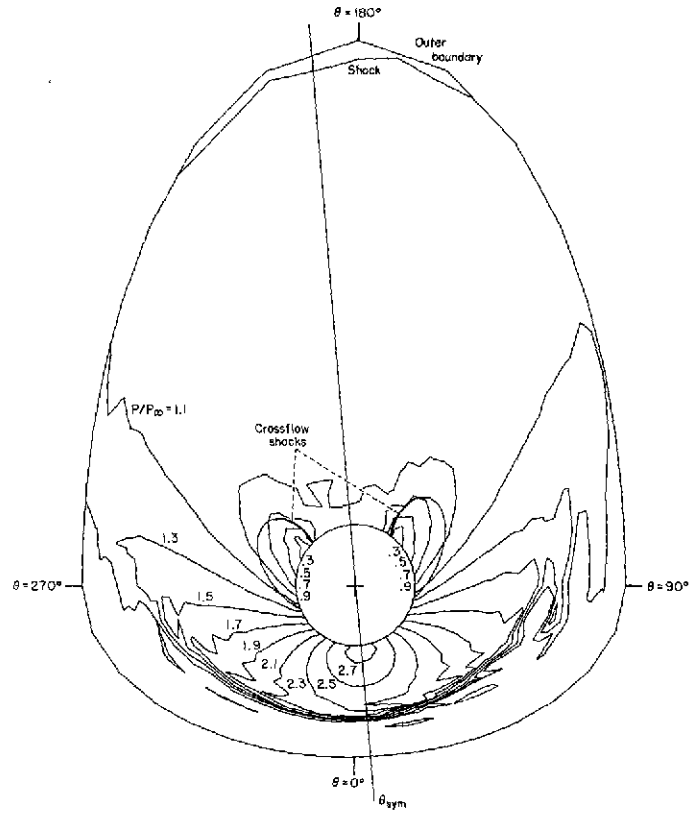

(f) $\sigma = 25.0°$, $\dot{\phi}/V = 0.15$

Figure 13.- Concluded.

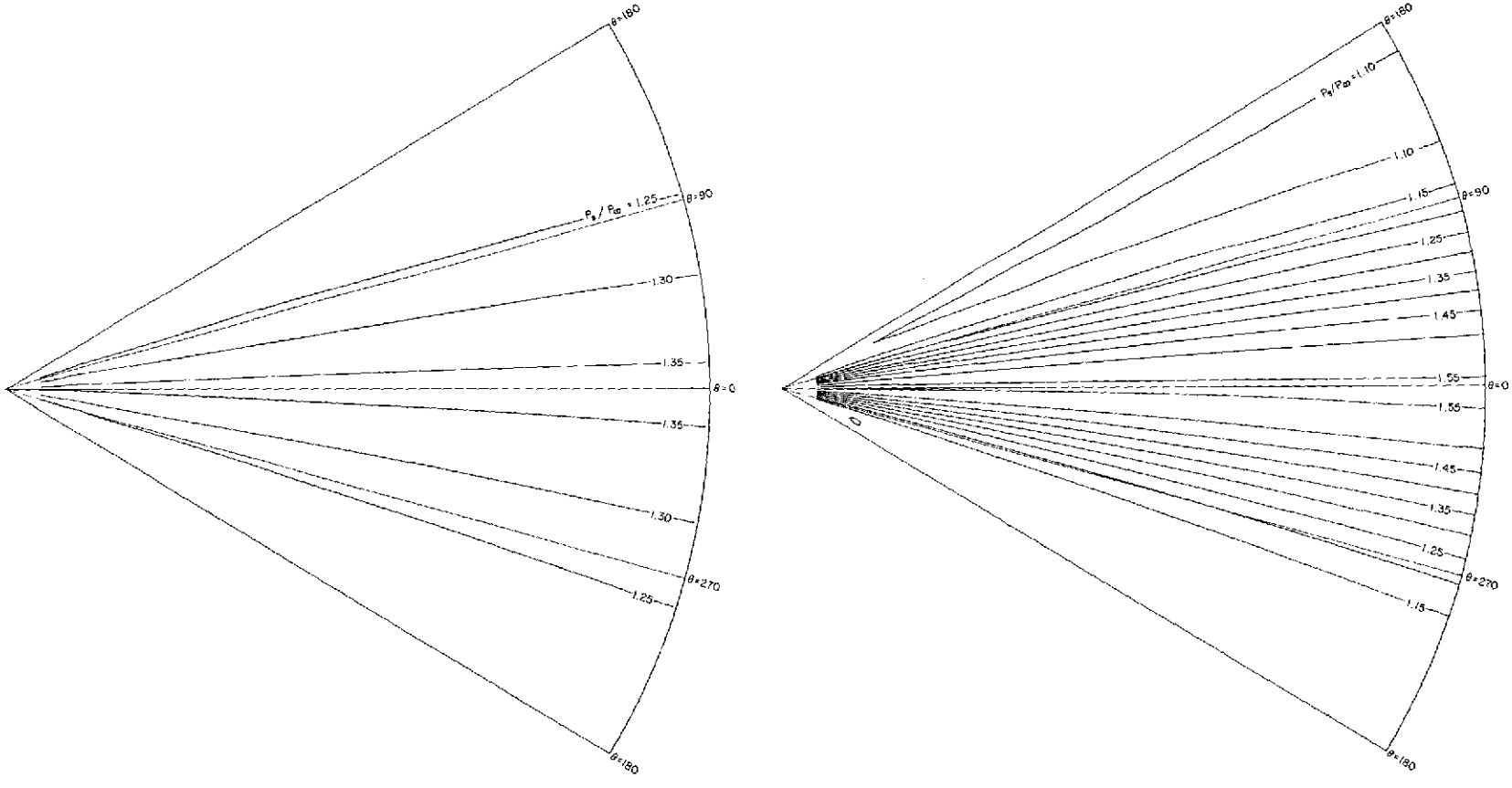

(a) $\sigma = 2.5°$, $\dot{\phi}/V = 0.12$

(b) $\sigma = 7.5°$, $\dot{\phi}/V = 0.12$

Figure 14.- Surface pressure contours for 10° half-angle cone; Mach number = 2.0.

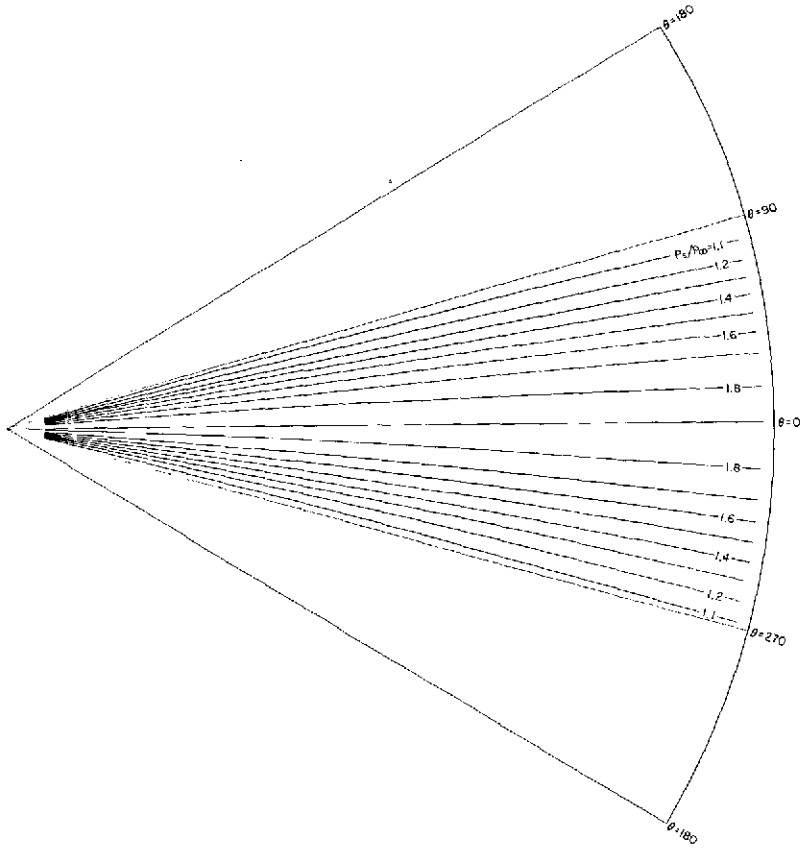

(c) $\sigma = 12.5°$, $\dot{\phi}/V = 0.12$

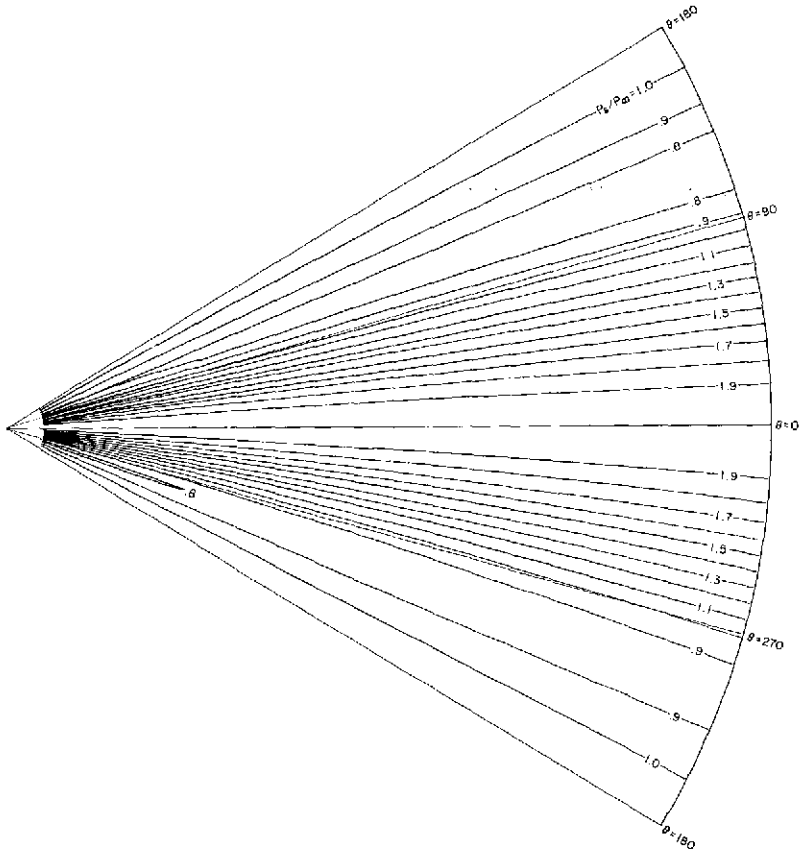

(d) $\sigma = 15.0°$, $\dot{\phi}/V = 0.15$

Figure 14.- Continued.

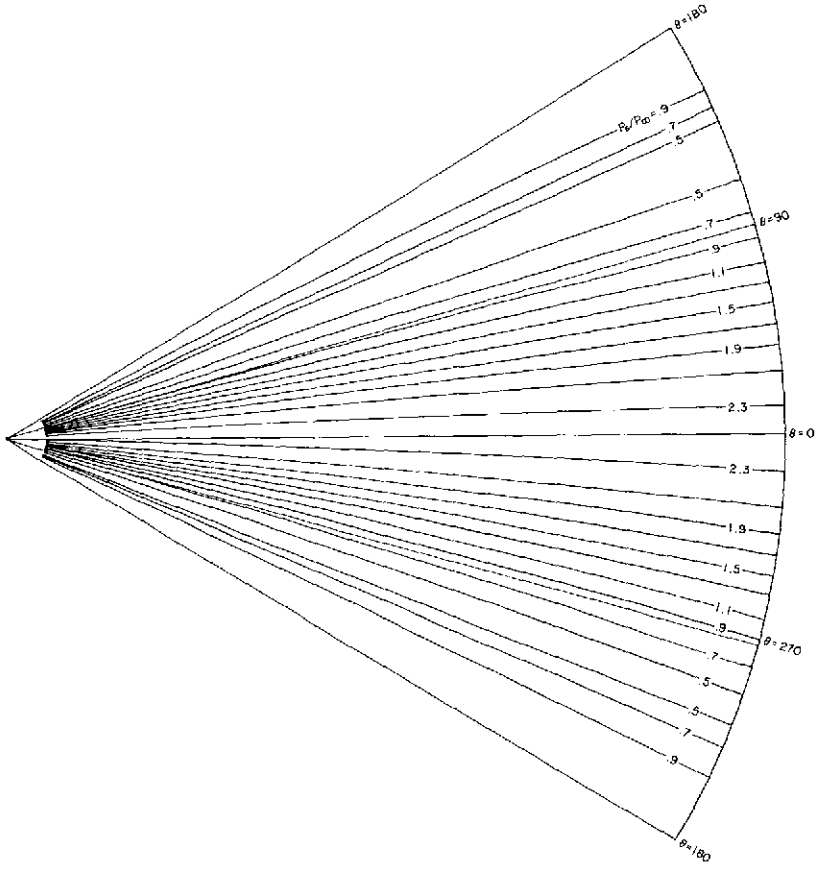

(e) $\sigma = 20.0°$, $\dot{\phi}/V = 0.15$

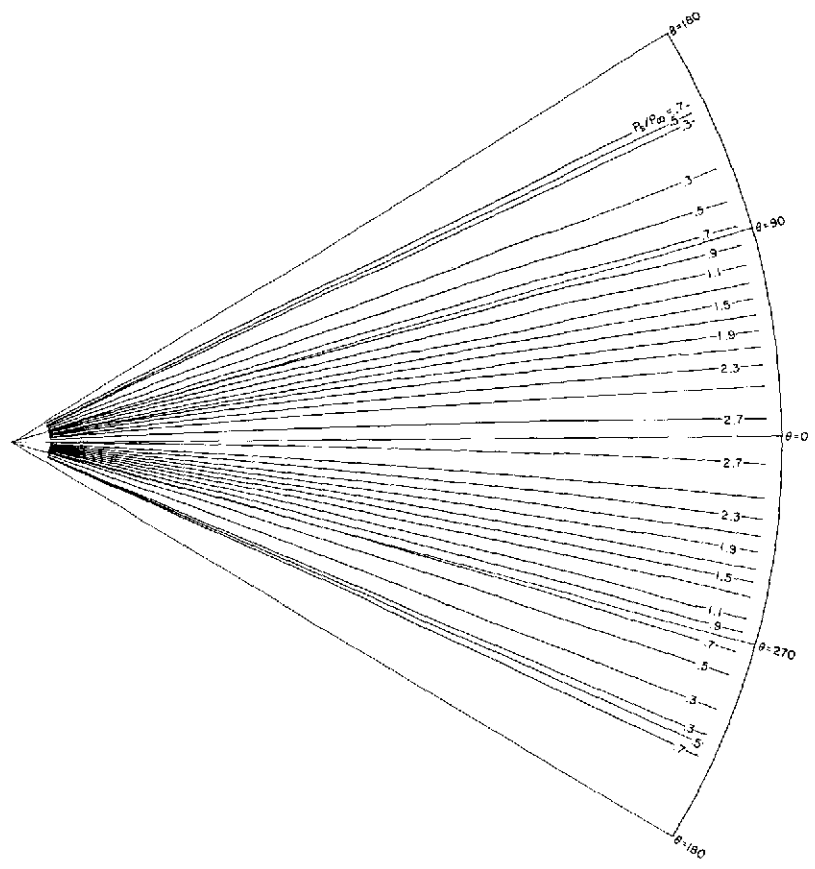

(f) $\sigma = 25.0°$, $\dot{\phi}/V = 0.15$

Figure 14.- Concluded.

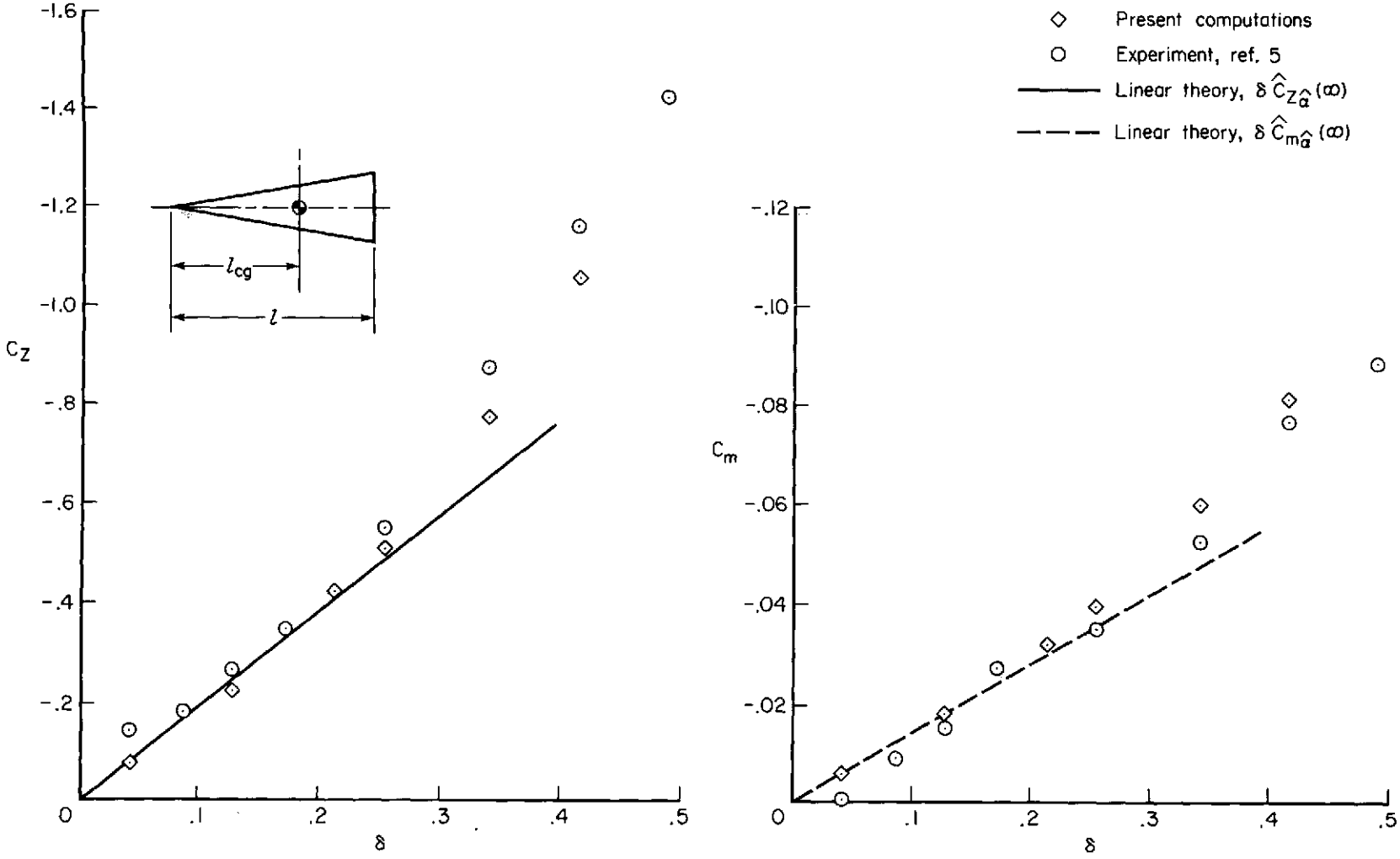

(a) Normal-force coefficient.

(b) Pitching-moment coefficient.

Figure 15.- Normal-force and pitching-moment coefficients for 10° half-angle cone; Mach number = 2.0, $\ell_{cg}/\ell = 0.61$.

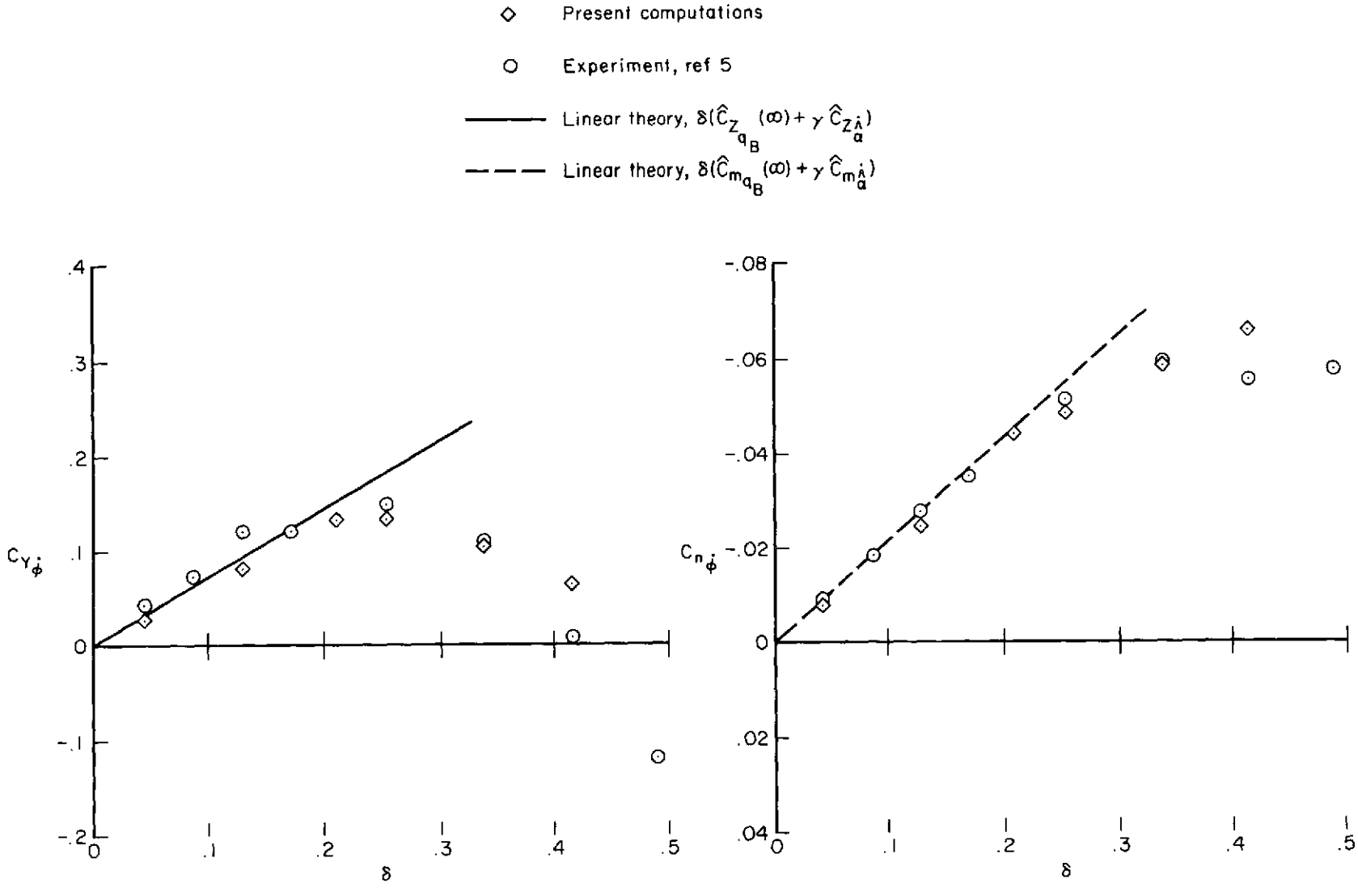

(a) Side-force coefficient.

(b) Side-moment coefficient.

Figure 16.- Side-force and side-moment coefficients on 10° half-angle cone caused by coning motion; Mach number = 2.0, ℓ_{cg}/ℓ = 0.61.

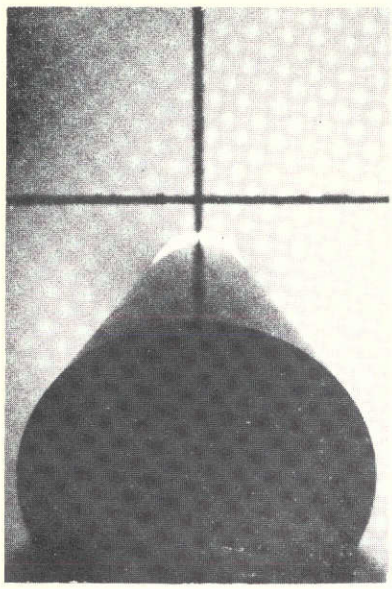

$\delta = 0.26$

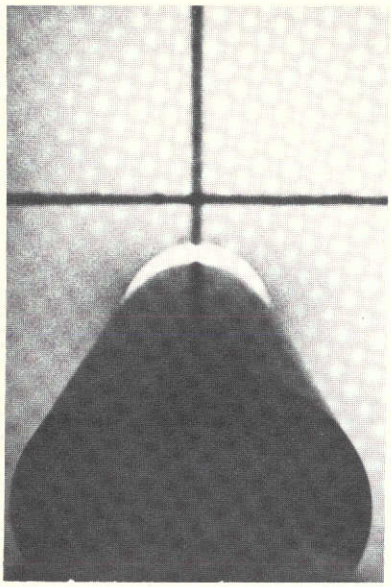

$\delta = 0.34$

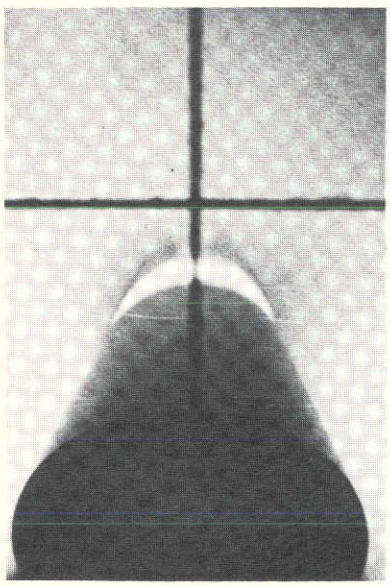

$\delta = 0.42$

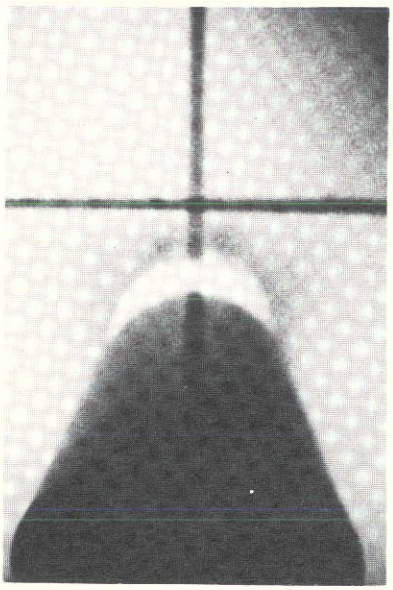

$\delta = 0.50$

Figure 17.- Typical vapor screen photographs; 10° half-angle cone, Mach number = 2.0.

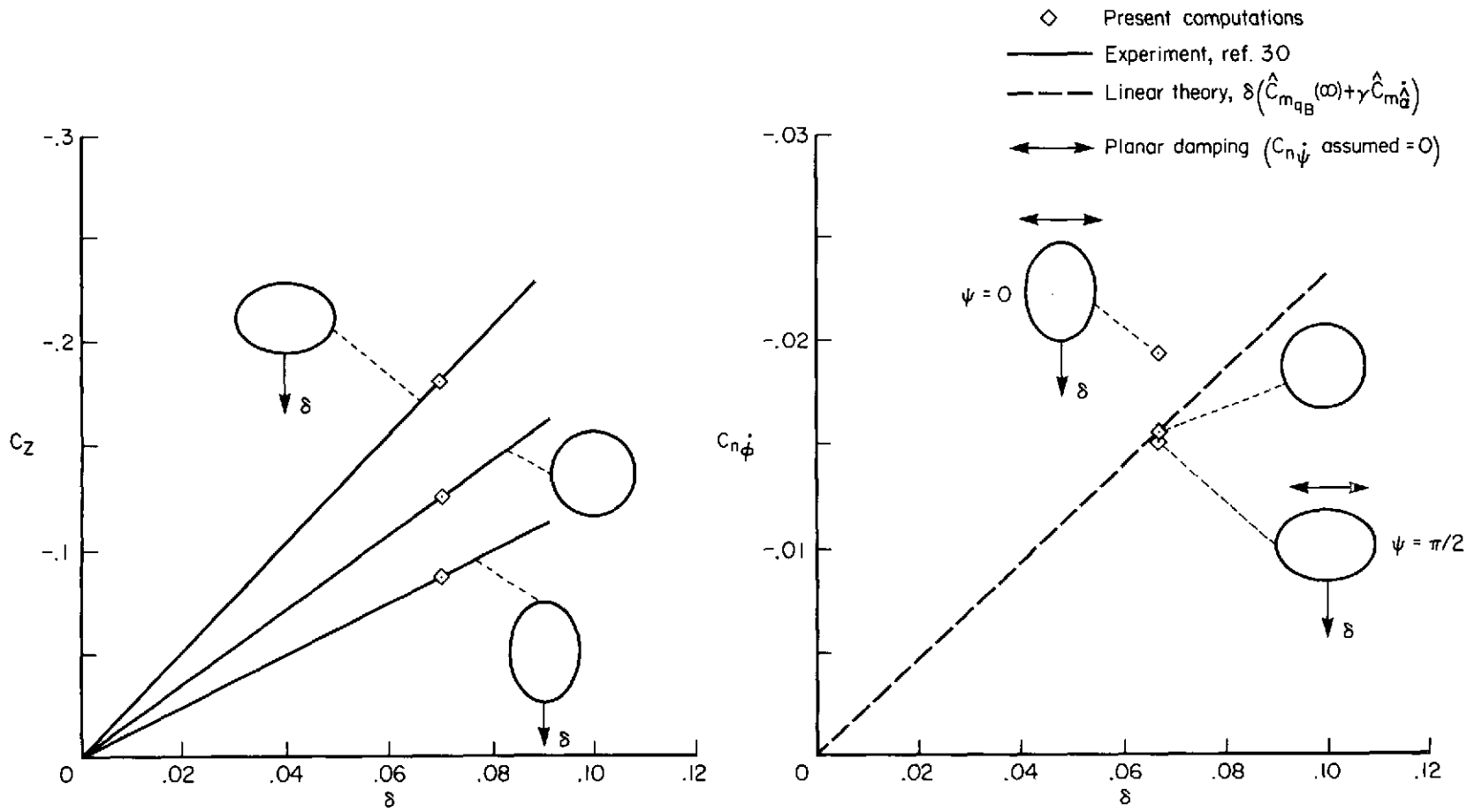

(a) Normal-force coefficient.

(b) Side-moment coefficient.

Figure 18.- Normal-force and side-moment coefficients on elliptic cones caused by coning motion; Mach number = 1.97, ℓ_{cg}/ℓ = 0.61.